

**Cationic polymer coating of PLGA
nanoparticles
for enabling cellular delivery of siRNA**

Dissertation

zur Erlangung des Grades

des Doktors der Naturwissenschaften

der Naturwissenschaftlich-Technischen Fakultät

der Universität des Saarlandes

von

Nicole Liebsch

Saarbrücken 2017

Die vorliegende Arbeit entstand in der Zeit von November 2012 bis November 2015

an der Universität des Saarlandes

am Lehrstuhl für Biopharmazie und Pharmazeutische Technologie und
dem Helmholtz-Institut für Pharmazeutische Forschung Saarland (HIPS).

Tag des Kolloquiums:	06. März 2018
Dekan:	Prof. Dr. Guido Kickelbick
Vorsitzender:	Prof. Dr. Marc Schneider
Berichterstatter:	Prof. Dr. Claus-Michael Lehr Prof. Dr. Thorsten Lehr
Akad. Mitarbeiter:	Dr. Matthias Engel

Alle Wahrheiten sind paradox.

Leo N. Tolstoi

This thesis was conducted as part of the project
“Collaboration on the Optimization of Macromolecular Pharmaceutical Access
to Cellular Targets (COMPACT)”,
financially supported by the Innovative Medicines Initiative (IMI)
Joint Undertaking under grant agreement n° 115363.

Table of Contents

ABSTRACT	IX
KURZZUSAMMENFASSUNG	X
CHAPTER 1 - GENERAL INTRODUCTION	1
1.1 Biomacromolecules as pharmaceutical ingredients	1
1.1.1 Definition of biomacromolecules and their impact on the market	1
1.1.2 Gene suppression via RNA interference	3
1.2 The lung as a target	6
1.2.1 Morphology and anatomy of the human lung	6
1.2.2 Pulmonary diseases and current medical applications	8
1.3 Nanoparticles as a system to overcome biological barriers	9
1.3.1 Nanoparticles or nanopharmaceuticals - what makes the difference?.....	9
1.3.2 Interactions with cellular and non-cellular barriers inside the lungs	10
1.3.3 A combined system of siRNA and nanoparticles as a new approach for pulmonary treatment.....	12
1.4 Aim of this research study	13
CHAPTER 2 - OPTIMIZATION OF THE PREPARATION TECHNIQUE ON THE BASIS OF CHITOSAN-COATED PLGA NANOPARTICLES (1ST GENERATION)	16
2.1 Introduction	17
2.2 NPs preparation	19
2.2.1 Materials.....	19
2.2.2 PLGA-Chitosan NPs.....	20
2.2.3 Flu-labeled NPs.....	21
2.3 NPs characterization	24
2.3.1 Colloidal characteristics.....	24
2.3.2 Purification techniques	25
2.3.3 Passive surface loading.....	26
2.3.4 Particle imaging (SEM/SPM)	28
2.4 Results and discussion	29
2.4.1 Preparation technique	29
2.4.2 FA- and DiI-labeled NPs.....	35

2.4.3 Purification.....	36
2.4.4 Loading efficiency.....	37
2.5 Conclusion.....	39
CHAPTER 3 - SUITABLE COATING MATERIALS FOR TRANSFECTING PLGA-BASED NANOPARTICLES (2ND GENERATION).....	41
3.1 Introduction	42
3.2 Materials and methods	44
3.2.1 Materials.....	44
3.2.2 Characterization of coating materials	45
3.2.3 Characterization of coated PLGA NPs	50
3.3 Results and discussion.....	53
3.3.1 Characterization of pure coating materials	53
3.3.2 Characterization of coated PLGA NPs	57
3.4 Conclusion	65
CHAPTER 4 - STABILITY OF DRUG DELIVERY SYSTEMS FOR PULMONARY APPLICATION	67
4.1 Introduction	68
4.2 Materials and methods	69
4.2.1 Storage stability	70
4.2.2 Freeze dried NPs.....	70
4.2.3 Nebulization.....	70
4.3 Results and discussion.....	73
4.3.1 NPs stability at 4 °C, RT and 37 °C	73
4.3.2 Re-dispersibility after lyophilization.....	75
4.3.3 Stability after nebulization.....	76
4.4 Conclusion	78
CHAPTER 5 - CELL VIABILITY AND IMMUNOGENICITY	81
5.1 Introduction	82
5.2 Materials and methods	83
5.2.1 Cell viability	83
5.2.2 Immunogenicity	87
5.3 Results and discussion.....	91

5.3.1 Cytotoxicity	91
5.3.2 Immunogenicity	96
5.4 Conclusion	100
CHAPTER 6 - TRANSFECTION EFFICIENCY OF DRUG DELIVERY SYSTEMS	102
6.1 Introduction	103
6.2 Materials and methods	104
6.2.1 Cultivation of A549 and hAELVi cells	104
6.2.2 Extraction of pGL3 plasmid from <i>E.coli</i>	106
6.2.3 Simultaneous co-transfection	106
6.2.4 Screening of transfection reagents.....	107
6.2.5 BCA vs. BCA-RAC for normalization	108
6.2.6 Luciferase assay.....	109
6.3 Results and discussion.....	109
6.3.1 Reagent screening	109
6.3.2 Transfection experiments on A549 cells.....	111
6.3.3 Transfection of hAELVi cells.....	113
6.4 Conclusion	114
CHAPTER 7 - UPTAKE AND LOCALIZATION OF NANOPARTICLES ON CELLS	
(IN-VITRO)	116
7.1 Introduction	117
7.2 Materials and methods	118
7.2.1 Cell culture	118
7.2.2 Uptake and localization	119
7.2.4 Fluorescent correlation spectroscopy.....	119
7.2.5 Correlative microscopy	120
7.3 Results and discussion.....	121
7.3.1 Uptake by different cell culture cells	121
7.3.1 Localization via LysoTracker [®] dye on A549 cells	124
7.3.2 FCS analysis	125
7.3.3 Correlative microscopy	126
7.4 Conclusion	128
CHAPTER 8 - SUMMARY AND OUTLOOK.....	129

CHAPTER 9 - ZUSAMMENFASSUNG UND AUSBLICK.....	132
ABBREVIATIONS.....	135
REFERENCES.....	140
DANKSAGUNG.....	153
SCIENTIFIC OUTPUT.....	155
CURRICULUM VITAE.....	157

Abstract

As part of the 'COMPACT' (*Collaboration on the Optimization of Macromolecular Pharmaceutical Access to Cellular Targets*) project a consortium of partners from academic and industrial research set the aim of developing a carrier system for the transport of siRNA (small interfering RNA) into the lung to overcome the pulmonary barrier. For this purpose, an established nanoparticulate system consisting of two polymers, PLGA poly(lactide-co-glycolide) and Chitosan, was applied and optimized concerning particle characteristics (size, distribution, and charge) potential automation and upscaling processes.

Within the development of the second generation of biodegradable drug delivery systems, a novel combination of Protamine + PLGA and CatStarch (a synthesized water-soluble cationic starch) + PLGA was used and characterized with regards to its application.

In vitro studies were performed to investigate the carriers biocompatibility (cytotoxicity and immunogenicity) and efficacy (cellular uptake, localization and transfection). Within this examination, a method to show knock-down results without the availability of cost-intensive stable transfected cell lines was developed.

Kurzzusammenfassung

Im Rahmen des „COMPACT“ (*Collaboration on the Optimisation of Macromolecular Pharmaceutical Access to Cellular Targets*) Projektes wurde in Kooperation mit Partnern aus Industrie und universitärer Forschung das Ziel gesetzt, einen Träger für den Transport von siRNA (small interfering RNA) in die Lunge zu entwickeln, um die Lungenbarriere zu überwinden. Zu diesem Zweck wurde auf ein bestehendes nanopartikuläres System bestehend aus zwei Polymeren, PLGA (Polylactid-co-Glycolid) und Chitosan, aufgebaut und die Herstellung bezüglich Partikeleigenschaften (Größe, Partikelgrößenverteilung und Ladung), möglicher Automatisierungs- und späterer Upscaling-Prozesse optimiert.

Bei der Entwicklung einer zweiten Generation an bioabbaubaren Wirkstoffträgersystemen wurde eine neuartige Kombination aus Protamin und PLGA und CatStarch (eine synthetisierte wasserlösliche kationische Stärke) und PLGA verwendet und unter applikationsspezifischer Gesichtspunkten charakterisiert.

Zur Beschreibung der Trägersysteme gehörten neben *in vitro* Untersuchungen zur Zelltoxizität, Immunogenität, Zellaufnahme und Lokalisierung, die Überprüfung der jeweiligen Transfektionseffizienz. Innerhalb dieser Versuche konnte eine Methode entwickelt werden, die die Darstellung von knock-down Prozessen ohne Vorhandensein einer kostenintensiven stabil transfizierten Zelllinie ermöglicht.

Chapter 1 - General introduction

1.1 Biomacromolecules as pharmaceutical ingredients

1.1.1 Definition of biomacromolecules and their impact on the market

The definition of biomacromolecules consists of the combination of the terms biological molecules (or biomolecules) and macromolecules. Biomolecules include all chemical structures which can be found in living organisms and all types of their metabolites, this includes hormones, proteins, lipids, nucleic acids and other natural products (e.g. cellulose, rubber). Macromolecules, however, describe all large, usual molecules with Mw ('relative' molecular weight/mass) of more than 10,000 [1], irrespective of their synthetic or natural origin.

The combined term biomacromolecules implies a limited group of only large biomolecules. Polymeric structures consisting of smaller units or monomers (e.g. proteins and nucleic acids) are part of this definition as well as non-polymeric lipids. Therefore, these molecules have different (not typically 'drug like') characteristics and are substantial more dependent on delivery technologies than smaller molecules.

Biomacromolecules as a powerful new class of active pharmaceutical ingredients (API) offer an improvement in drug efficiency and safety (low capability of unintended side-effects) resulting from an exquisite specificity and a highly selective mode of action. With this it is possible to intervene directly in disease pathways. Nevertheless the *in vivo* stability and the lack of cellular uptake (insufficient capability to reach intracellular targets: essential particularly for nucleic acids) are some restrictions which need to be considered [2-4]. Therefore new barrier-crossing formulations are required beside the development of new APIs.

In the range of proteins and peptides, many candidates e.g. insulin and monoclonal antibodies (Humalog[®], Humira[®]; proteins) or the gonadotropin-releasing hormone Leuporelin (Lupron[®]; peptide) just to mention some are already available on the market [5-8]. Currently, Humira[®] even ranks at the very top position of drugs with the highest sale numbers. This perspective a high target specificity and a low potential to

fail in late developmental stages are reasons why the pharmaceutical industry count on biomacromolecules.

Till now, the FDA (Food and Drug Administration) approved two antisense oligonucleotides (ASO) Fomivirsen (Vitravene[®]) against cytomegalovirus retinitis and Mipomersen (Kynamro[®]), used for treating homozygous familial hypercholesterolemia. These intravitreal or subcutaneous applied medicines from Ionis Pharmaceuticals, formerly known as ISIS Pharmaceuticals [9] were the first antisense therapeutics on the US-market; to date, the European Medicine Agency (EMA) however refused the approval of Mipomersen [10] due to relatively high dropout rates in the proband group.

Currently, approximate 30 therapeutics can be found in clinical trials which include two intravenously administered siRNA-based formulations from Alnylam Pharmaceuticals against Transthyretin-mediated amyloidosis [11]. Both are enrolled in phase III trials: Revusiran within the ENDEAVOUR study [12] and Patisiran within the study APOLLO [13]. First statements concerning the outcome can prospectively be expected in 2018 [14]. Notwithstanding rapid advances in research, no non-invasive antisense oligonucleotides are present on the market or in late-stage studies.

Biomacromolecules in general have a great potential which could be exploit much better if more suitable carriers for intracellular targeted delivery were available. Within the COMPACT project (see section 1.4) different delivery technologies were used to enable a transport of biomacromolecules through the epithelium. Within this thesis one side project of COMPACT will be presented and focuses on the pulmonary delivery of a delimited group of nucleic acids, in specific siRNA.

1.1.2 Gene suppression via RNA interference

Eukaryotic cells have sophisticated antisense mechanisms to regulate or suppress gene expression [15, 16]. One very important post-transcriptional [17, 18] pathway to inhibit the function of a target RNA is the mechanism of RNA interference (RNAi) [19], which was discovered in 1998 by Fire et al. [20]. Only a few years later in 2006, the Nobel Prize in Physiology or Medicine was awarded to Andrew Z. Fire and Craig C. Mello “for their discovery of RNA interference – gene silencing by double-stranded RNA” [21].

Before then studies demonstrated possible gene silencing caused by antisense [22] and remarkable sense [23] strands. These results were inconsistent so that interfering effects could not be explained by the simple pairing of antisense RNA to mRNA [24]. Within their work Fire et al. were able to observe an enhanced silencing effect of double-stranded RNA (dsRNA) in contrast to sole sense or antisense strands [20]. This new insight and further conclusions about the specificity of dsRNA to homologous mRNA and the loss of mRNA (degradation) put the pieces together and led to the explanation of the RNAi mechanism.

The RNA interference by mRNA cleavage or translational repressions is mediated by the same protein complex, called RISC (RNA-induced silencing complex). The crucial template for the interference, however, can be either siRNA or miRNA. SiRNA (small interfering RNA) is a short double-stranded RNA oligonucleotide with a prevalent length of 21-23 nucleotides (nt) [25] with a two nucleotide 3'-overhang on each strand and leads to mRNA cleavage. In contrast, miRNA (micro RNA) [26-28] is a single-stranded RNA oligonucleotide with a prevalent length of 19-25 nt [29] and leads to translational repression or mRNA cleavage. The crucial small non-coding oligonucleotides for RNAi pursue in general the same mechanism, but slightly differ in their emergence and binding to target mRNA (see Figure 1.1).

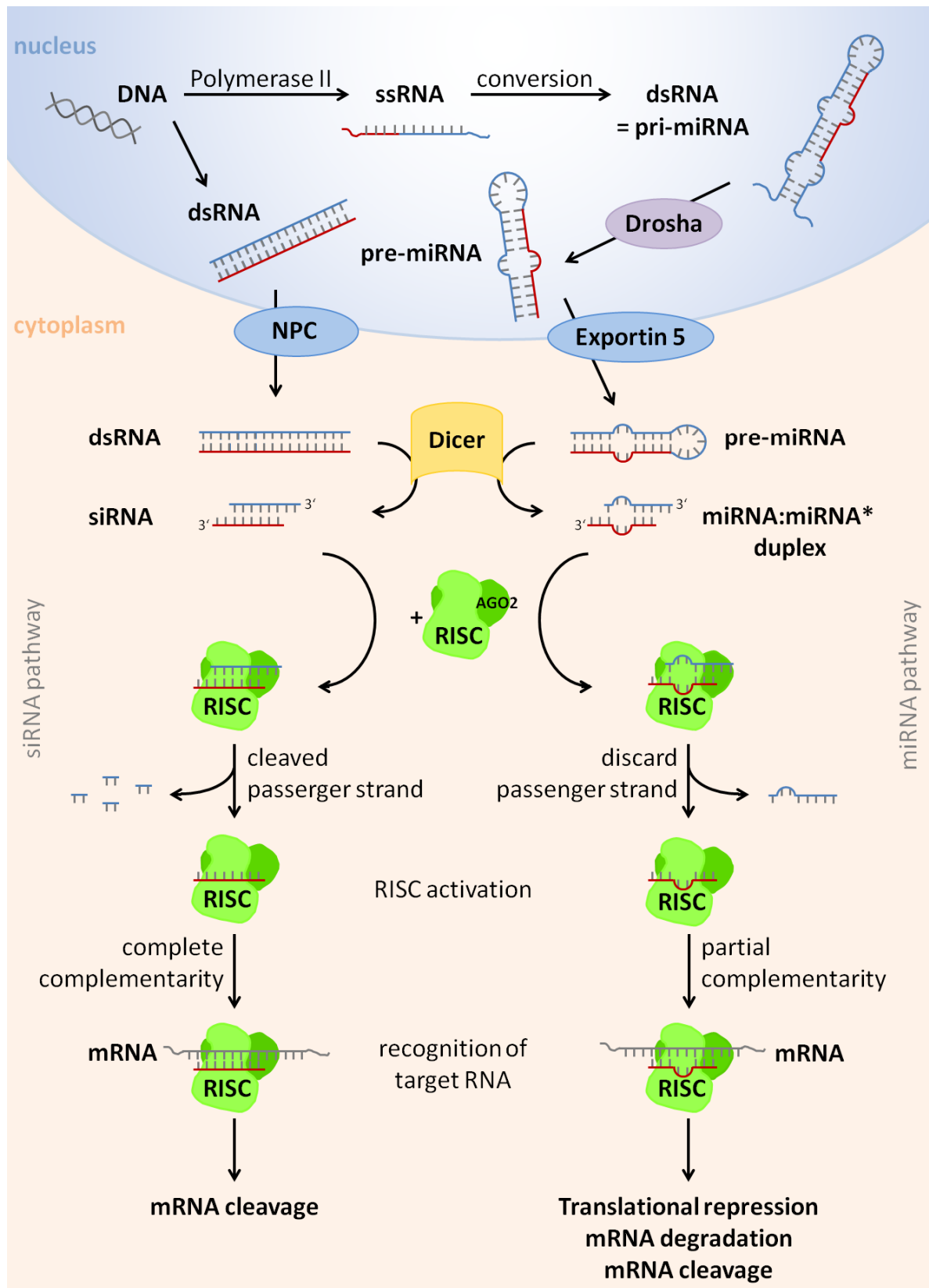


Figure 1.1: RNA interference by siRNA and miRNA and the different pathways. NPC: nuclear pore complex, AGO2: argonaute protein 2, RISC: RNA-induced silencing complex. This figure was compiled based on Lam 2015 [30], Ozcan 2015 [31] and Davidson 2011 [32].

siRNA pathway

In the nucleus siRNA can arise from an endogenous source naturally produced in the body or by viral genetic material. It is primarily known as a defense mechanism against viruses and genome transposons. Therefore, a degradation of target mRNA is essential. The transcription of both 'sense' and 'antisense' RNA from the same loci results in the assembly of long double stranded RNA (dsRNA). After the transport of dsRNA into the cytoplasm via the nuclear pore complex (NPC), the enzyme "Dicer", a RNase-III-like endoribonuclease [19, 33], starts with a subsequent cleavage of the RNA molecule. An exogenous source is the direct injection or transfection of synthetic siRNA [34]. The synthesis of short RNA molecules is an easy operation to create effective active ingredients. Once in the cytoplasm, the siRNA is creating an RNA-induced silencing complex (RISC). Within this multiprotein complex, the double strand will be unwound and separated (Helicase function) [16] so that only the antisense (or guide) strand is remaining. The sense (or passenger) strand will be degraded [29] whereas the antisense strand incorporated in the RISC complex binds completely complementary to one target mRNA. The Argonaut (AGO2) as the major catalytic part of the RISC complex causes cleavage of the mRNA (RNase H function). Thus, the translation of the mRNA into a protein is inhibited or the mRNA itself destroyed.

miRNA pathway

MiRNAs are products of dsRNAs encoded in genes of our genome and support the control of gene expression and cell functions (e.g. differentiation, development). DNA is transcribed (via polymerase II) into single-stranded RNA (ssRNA) and converted into dsRNA (pri-miRNA) [35] due to the sequence complementarity. First, the RNase-III-enzyme "Drosha" [36] cuts the pri-miRNA into smaller fragments (pre-miRNA) [37], then "Exportin 5" guides the pre-miRNA from the nucleus into the cytoplasm. There, the enzyme "Dicer" cuts off the stem-loop [38] and forms a miRNA:miRNA* duplex [39, 40]. After binding to RISC, the passenger strand is discarded, and the mature single-stranded miRNA (guide strand) within the RISC complex binds partially complementary to multiple mRNAs via short complementary

sections (“seed region”: 2-7 nt) [41, 42]. In this way the mRNA is degraded, cleaved (only by a high level of complementarity) or its translation is repressed.

Although siRNA and miRNA have different functions, their respective pathway appears very similar. Both use the same silencing complex (RISC) to receive a ssRNA template and to reach target mRNA. Based on the high similarity of siRNA and miRNA similar carrier systems can be used to deliver nucleic acids (see section 2.1). Sometimes in the context of gene silencing the terms short hairpin RNA [43] (shRNA), piwi-interacting RNA (piRNA) and repeat-associated small interfering RNA (rasiRNA) may be used. ShRNAs are foreign vector-based RNAs, serve as precursors [44, 45] and assimilate into the miRNA pathway [46]. PiRNAs are small non-coding RNAs (24-31 nt in length) interacting with P-element induced wimpy testis (PIWI) proteins and occur in germline cells [44, 47, 48]; rasiRNAs are merely a group of piRNAs [49, 50].

Therapeutic siRNA often looks like a degradation product (sometimes longer dsRNAs) of the enzyme ‘dicer’. This is the reason why siRNA only need to be delivered into the cytosol to be effective. Especially the targeted compartment needs to be considered when developing a specific delivery system. Otherwise highly effective drugs are not able to show their mode of action.

1.2 The lung as a target

1.2.1 Morphology and anatomy of the human lung

The lung is a part of the lower respiratory tract and the responsible organ for gas exchange. In humans (and mammals in general) two lungs are located in the thoracic cavity. The conductive section comprises the windpipe (*trachea*), which branches into two main bronchi and separates the right lung (*pulmo dexter*) with three lobes from the left lung (*pulmo sinister*) with two lobes. The respiratory section comprises the cartilaginous bronchi branching again into smaller bronchioles, finally ending into alveolar ducts with a terminal collection of alveoli. The alveoli consist of flattened epithelial cells and are surrounded by a mesh of capillaries to ensure the exchange of oxygen versus carbon dioxide (via diffusion). An adult pair of human lungs

contains approximately 700 million alveoli. With a diameter of $\sim 200 \mu\text{m}$ the total respiratory surface area estimates about 90 m^2 [51]. Therefore, the pulmonary route represents an interesting target structure for the deposition of drugs in current research activities.

The gross anatomy of the lung differs from the bronchial to the alveolar level as well as the microscopic anatomy of these regions (see Figure 1.2, adapted from Klein 2011 and modified from Ochs/Weibel 2008).

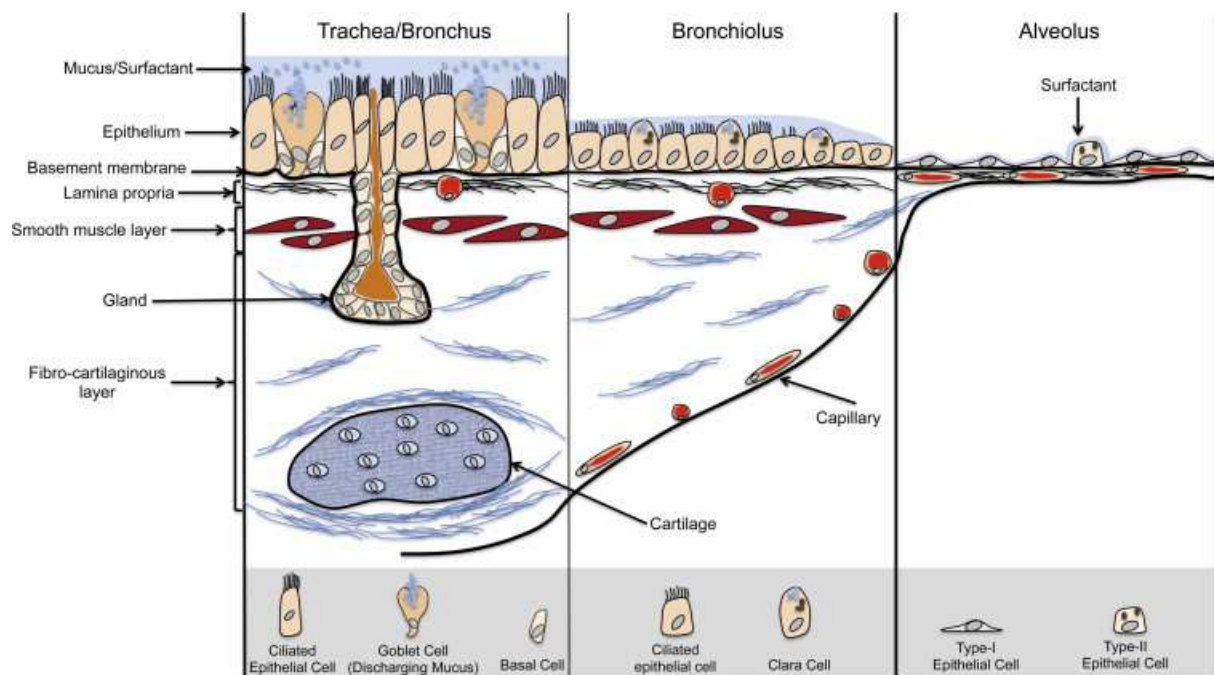


Figure 1.2: Scheme of the respiratory wall, divided in three main parts: mucus-producing bronchus, bronchioles and surfactant-producing alveolus. Adapted from Klein 2011 and modified from Ochs and Weibel 2008.

The upper rigid part, trachea and bronchus, consists of a thick fibro-cartilaginous layer with many embedded glands, a smooth muscle cell layer and the *lamina propria* (connective fibro-elastic tissue and blood vessels). The epithelium implies ciliated pseudostratified epithelial cells, mucus-producing goblet cells and basal cells [52]. The intermediate bronchioles contain no longer cartilage cells and glands but more blood vessels and capillaries. The epithelium has still ciliated but cuboidal epithelial cells and secretory dome-shaped Clara cells (also known as club cells or bronchiolar exocrine cells) [53]. The terminal alveolus mainly consists of a mono-layer-mosaic of flat ($\sim 0.2 - 0.3 \mu\text{m}$ thick) structure-lending Alveolar Type-I (AT I) epithelial cells that

cover roughly 90% of the total alveolar surface [54] surrounded by numerous capillaries embedded in elastic and collagenous fibers without any muscle cells. The remaining part occupy granular Alveolar Type-II (AT II) epithelia cells [55] which secrete surfactant to avoid collapsed alveoli by the reduction of surface tension [56, 57]. Especially the presence of a mono-cell-layer in the deep lung makes a topic treatment of appropriate lung diseases feasible.

1.2.2 Pulmonary diseases and current medical applications

Following the *World Health Organization* and the *European Centre for Disease Prevention and Control*, many diseases may affect the human lung. Asthma, chronic obstructive pulmonary disease (COPD), pneumonia and lung cancer are just some of the most common ones. The *European Respiratory Society* published the *European Lung White Book* with the latest data about respiratory deaths in European countries [58] (see Figure 1.3).

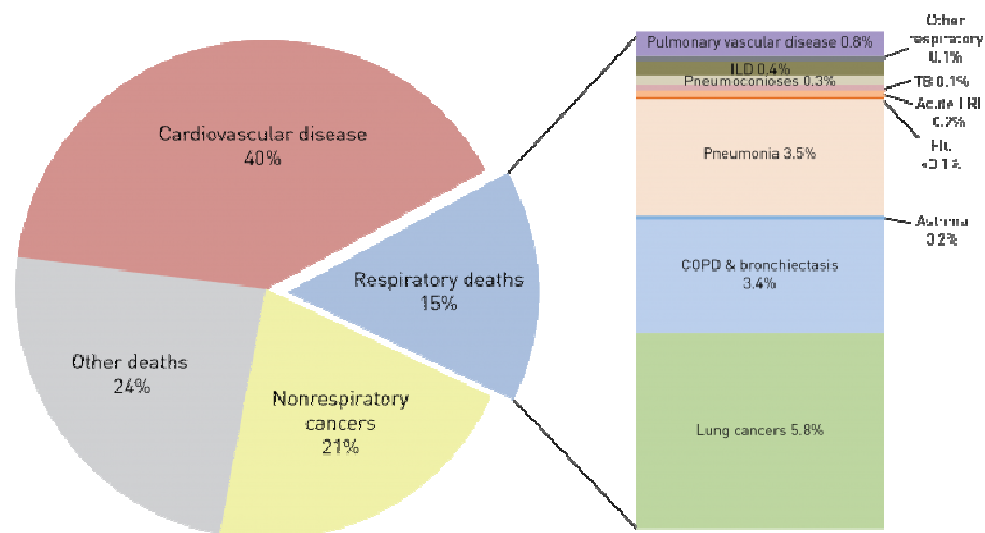


Figure 1.3 Deaths caused by respiratory conditions in selected European Union countries* (in percent). ILD: interstitial lung disease; TB: tuberculosis; LRI: lower respiratory infections; COPD: chronic obstructive pulmonary disease from World Health Organization World and Europe Detailed Mortality Databases. Adopted from webpage: <http://www.erswhitebook.org/chapters/the-burden-of-lung-disease/>; 25.04.2016.

*countries with available full ICD-10 coding diagnoses for both hospital admissions and deaths

The major proportion of lethal pulmonary diseases can be reduced to lung cancers, pneumonia, COPD, and bronchiectasis. Therefore a curative therapy of these maladies is particularly relevant.

To treat respiratory disorders in general, it is possible to hit the lung via the systemic (“blood-to-lung”) or topical (“air-to-lung”) route. A systemic application of several drugs e.g. chemotherapeutics was established, but due to relatively high required doses (caused by high protein binding or interactions with Cytochrome-P-450) adverse effects like tissue necrosis, hematological toxicity or cytostatic induced vomiting may endanger the success of a cancer therapy. A standard [59] topical therapy for the symptomatic treatment of Asthma [60] and COPD [59, 61] are bronchodilators (e.g. Formoterol, Tiotropium bromide) and corticosteroids (Budesonide).

It is obvious that a great need for inhalable drugs is present. Biopharmaceuticals and siRNA may reach new (not available with small molecule drugs) target proteins and enable an easier personalized medicine (e.g. in tumor therapy). First studies with naked siRNA showed an insufficient potency. Therefore, possibilities to maintain the stability of a therapeutic agent and to assure a controlled drug release were explored. Here, the scientific focus is especially set on nanotechnology and nanoparticle-based carrier systems.

1.3 Nanoparticles as a system to overcome biological barriers

1.3.1 Nanoparticles or nanopharmaceuticals - what makes the difference?

Nowadays nanotechnology, the production technology of nanoparticles (NP) [62], constitutes in many disciplines from e.g. electronics [63, 64] to life science applications [65-68]. Here, the effect of modified properties of nano-materials can be turned into a benefit. When talking about nanoparticles, the definition seems to be obvious: Nanoparticles are particles (spheres, tubes, fibers or miscellaneous) in the nano-scale from 1 nm to 1,000 nm. This size range is universally accepted, but

depending on the field of action or the type of material the described size range may differ and comprises particles smaller 1 nm or even larger than 1,000 nm [69]. Particularly because the term nanoparticle describes so many different types of particles including non-engineered particles (pollutants as side-products of incomplete combustion, pathogens, and other airborne particles) it makes sense to carry out a classification referred to its application area or occurrence.

With the beginning of the National Nanotechnology Initiative (NNI) in 2000, the terminology in the medical field with the focus on health-sciences changed. “Nano” replaced “colloidal” [70] and terms like nanopharmaceuticals, nanomedicines, nanodrugs or nano-formulations were utilized more and more frequent. Here, nanopharmaceuticals can be described as nanoparticles for therapeutic [71-73] as well as diagnostic [74-76] purposes and automatically imply a thorough selection of suitable materials manufacturing and characterization methods to ensure an adequate drug safety. But that does not necessarily mean the absence of nanopharmaceuticals till then. In 1995 the FDA approved Doxil[®], a liposomal doxorubicin hydrochloride formulation and thus the first nano-drug [77]. Further approved nanopharmaceuticals were reviewed by Weissig et al. There, they classified nanopharmaceutical drugs due to their structure and material: liposomes (Doxil[®], AmBisome[®]), non-liposomal lipid-based formulations (Abelcet[®]), PEGylated compounds (Pegasys[®]), nanocrystals (Emend[®], Rapamune[®]), polymer-based formulations (Copaxone[®]), protein-drug conjugates (Abraxane[®]), surfactant-based (Strasorb[™]) and metal-based (Feridex[®]) formulations as well as virosomes (Gendicine[®], approval only in China) [70]. Based on various existing nano-formulations the development of novel and innovative formulations will continue, and future results will follow [78].

1.3.2 Interactions with cellular and non-cellular barriers inside the lungs

Pulmonary barriers are intended to protect the human body against external influences. They do not differentiate between pathogens, pollutants or even nanopharmaceuticals and consist of cellular (e.g. epithelial cells) and non-cellular

(lining fluid) components [79]. The anatomy and physiology of the pulmonary mucosa of the central airways (trachea/bronchus and bronchioles) differs from the peripheral region (= alveolus region or deep lung) (see Chapter 1.2.1.). Therefore, inhaled particles need to be analyzed to predict their flying characteristics and their deposition at the targeted tissue. To estimate what happens after landing and what mechanisms can thwart an efficient delivery of nanopharmaceuticals some aspects of particle interactions need to be considered (see Figure 1.4). In the conducting airways (central lung), inhaled particles are mainly eliminated by the mucociliary clearance [80]. This process describes the entrapment of particles in mucus and the movement in cranial direction accomplished by ciliated epithelial cells. In humans, the velocity of this expulsion ranges individually between 3-25 mm/min [81, 82] which reveals a residence time of about 6 hours [83]. Within that period therapeutic particles need to penetrate the mucus to reach the epithelial cells underneath. Depending on the composition of the mucus (amount of water, mucins, proteins, lipids...) it consists of a viscous upper gel layer and a lower aqueous sol-like layer [52]. Both together create a complex and heterogeneous mesh with various pore sizes from 100 nm up to some micrometers [84] to hinder particulates from entering.

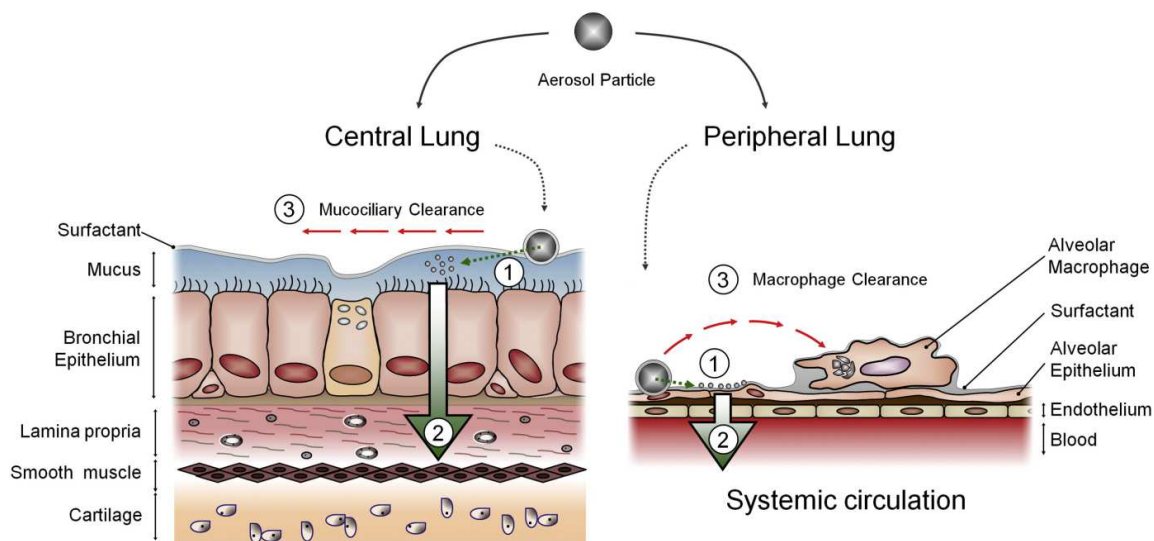


Figure 1.4 Particle-lung interactions with cellular and non-cellular barriers, adopted from de Souza Carvalho 2014 [91], modified from Ruge 2013 [79]. 1: deposition on lining fluids 2: delivery of drugs, DDS or particles to/through underlying cells 3: clearance mechanisms.

Regarding the alveolar section, the macrophage clearance removes most of the inhaled particles. More than 50 % of them are eliminated after 2-3 hours and nearly 100 % after 24 hours [85]. Beside AT I and AT II cells joint by tight junctions to impede paracellular transport [86, 87] (which is relevant to reach underlying tissue or the bloodstream) alveolar macrophages are present in alveolar spaces of the deep lung. Triggered by hydrophilic proteins in the surfactant [88, 89] macrophages preferably catch and degrade particles in size range of 1-5 μm [90]. If not eliminated by the clearance mechanisms APIs or formulations have the chance to reach the next barrier, the cell membrane of underlying cells. At this point particulate properties like molecular weight, size, charge, lipophilicity, solubility, etc. are decisive criteria for further transport.

Naked siRNA as an example should get into the alveolar cytoplasm. However, due to a relatively high molecular weight, large size, hydrophilicity and a negative charge (from the phosphate groups of the backbone) the API is not able to easily pass anionic cell membranes [92, 93]. To overcome this barrier, cationic siRNA-formulations can be designed to enter the cell by endocytosis [94]. (Particles with a size around 100 nm may pass the alveolar epithelium [95] whereas bigger ones are internalized by endocytic pathways [96].) Contingent on the API and the reason for limited uptake and transport a suitable DDS is necessary.

Considering these barriers and particle-lung interactions in developing novel DDS it is also important not to ignore differing properties of the biological barriers depending on the affecting disease and the pathological conditions of the lung [97].

1.3.3 A combined system of siRNA and nanoparticles as a new approach for pulmonary treatment

Although the general concept of siRNA-based therapeutics remains as a promising approach in medical research the development of siRNA-based formulations must not be neglected. As almost all of the approved and in clinical trials situated antisense oligonucleotides need to be applied via injection - to ensure a locally easy access or to target systemically cancer cells [98] - a lack of non-invasive medicines in

antisense therapy (e.g. inhalable drugs against alveolar epithelia affecting disorders) is apparent.

Within this work, the focus is basically on the development and evaluation of new nanoparticulate systems for the intracellular delivery of siRNA. To ensure a successful pulmonary application the implemented materials need to be from the outset biocompatible, biodegradable, non-toxic and non-immunogenic - the DDS itself needs to be intact stable and reproducible. The approach to create nanoparticles to load its surface with siRNA has some clear benefits: Two independent preparation steps to create the carrier first and load the cargo on this system afterwards in a second step allow a direct correlation in characterizing and analyzing the same manufactured batch of the system in a loaded and unloaded version. Furthermore, a post-loading has the chance to save limited amounts of siRNA and to enable quality control within the formulation process. With the view on later industrial perspectives, this systematic to create a DDS holds the opportunity to obtain a stable and reproducible (especially important for carriers for high potent molecules) and a flexible preparation technique. Here, a later scale-up should be possible, to have the capacity when higher amounts are needed and the production converts from laboratory scale over pilot scale to production scale.

Next to polymer-based nanoparticulate systems for the pulmonary delivery of siRNA research activities focus on diverse possible carrier systems. Some also use PLGA [101] or chitosan [102-104] to create NPs. Others use for instance lipids to create nanostructured lipid carriers [105] or create self-assembled micelles [106] and cyclodextrin-siRNA nanoplexes [107] to deliver siRNA. Within COMPACT, project partners worked inter alia on surface functionalized lipid polymer hybrid NPs (University of Copenhagen, P3) and DARPin-siRNA conjugates or DARPin-siRNA perfect conjugates (University of Vienna, P8).

1.4 Aim of this research study

Nucleic acid based biopharmaceuticals represent an emergent group in drug development. Their therapeutic efficacy however, is restricted due to their limited cellular uptake and poor *in-vivo* stability. Applying non-viral vectors different

formulation strategies (e.g. polymeric NPs as a carrier system) may address these restrictions.

This doctoral thesis was part of the collaborative research project COMPACT (Collaboration on the Optimization of Macromolecular Pharmaceutical Access to Cellular Targets) which was initiated by an association of scientific experts in pharmaceutical industry and academia supported by the innovative medicine initiative (IMI), a partnership between the European Commission and the European Federation of Pharmaceutical Industries and Associations (EFPIA) [99]. To progress with a preferably high effectiveness project partners were divided into several preconceived work packages (WP) with the focus on the investigation of various applications and delivery routes. The development and characterization of drug delivery systems (DDS) for proteins or peptides (WP1) and nucleic acids (WP2) for different application sites (oral delivery (WP4), brain delivery (WP5), pulmonary delivery (WP6), (trans)dermal delivery (WP7)) and *in vitro* / *in vivo* testing (preclinical validation and identification of transport pathways; WP3) of diverse formulations comprised the major goals of the consortium. The framework conditions of this research work to develop a drug delivery system for the pulmonary delivery of siRNA (WP 2 and 6) needed to be observed by putting emphasis on testing the intracellular delivery first. Chitosan coated PLGA NPs as a well-established non-toxic polymeric DDS for the delivery of antisense oligonucleotides, 2'-*O*-methyl-RNA, functioned as a starting point for this study (see prior work by Nafee et al. [100]).

Within this context, 4 major aims of this thesis were identified:

1 to enhance system robustness by optimizing the particle preparation process

Determining process parameters of the emulsion-diffusion-evaporation technique were identified and optimized to ensure reproducibility, scalability and shelf life of the particulate system (chapter 2 - 4).

2 to evaluate the impact of applied cationic polymer on particle characteristics and stability

Three biodegradable and biocompatible cationic polymers with promising transfection properties were found to investigate the binding and release behavior by an exchange of the respective coating material. In this connection, different material

properties (e.g. size, surface charge) were investigated to define diverse particle characteristics (chapter 3).

As the deposition of sole NPs in the deep lung is limited, NP suspensions need to be aerosolized. Hence, a particulate system for pulmonary application should be retained stable after nebulization by using diverse devices (chapter 4).

3 to perform suitability testing for siRNA delivery

Functional *in-vitro* transfection studies build a scientific basis for later *in-vivo* tests. Here, a method to visualize a knock-down on different pulmonary alveolar cells by transfected siRNA needed to be invented due to the unavailability of stably transfected cell lines (chapter 6)

4 to assess the safety of the DDS in cell-viability and immunogenicity studies

To investigate a possible harmful potential of the DDS cytotoxicity and immunogenicity assays were performed (chapter 5).

Chapter 2 - Optimization of the preparation technique on the basis of chitosan-coated PLGA nanoparticles (1st generation)

The author of this thesis made the following contribution to this chapter:

Planned and performed all experiments related to particle preparation and characterization, analyzed all the data from the mentioned studies, interpreted all experimental data and wrote the chapter, it not stated otherwise.

2.1 Introduction

As the access of naked nuclease-sensitive siRNA through the cell membrane into the cytoplasm is restricted nanocarriers may act as promising delivery systems for genes [108]. A commonly used and well investigated material for nanoparticle preparation is PLGA (Figure 2.1), a clinical approved biocompatible and biodegradable copolymer of glycolic and lactic acid (associated as polyester). Through the presence of methyl groups on the one hand and free carbonyl groups on the other PLGA nanoparticles show hydrophobic properties and a negative surface charge.

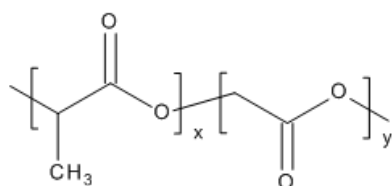


Figure 2.1 Chemical structure of Poly(D,L-lactide-co-glycolide) polymer

Thus, hydrophobic and/or cationic drugs can easily be encapsulated into PLGA nanoparticles with the help of the emulsion-evaporation technique, a standard NPs preparation procedure. Although it has been shown that PLGA nanoparticles can function as delivery systems for hydrophilic and negatively charged drugs like siRNA [109] as well, the utilization of a cationic polymer (e.g. polyethyleneimine, chitosan [110]) as a complexing agent is still required. Here, the double-emulsion technique [111] needs to be applied to encapsulate sufficient amounts of nucleotides since otherwise electrostatic and hydrophilic-hydrophobic repulsion effects prevent any encapsulation. However, this preparation technique leads to relatively large particles with a broader size distribution and a minor cargo stability [112] due to contact of DNA or siRNA with organic solvents, which are necessary to solve the PLGA polymer. Kumar et al. already saw the demand for a novel approach and designed nanocomposite particles. To enable a surface loading after NP preparation: PLGA-based NPs with an outer cationic coating, PVOH, and chitosan (Figure 2.2) blends [113] were used.

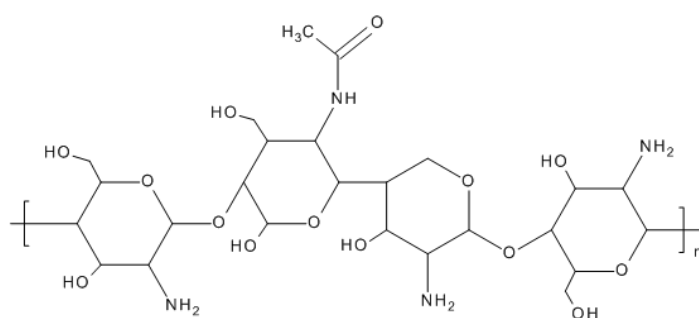


Figure 2.2 Chemical structure of Chitosan polymer

This manufacturing process represents an easy and robust way to prepare PLGA-based NPs with the ability to load hydrophilic negative charged drugs by keeping the advantage of a small size distribution and though a better cellular uptake [114] (see chapter 7). Possible concerns about DNA or siRNA stability can be neglected since surface loaded nucleotides stay protected against degradation through condensation (especially of DNA) [115] or steric hindrance [116, 117].

Since particle size and surface charge represent determining colloidal characteristics of nanoparticles for cellular uptake, trafficking [100, 118] and transfection efficiency [114] Nafee et al. analyzed the effect of different formulation parameters and their impact on particle properties [100]. Within this chapter the foregone work regarding critical formulation parameters will be verified and single steps will be adopted and optimized to gain a standard preparation method to create suitable NPs with a mean size smaller 200 nm, a narrow size distribution ($PdI < 0.2$) and a strong positive surface charge (zeta-potential) to transfect human lung epithelial cells.

*Beside of the COMPACT project Chitosan-coated PLGA NPs (PLGA-Cs NPs) were sent to Dr. Carolin Daniel¹ (Institute for Diabetes Research, München) and Dr. Benno Weigmann² (Department of Medicine, University of Erlangen-Nuremberg). Here, these nanoparticles were used for miRNA mimic applications to investigate “miRNA92a targets KLF2 and the phosphatase PTEN signaling to promote human T follicular helper precursors and T1D islet autoimmunity” [119]. With the help of confocal microscopy, it could be shown, that FA-PLGA-Cs NPs can successfully deliver miRIDIAN miRNA mimic transfection control (Dy 547) into human naïve CD₄⁺T cells (mature T helper cells expressing surface protein CD₄). A research paper

has been published in PNAS (Proceedings of the National Academy of Sciences). Up to now, a second manuscript is still in progress.

¹ Institute for Diabetes Research, Independent Young Investigator Group Immune Tolerance in Type 1 Diabetes, Helmholtz Diabetes Centre at Helmholtz Zentrum München; German Centre for Diabetes Research (DZD)

² Department of Medicine 1, University of Erlangen-Nuremberg, Kussmaul Campus for Medical Research

2.2 NPs preparation

2.2.1 Materials

Poly(D,L-lactide-co-glycolide) (PLGA, CAS No: 26780-50-7)

Resomer[®] RG 752 H from Evonik Industries is a free carboxylic acid terminated biodegradable synthetic and amorphous copolymer (lactide:glycolide 75:25) with a M_w 4,000 – 15,000. Degraded and metabolized in the human body (through the citric acid cycle) into non-toxic amounts of lactide and glycolide [120].

Polyvinyl alcohol (PVOH, CAS No: 9002-89-5)

Moviol[®] 4-88 from Kuraray (new grade name Kuraray Poval[™] 4-88), is a partially saponified (grade of hydrolysis 86.7 – 88.7 mol%) synthetic, biodegradable and water soluble (10.0-11.6 residual content of acetyl) polymer with a M_w ~ 31,000 and a high standard purity. Within the scope of nanoparticle formation, PVOH is commonly used as an emulsifier/surfactant for stabilization of the emulsion in emulsion-solvent evaporation technique to form small and uniform particles.

Chitosan (Cs, CAS No: 9012-76-4)

Protasan[®] UP CL 113 from Novamatrix (Sandvika, Norway) is an ultrapure (low level of endotoxin and proteins) biopolymer (water-soluble chitosan chloride) in accordance with GMP guidelines; ICH Q7; and ISO standards: ISO 9001:2008, ISO 13485:2003 and ISO 22442:2007. 75 - 90 % of the acetyl groups are removed. The degree of deacetylation (batch no. BP-0806-01: 83 %) was verified by an

acid-base-titration according to Yuan et al. [121] with a value within the range of 76.8 ± 1.0 %. Mw 50,000-150,000 g/mol (measured as Chitosan acetate).

Fluorescein amine isomer I (FA, CAS No: 3326-34-9) or 5-Aminofluorescein = 6-Amino-3',6'-dihydroxyspiro[2-benofuran-3',9'-xanthene]-1-one; used to label covalently PLGA polymer (see chapter 2.2.3 for FA-PLGA synthesis) and Dil 1,1'-Dioctadecyl-3,3,3',3'-tetramethylindocarbocyanine perchlorate 97 % (CAS No: 41085-99-8) was purchased from Sigma-Aldrich, Germany.

All other used solvents, chemicals and materials are designated in the related sections.

2.2.2 PLGA-Chitosan NPs

Poly (D,L-lactide-co-glycolide (PLGA) based nanoparticles coated with a cationic polymer were prepared via the emulsion-diffusion-evaporation technique [100, 113]. 15 - 25 mg (0.3 – 0.5 % (w/v)) of chitosan was solved in 5 mL of an aqueous 2.5 % (w/v) polyvinyl alcohol (PVOH) solution. The organic phase consisting of 100 mg PLGA in 5 mL ethyl acetate (EtOAc, CAS No: 141-78-6, Chomasolv[®] for HPLC 99.8 % from Sigma-Aldrich, Germany) was added dropwise to the stirring (on magnetic stirrer VRW VMS-D from VWR at 900 rpm) aqueous solution to create a primary emulsion. After homogenizing with a high-performance dispersing instrument (stand dispersion unit: Polytron[®] PT 2500E; dispersing aggregate: Polytron[®] PT-DA 20+/2+ EC-E 192 from Kinematica, Eschbach, Germany) at 15,000 to 17,000 rpm for 5 – 10 min. ultrapure (type I) purified water (Millipore Milli-Q[®] Integral water purification System, sourced from a Q-POD[®] unit with a BioPak[®] filter from Merck, Germany) was added to a final volume of 50 mL to let the ethyl acetate evaporate overnight (Figure 2.3). The dropwise addition of the organic phase into the aqueous phase was implemented in a manual, semi-automatic and automatic manner. For the manual dropping method Pasteur pipettes (145 mm or 225 mm) soda-lime-glass ISO 7712 (Brand GmbH & Co. KG, Germany), for the semi-automatic method a peristaltic pump (Minipuls[®] 2 from Gilson, Middleton, USA) with N needle (from Hamilton \varnothing 0,26 mm; \varnothing 0,41 mm; \varnothing 0,13 mm) and for the automatic method a syringe pump (Harvard

Apparatus PHD ultra) with a glass syringe 5 mL 1005 TLL (from Hamilton) with N needle (from Hamilton \varnothing 0,26 mm; \varnothing 0,41 mm; \varnothing 0,13 mm) was used.

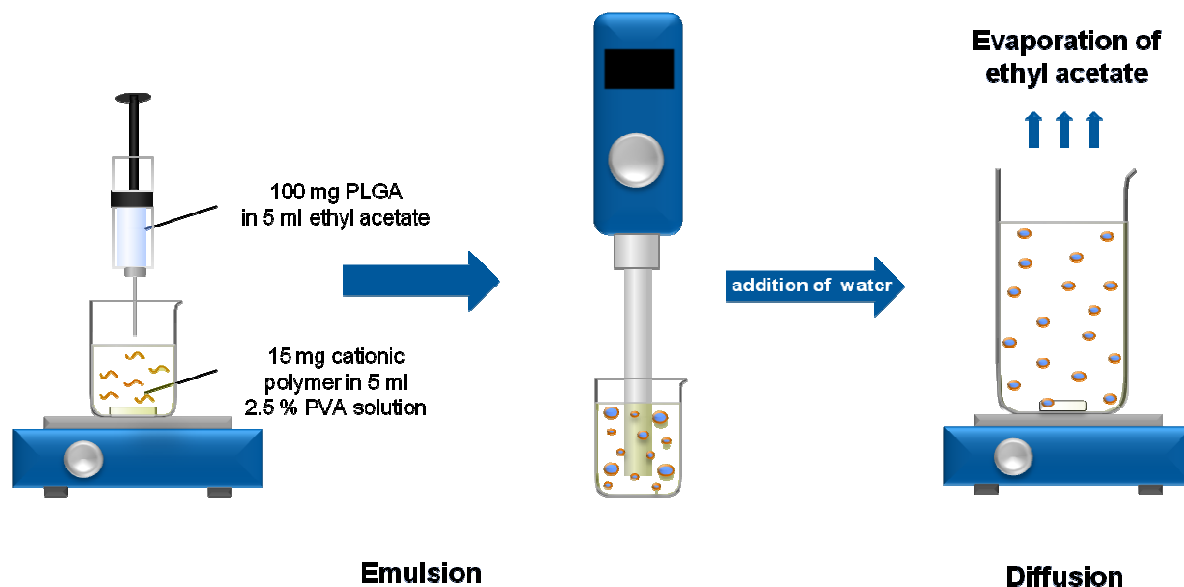


Figure 2.3 Emulsion-Evaporation-Preparation-Technique of PLGA NPs with a cationic coating.

2.2.3 Flu-labeled NPs

Fluorescent nanoparticles have a great significance for carrier visualization and localization (see chapter 7). A most widely used fluorescent dye is fluorescein, first synthesized in 1871 from Adolf von Baeyer. Its absorption (excitation) and emission spectra have their maximum peaks ($= \lambda_{\max}$) at 489 and 519 nm and show a green color. Meanwhile many fluorescein derivatives like fluorescein amine (FA) are available.

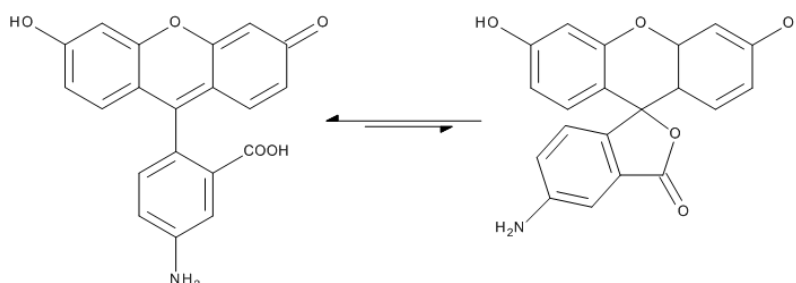


Figure 2.4 The Structure of fluoresceine and fluorescein amine is present in two different conformations; left: stable open carbolic acid form (red, in solid state) and right: a more instable spiro form (yellow) of fluorescein amine.

One advantage of this component is that the primary amine group from fluorescein amine (FA) can easily be coupled with the carboxylic acid of the PLGA polymer [122, 123].

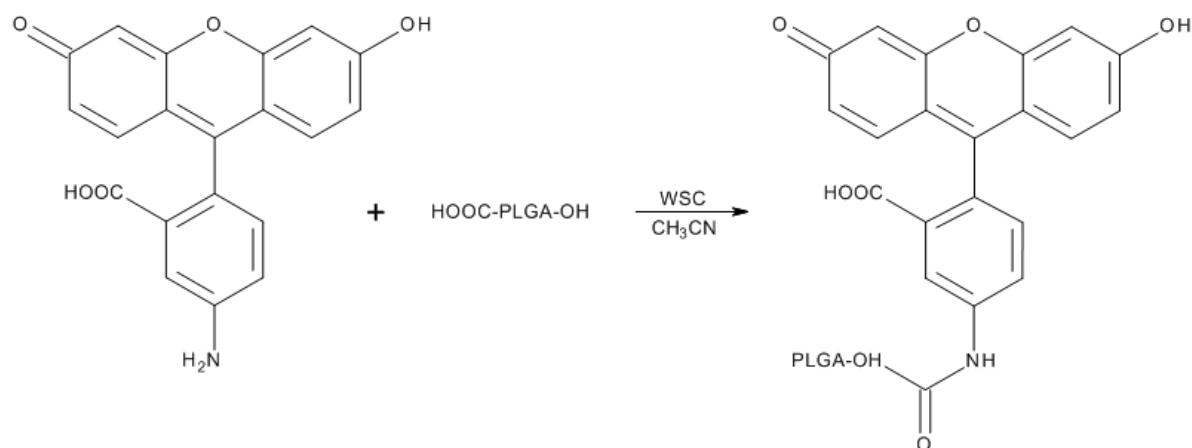


Figure 2.5 Schematic coupling reaction of fluorescein amine and PLGA to create fluorescent FA-PLGA.

For this purpose 3.07 g PLGA and 0.0583 g Fluorescein amine isomer I or 5-Aminofluorescein (= 6-Amino-3',6'-dihydroxyspiro[2-benofuran-3',9'-xanthene]-1-one) were solved in 30 mL acetonitrile. After the addition of 0.0408 g 1-ethyl-3-(3-Dimethylaminopropyl)-carbodiimide Hydrochloride (WSC), the solution remained stirred overnight (up to 24 h) under the exclusion of light to activate the carboxylic groups. To precipitate FA-PLGA Milli-Q purified water was added and the aqueous supernatant was discarded after centrifugation (6 min, 6,000 x g, Hettich Rotina 420R). The generated pellet was solved in acetone (CAS No: 67-64-1, Chomasolv[®] for HPLC 99.8 % from Sigma-Aldrich, Germany) and subsequently washed with ethanol (EtOH, CAS No: 64-17-5, absolute from Sigma-Aldrich) until all FA-PLGA was precipitated. The liquid phase was discarded, and the FA-PLGA pellet was dried via lyophilization (Alpha 2-4, Martin Christ GmbH, Osterode, Germany). The resulting FA-PLGA was crushed into a fine powder (Figure 2.6) and stored under exclusion of light at 4 °C or directly used for the preparation of NPs.



Figure 2.6 PLGA (left, white) and FA-PLGA (right, yellow-green) after lyophilization as dry powder

To create green fluorescent NPs the same amount of FA-PLGA as PLGA (= 20 mg/mL) for non-labeled NPs was used. All further preparation steps had to be performed analog to non-labeled NPs but under strict exclusion of light to avoid chemical destruction of the fluorochrome (= photobleaching) [124].

Next to the relatively high proneness of fluorescein to get impaired by photobleaching effects [125] this fluorescent dye shows a relatively broad emission spectrum which may cause limitations in some multicolor applications (absorption overlaps with 488 nm spectral line of the argon laser). In the course of confocal spectroscopy a second fluorescent dye to visualize the carrier system benefits when green fluorescent dyes are used to stain specific cell compartments. The existing filters are not able to differentiate between these two signals, cell and particle signal. An alternatively suitable red fluorescent dye is Dil (= 1,1'-Di-octadecyl-3,3',3',3'-tetramethylindocarbocyanine perchlorate (Figure 11) from Sigma-Aldrich, Germany) with a λ_{max} of 549 nm (absorption) and 565 nm (emission). The absorption and emission spectra of fluorescein and Dil are confronted via Fluorescence SpectralViewer from Thermo Scientific in Figure 2.8.

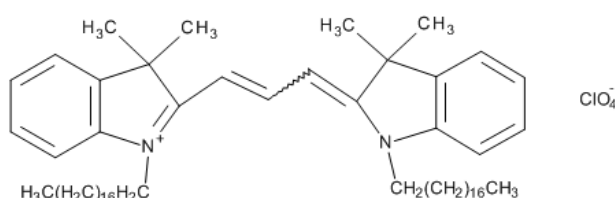


Figure 2.7 Chemical structure of Dil (1,1'-Di-octadecyl-3,3',3',3'-tetramethylindocarbocyanine perchlorate)

Although it cannot be (easily) coupled covalently with PLGA, it is possible to disperse the dye into a PLGA-ethyl acetate solution without a significant migration into any surrounding media [126]. Therefore, a Dil solution (Dil solved in ethyl acetate) was added to the solved PLGA solution to create a mixture with a final concentration of 20 mg/mL PLGA and 2 μ M Dil. The following preparation steps were performed analogously to the prior described emulsion-evaporation-technique. Nonetheless, FA-labeled PLGA particles remain first and foremost as the preferred type of fluorescently labeled particle.

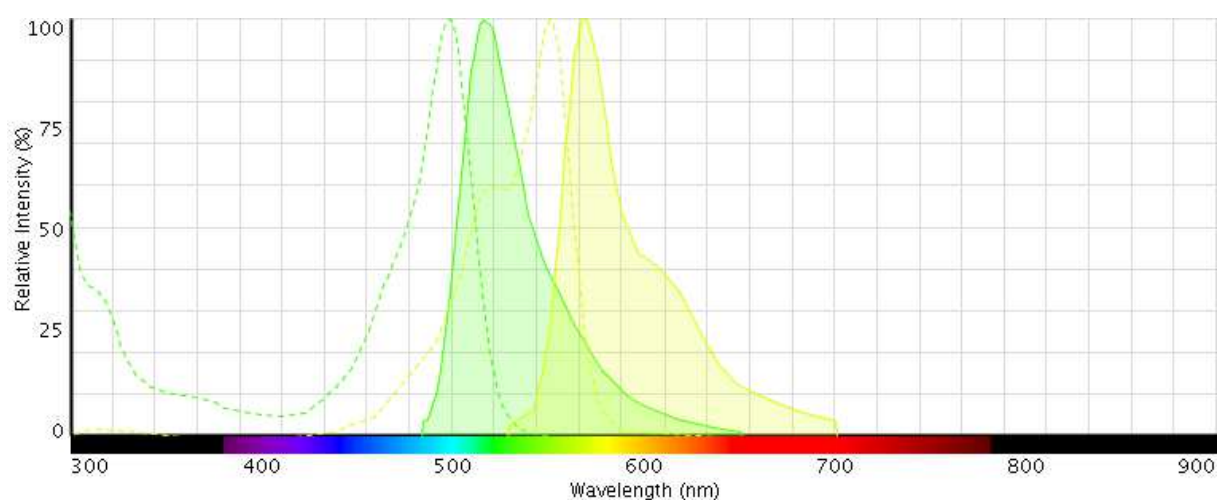


Figure 2.8 Comparison of the absorption (solid line) and emission (dashed line) spectra of fluorescein (green) and Dil (yellow). Visualized by Fluorescence SpectralViewer (Thermo Scientific).

2.3 NPs characterization

2.3.1 Colloidal characteristics

Photon correlation spectroscopy (PCS) was applied to measure particle size. Zetasizer Nano Series ZS (Malvern Instruments Inc., UK) was used with the following settings: Material: PLGA, RI: 5.500, Absorption: 0.010, dispersant: water, viscosity: 0.8872 CP, RI: 1.330, temperature: 25 °C, equilibration time: 120 sec, cell type: DTS 0012 disposable sizing cuvette, measurement/scattering angle: 173°, backscatter (NIBS default). Dilution: 1:10 diluted with Milli-Q water. For analysis, the method of cumulants was applied according to ISO13321 (1996) and ISO22412 (2008). Surface charge derives from the ζ -potential, measuring the electrophoretic

mobility with Zetasizer Nano Series ZS (Malvern Instruments Inc., UK). The ζ -potential is a pH-dependent value: hence the measurement was implemented in a 1:10 dilution of Milli-Q water in a standardized quality and a resulting pH value of the nanoparticle suspension of pH 5.

Ionic strength and pH are critical parameters for colloidal stability. Thus, nanoparticle stability was assessed in a set of standard buffers and cell culture media. Results were compared to the measurement in only purified water as dispersant. Exemplary Phosphate buffered saline (PBS) and a Krebs-Ringer Buffer (KRB) in a gradually pH range from 3.0 – 12.0 and Milli-Q at pH 3.5, 6.2 and 10.6 were compared respectively. PBS Buffer (137 mM NaCl, 2.7 mM KCl, 10 mM Na₂HPO₄, 2 mM KH₂PO₄) and Krebs-Ringer Buffer (142 mM NaCl, 3 mM KCl, 1.5 mM K₂HPO₄, 10 mM HEPES, 4 mM D-glucose, 1.4 mM CaCl₂, 2.5 mM MgCl₂) were adjusted to the required pH with 1 M NaOH or 1 M HCl.

All experiments were performed in triplicates.

NPs preparation in physiological buffer

2.3.2 Purification techniques

The purification of the DDS is an essential step to remove the excess of PVOH, which might influence further investigations or disturb different imaging techniques e.g. scanning electron microscopy (SEM; see Chapter 2.3.4). In Figure 2.9 the image of the NP morphology is interfered by the vast amount of PVOH.

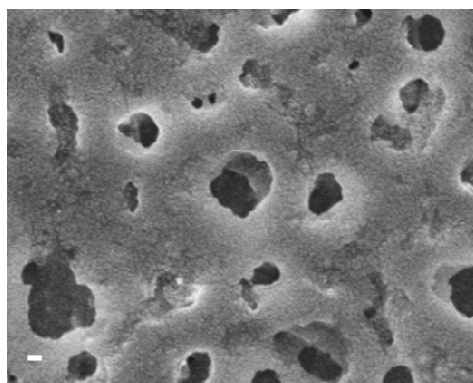


Figure 2.9 SEM-micrograph of non-purified PLGA-Cs NPs. Scale bar = 200 nm.

Various techniques are suitable to remove PVOH from the NP fraction. The most obvious way is to centrifuge the nanoparticle suspension (Hettich Rotina 420R centrifuge at 24400 x g for 10 min.), decant the supernatant, re-disperse with Milli-Q water and repeat this procedure at least three times (method A).

Centrisart[®] and Vivaspin[®] (both from Sartorius Stedim Biotech GmbH, Germany) are centrifugal ultrafiltration units with a cellulose triacetate (CTA) or polyether sulfone (PES) membrane. The material differs depending on the required molecular weight cut-off (MWCO). As Centrisart[®] I can be used only for small volumes (2.5 mL – 500 µL) the Vivaspin[®] 20 device, which can handle volumes up to 20 mL was used. As PVOH is a relatively long filamentary molecule, a Vivaspin[®] 20 unit with a 300,000 Da PES filter was utilized. The NPs were centrifuged at 6,000 x g for 15 min. (Hettich Rotina 420R), Milli-Q water was added to the concentrated NP suspension, and the procedure was repeated for three times (method B).

The Vivaflow[®] 50 (Sartorius Stedim Biotech GmbH, Germany) is a cross-flow / tangential flow system available with a PES or regenerated cellulose (RC) membrane with a maximum MWCO of 100,000. The nanoparticle suspension (50 ml) was concentrated with a flow rate of approximately 100 mL/min to a final volume of 25 ml and diluted with Milli-Q water to the initial volume of 50 ml. This procedure was repeated 20 times till 500 ml Milli-Q water were used (method C). Other methods like dialysis or asymmetric field flow fractionation (AFFF) are possible for particle purification but in this case not applicable. After the washing procedure, the main particle characteristics (size, charge, and Pdl) were analyzed to assess the impact of the procedure on the NPs.

2.3.3 Passive surface loading

Chitosan-coated NPs were loaded with siRNA in a siRNA: NP ratio of 1:100 and 1:50. The binding of siRNA onto the particle surface can be described as a passive surface loading and underlies the principle of electrostatic attraction of differently charged particles (see Figure 2.10). The loading procedure itself and the most promising siRNA :NP weight ratios were adopted and partially modified from Nafee et al. [127].

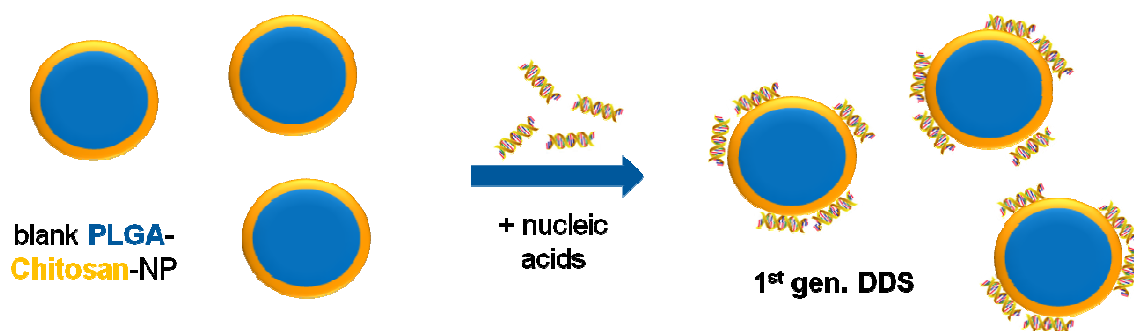


Figure 2.10 Scheme of the loading strategy of nucleic acids (siRNA) on PLGA-Cs NPs as 1st generation formulation.

Freeze-dried siRNA provided from GlaxoSmithKline (gsk), UK was solved in nuclease-free water (not DEPC treated, autoclaved, 0.2 μ m filtered) from Ambion by Life Technologies, USA and aliquoted in DNA LoBind Eppendorf Tubes[®] 1.5 mL/5 mL, PCR clean from Eppendorf AG, Germany in a final concentration of 1 mg/mL. The NP suspension was then filtrated with a Steriflip - Vacuum Filtration System (50 mL) with a Millipore Experess[®] PLUS Membrane (0.22 μ m) from Millipore to get rid of containing contaminations which enter the system during to the preparation procedure (e.g. dust, unsolved polymer). The yield of NPs in the suspension was defined via freeze-drying and calculated with regard to the applied mass. The final concentration of siRNA (1% (w/w) or 2% (w/w) of the calculated particle mass) achieved by pipetting an appropriate amount of the aqueous siRNA solution into the determined volume of NP suspension. To reach optimal binding conditions the mixture was vortexed for 20 sec. and incubated for at least 30 min. on an orbital shaker. The entire binding or loading procedure was performed at room temperature.

Detection of siRNA

Next to fluorescent measurements, UV-Vis-spectrometry is one of the standard methods to quantify single and double stranded DNA or RNA. This quick and simple method is suitable for purified nucleotides at 260 nm (A_{260}). An Eppendorf BioPhotometer was used to perform measurements at 260 nm and secondary wavelengths of 230 nm, 280 nm and 340 nm to control sample purity. Residual amounts of small particles may lead to unreliable results when measuring samples

with low concentrations < 1.0 – 1.5 µg/mL. For the 400 µL cuvette (UVette) a dilution was necessary because of the limited amount of sample. The following programs with predefined factors were eligible: dsDNA 50.0; ss DNA 37.0; RNA 40.0; oligo 30.0; x µg/mL = 1A.

Via an indirect UV measurement with an Infinite[®] 200 Pro microplate reader (Tecan, Switzerland) in UV-Star microplates 96 well, F-Bottom, chimney well, µclear (Greiner bio-one, Germany) the loading of the carrier system could be investigated. Here, the loaded particles were centrifuged, and the supernatant was analyzed relating to remaining free siRNA.

Fluorescent measurements, however, need specific fluorescent dyes (e.g. SYBR Green, Ribo Green, Pico Green, ethidium bromide) which react sensitively with a very high precision with the nucleotides. For siRNA detection, SYBR Green II RNA staining (directly added to the loading buffer in a final concentration of 1:100 from Lonza, Belgium) and ethidium bromide solution (Sigma-Aldrich, USA) were used, and the stained gel was illuminated at 300 nm ultraviolet transillumination (peqlab Fusion FX). Furthermore, gel electrophoresis was performed to observe surface properties and the ability to bind siRNA on the particle surface.

2.3.4 Particle imaging (SEM/SPM)

As PCS only calculates the mean hydrodynamic diameter of measured nanoparticles, it is important to get valid information about the morphology (real shape and its surface) of a particle fraction. Thus, a direct visualization via SEM, for instance, is necessary. Here, SPM or AFM measurements were additionally performed to observe gradual aggregation trends of the nanoparticles in different media at various pH values (without necessary purification steps).

Scanning electron microscopy (SEM)

As residual amounts of additives may prevent an appropriate imaging of the particles the NP suspension need to be removed from excess PVOH. Therefore, the suspension was treated as described in chapter 2.3.2 method A.

Sample preparation: A double-sided adhesive carbon tape was glued onto an aluminum stub. A drop (~ 1 μL) of the purified and diluted (1:1,000 with Milli-Q water) NPs was pipetted onto a silica wafer and this wafer was placed on top of the carbon tape. The particles were dried for at least 2 h at RT and were sputtered with a thin gold layer using a Quorum Q150R ES (Quorum Technologies, UK), a compact rotary-pumped combined sputter coater and SEM carbon coater (gold coating profile 'QT Timed Gold'). The sample was analyzed in a scanning electron microscope JSM 7001F Field Emission SEM (Jeol, Japan) using the control program "SmartSEM" from Zeiss, Germany.

Scanning probe microscopy (SPM)

With the help of an atomic force microscope (MultiMode AFM from Bruker, USA) the NP suspension could be analyzed without any additional treatment (e.g. purification); the liquid sample was solely pipetted onto a mica lamella and imaged at tapping mode (intermittent contact mode) for a quick visualization of the effect of different pH values in water, KRB buffer or PBS buffer on PLGA-Cs NPs.

2.4 Results and discussion

2.4.1 Preparation technique

At the beginning, a well established particulate system of chitosan-coated PLGA-NPs (1st generation formulation) was used to decide on a preferred preparation technique, which can be borrowed for 2nd generation formulations (see chapter 3). Significant differences at important preparation steps could be observed by comparing the following parameters:

- a) dropping methods: Pasteur pipette (manual), peristaltic pump (semi-automatic) and syringe pump (automatic) at two different injection rates (Figure 2.11)
- b) homogenization speed (rpm) and time (min) (Figure 2.12)
- c) content of Chitosan (Figure 2.13)

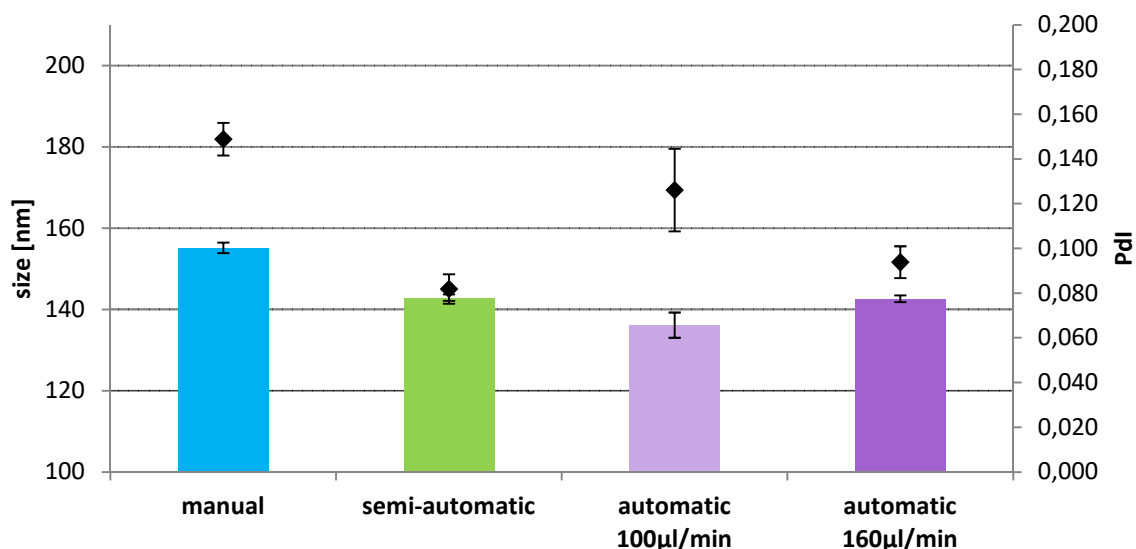


Figure 2.11 Comparison of different dropping methods from the solvent to the aqueous phase and their impact on size and size distribution. Manual method using a Pasteur pipette, semi-automatic method via a peristaltic pump (each 150 - 170 $\mu\text{L}/\text{min}$) and an automatic method via a syringe pump (100 $\mu\text{L}/\text{min}$ and 160 $\mu\text{L}/\text{min}$). [Homogenization: 15,000 rpm, 10 Min.; 15 mg chitosan/100 mg PLGA].

As a starting point, the effect of different dropping methods was analyzed. All other parameters were maintained as described in Nafee et al. [100]. All three observed methods to join the aqueous and solvent phase are suitable for a proper nanoparticle production. The automatic (both injection rates, see below) and semi-automatic manner (142.9 ± 0.8 nm; Pdl: 0.082 ± 0.007) showed good results concerning particle size around 140 nm. Slight differences could solely be observed concerning particle distribution. Here, a slower injection rate resulted in little smaller particles (100 $\mu\text{L}/\text{min}$.: 136.1 ± 3.1 nm; 160 $\mu\text{L}/\text{min}$.: 142.6 ± 0.8 nm) with a higher Pdl (100 $\mu\text{L}/\text{min}$.: 0.126 ± 0.018 ; 160 $\mu\text{L}/\text{min}$.: 0.095 ± 0.007). Thus, a reduced dropping rate seemed to have a higher influence on the particle distribution as the size itself. The manual one revealed slightly bigger particles with 155.2 ± 1.3 nm and a broader but still acceptable size distribution (Pdl 0.149 ± 0.007 , < 0.200). As a result, all further preparations will be performed via the automatic implementation with an injection rate of 160 $\mu\text{L}/\text{min}$.

Besides the dropping method, the homogenization speed and time was considered. A homogenization via sonification with an amplitude of 40 – 60 % created acceptable nanoparticles with a mean diameter of ~ 190 nm and a Pdl < 0.2 . However, in contrast to the homogenization via Ultrathurrax the use of a sonification unit offered

no benefit. Hereafter two different homogenization rates (15,000 rpm and 17,000 rpm) and durations (5 min. and 10 min.) were conferred against one another. To protect the equipment against excessive attrition a maximum utilization of 17,000 rpm for 10 min. was identified. Apparent from Figure 14 the particle size is more influenced by the length of time as by the homogenization rate. A homogenization for 5 min. created relatively large particles (15,000 rpm: 160.7 ± 0.8 nm, Pdl: 0.084 ± 0.014 ; 17,000 rpm: 157.8 ± 1.0 nm, Pdl: 0.084 ± 0.014), thus a homogenization for 10 min. seems to be necessary. However, both observed variables had no significant influence on the Pdl with the result that this preparation step only seems to determine the absolute particle size but not the quality of the comminution.

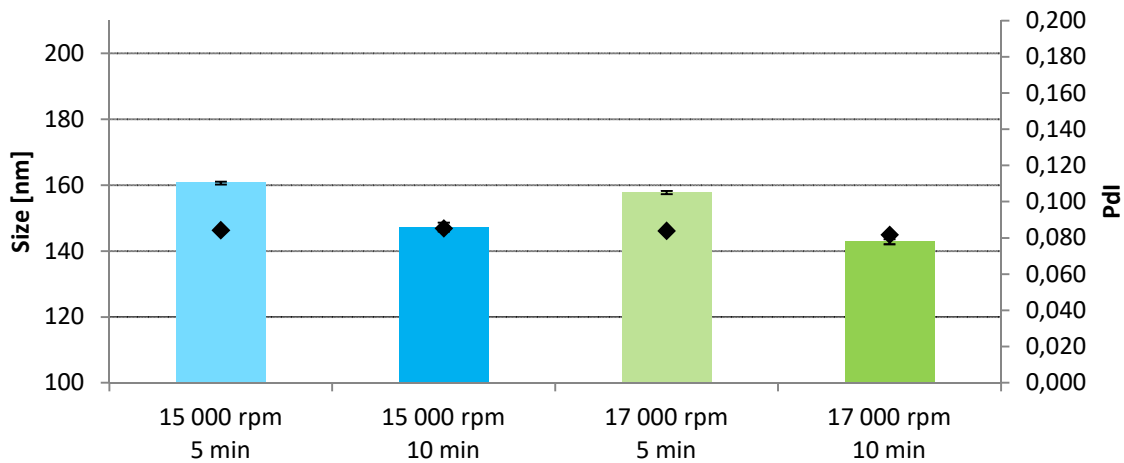


Figure 2.12 Impact of homogenization speed (15,000 rpm vs. 17,000 rpm) and homogenization duration (5 min. vs. 10 min.) on size and size distribution.

[Dropping method: automatic (syringe pump) with 160 μ L/min; 15 mg chitosan/100 mg PLGA].

Following this, the content of the coating material Chitosan was observed by applying 15 mg and 25 mg Chitosan at a time to 100 mg PLGA. The ambition was to use as little cationic material as possible, as much as necessary.

Here, the combination of 100 mg PLGA and 15 mg Chitosan formed NPs with the following characteristics: 142.6 ± 1.6 nm, Pdl: 0.094 ± 0.014 , 29.1 ± 2.5 mV. A higher amount of Chitosan (25 mg) resulted in clearly bigger particles (161.1 ± 0.7 nm, due to a thicker Chitosan shell on the PLGA core) with a higher ζ -potential (47.9 ± 5.1 mV).

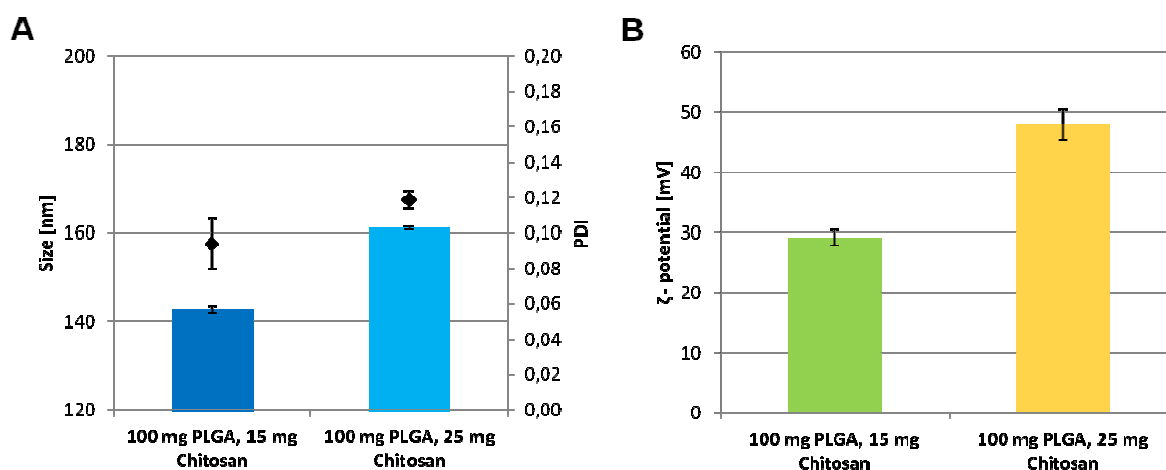


Figure 2.13 Impact of chitosan content on NPs characteristics: size and PDI (A) and ζ -potential (B). [Dropping method: automatic (syringe pump) with 160 μ L/min.; homogenization: 15,000 rpm, 10 Min.].

The size distribution was just a little bit affected to a marginal higher PDI (0.119 ± 0.005). As a result of the combination of 100 mg PLGA with 15 mg Chitosan appeared as the better option without gaining too large particles and applying too much Chitosan. For the sake of completeness, PLGA NPs were compared with chitosan-coated NPs (PLGA-Cs; 15 mg Cs/ 100 mg PLGA). Plain PLGA NPs show a mean size of 128.7 ± 1.0 nm, PDI: 0.043 ± 0.025 and a negative ζ -potential of -14.2 ± 1.5 mV. The addition of chitosan results in clearly bigger particles (142.6 ± 1.6 nm, PDI: 0.094 ± 0.014) with a positive ζ -potential of 29.1 ± 2.5 mV. The change of the ζ -potential (from negative to positive values) and the increased mean size supports the thesis of an outer chitosan shell.

Negligible examined preparation modifications were the usage of a smaller syringe cannula (with an inner diameter of 0.26 mm vs. 0.41 mm) and PEG 1000 (2.5 % and 5 %) as an alternative stabilizer (instead of PVOH). Whereas the homogenization step needed to be performed in a small (= 25 mL) glass beaker. The usage of a plastic falcon tube resulted in an inhomogeneous mixture with excessive frothing.

NPs imaging via SEM

An image captured by scanning electron microscopy allowed a proper assessment of the nanoparticulate system by providing direct information about size, shape and size distribution. In Figure 2.14 a micrograph of purified (method A) PLGA-Cs NPs show

consistent spherical shaped nanoparticles with a smooth surface. The projected mean size seems to be in the same scale, but a little bit smaller compared with the DLS measurement. This impression can be explained by the calculation of the mean hydrodynamic diameter via Stokes-Einstein equation, where the solvent layer attached to a particle is included. Hence, the hydrodynamic diameter is always greater than the size estimated by SEM [128] or other direct imaging techniques. Nevertheless, due to time- and cost-saving reasons DLS measurement remains as the preferred sizing technique for nanoparticulate systems.

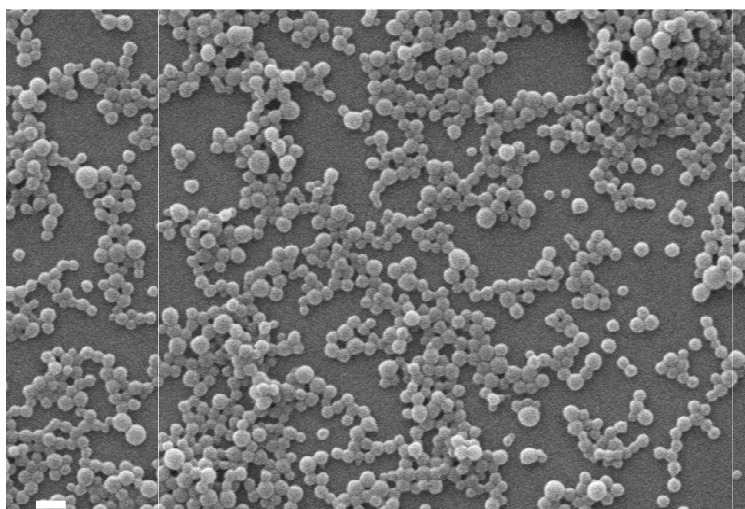


Figure 2.14 Image of purified PLGA-Cs NPs captured by SEM. Scale bar = 200 nm.

NPs preparation in media

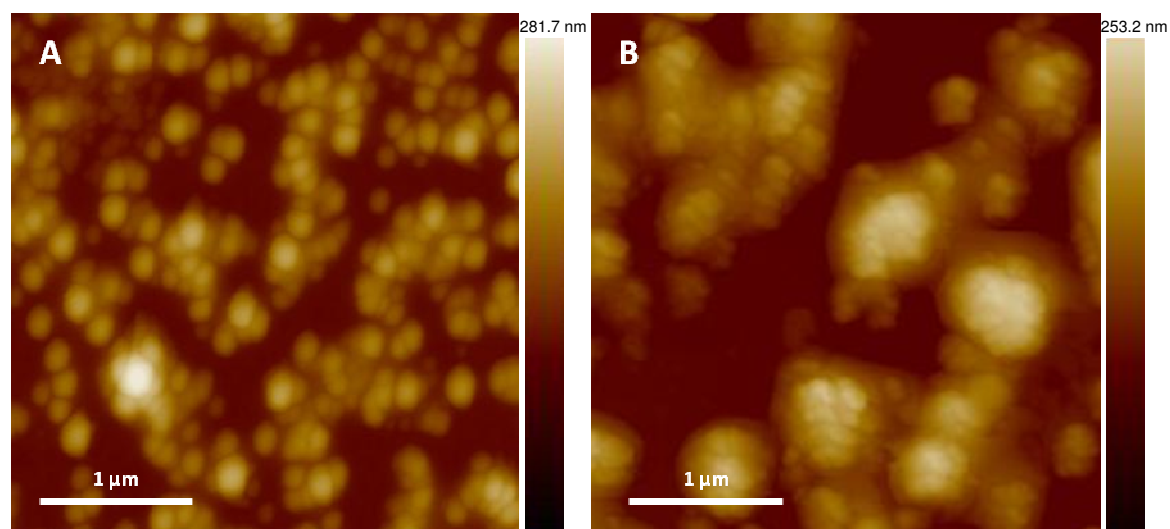
The resulting PLGA-Cs NPs-suspension (as described in Chapter 2.2.2) showed a slightly acidic pH of 5.5 (Table 2.1, shaded in gray). Due to the lack of buffering capacity further pH values (acidic, neutral and alkaline) could only be adjusted to 3.5, 6.2 and 10.6. Comparable values of the buffered systems (pH 4.0, 7.0 and 9.0) were identified. In KRB and PBS buffered systems with a pH > 9.0 reliable results could not be calculated.

Apparent from Table 1 the pH value had a significant influence on the system stability. This impact can easily be explained by ionizable amine groups of chitosan, pKa ~ 6.5 [129], and the relating pH-dependency of the ζ -potential. In this setup with a higher pH value, fewer ions (here: anions) can attach to the positive surface of the NPs and resulted in a decreased ζ -potential.

Table 2.1 Overview of PLGA-Cs NPs characteristics in Milli-Q water, KRB buffer and PBS buffer at acidic (3.5 – 4.0), roughly neutral (6.2 – 7.0) and alkaline (9.0 -10.6) pH values.

<i>Milli-Q water</i>						
<i>pH</i>	<i>size [nm]</i>	<i>Pdl</i>	<i>ζ-potential [mV]</i>			
3.5	166.1 ± 2.2	0.155 ± 0.012	43.8 ± 2.3			
5.5 (as produced)	152.4 ± 1.2	0.085 ± 0.008	28.4 ± 0.8			
6.2	164.6 ± 3.1	0.219 ± 0.010	24.9 ± 0.5			
10.6	223.9 ± 4.4	0.295 ± 0.005	1.8 ± 1.1			
<i>KRB buffer</i>			<i>PBS buffer</i>			
<i>pH</i>	<i>size [nm]</i>	<i>Pdl</i>	<i>ζ-potential [mV]</i>	<i>size [nm]</i>	<i>Pdl</i>	<i>ζ-potential [mV]</i>
4.0	131.2 ± 1.4	0.014 ± 0.004	14.4 ± 0.8	139.3 ± 2.6	0.097 ± 0.021	7.6 ± 0.6
7.0	135.1 ± 0.4	0.062 ± 0.018	5.3 ± 0.4	138.1 ± 0.9	0.115 ± 0.013	2.9 ± 0.4
9.0	175.6 ± 10.7	0.344 ± 0.018	-2.2 ± 1.2	138.0 ± 2.3	0.214 ± 0.028	-1.6 ± 0.5

As the system is electrostatically stable with a preferably high or low ζ -potential (+20 to +40 mV or -20 to -40 mV), the presence of values close to zero (0 to ± 10 mV) results in particle aggregation indicated by the Pdl. The particle size itself seemed to rise but is just a mean size of single particles and particle aggregates. As a generic example for this particle aggregation caused by a changing pH (from acidic towards alkaline conditions) of the system, particles in KRB buffer at pH 4.0 and pH 9.0 were depicted below (Figure 2.15).

**Figure 2.15** AFM micrograph (height image) of PLGA-Cs NP in KRB-buffer at pH 4.0 (A) and pH 9.0 (B).

2.4.2 FA- and DiI-labeled NPs

With the resulting standard method (see Chapter 2.3.1) flu-labeled and non-labeled NPs were prepared. An observation on possibly different NP characteristics is necessary to interpret later experiments with labeled particles accurately. A juxtaposition of the main parameters is listed below (Table 2.2).

Table 2.2 NPs characterization (size, Pdl and ζ -potential) of flu- and non-labeled PLGA-Cs NPs

	<i>size [nm]</i>	<i>Pdl</i>	<i>ζ-potential [mV]</i>
PLGA-Cs NPs	142.6 ± 1.6	0.094 ± 0.014	29.1 ± 2.5
FA-PLGA-Cs NPs	147.0 ± 1.8	0.062 ± 0.014	25.8 ± 0.6
DiI-PLGA-Cs NPs	146.2 ± 1.7	0.126 ± 0.021	36.2 ± 0.5

PLGA-Cs NPs, FA-PLGA-Cs NPs, and DiI-PLGA-Cs show all very similar values whereas DiI-PLGA-Cs NPs offered a slightly increased deviation from the ζ -potential. To assign the results from flu-labeled samples to non-labeled ones it has additionally been shown that the flu-label is incorporated in the NPs. In Figure 2.16 both NP suspensions were pictured; the different color of the labels is clearly visible.

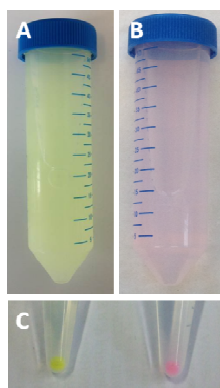


Figure 2.16 FA-PLGA-Cs NPs (A, yellow-green), DiI-PLGA-Cs NPs (B, red) and spun down (24,000 x g for 15 min.) fluorescent-labeled NPs (C).

After spinning down the particles, the color remains at the bottom (particle pellet) and is not free in the supernatant. That implies the presence of the dye inside the particles, which especially was relevant for the DiI-labeled particles since the dye is not covalently bound to the PLGA (as with FA, see Chapter 2.2.3) but dispersed and embedded into the PLGA core (see Figure 2.17).

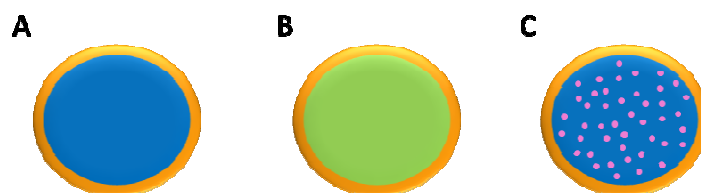


Figure 2.17 A highly simplified and enlarged sketch of a NP cut through: PLGA-Cs (left), FA-PLGA-Cs NPs (middle) and DiI-PLGA-Cs NPs (right) [blue = PLGA; orange = Chitosan; green = FA-PLGA; red = DiI].

2.4.3 Purification

In this context, the purification of the particles was meant to remove excessive amounts of PVOH which had functioned as a stabilizer. As the purification technique itself may have an impact on the stability of a particulate system NP characteristics were analyzed after the completed clean-up procedure (Table 2.3 and Figure 2.18).

Table 2.3 NPs characteristics (size, Pdl and ζ -potential) depending on purification technique. [Method A = spin down and wash, method B = VivaSpin[®] and method C = VivaFlow[®].]

	size [nm]	Pdl	ζ -potential [mV]
particles as produced	151.9 ± 2.6	0.143 ± 0.008	43.4 ± 0.5
method A	354.5 ± 40.9	0.386 ± 0.016	6.5 ± 0.4
method B	199.3 ± 1.7	0.229 ± 0.001	49.4 ± 0.6
method C	156.8 ± 2.4	0.178 ± 0.005	42.8 ± 1.5

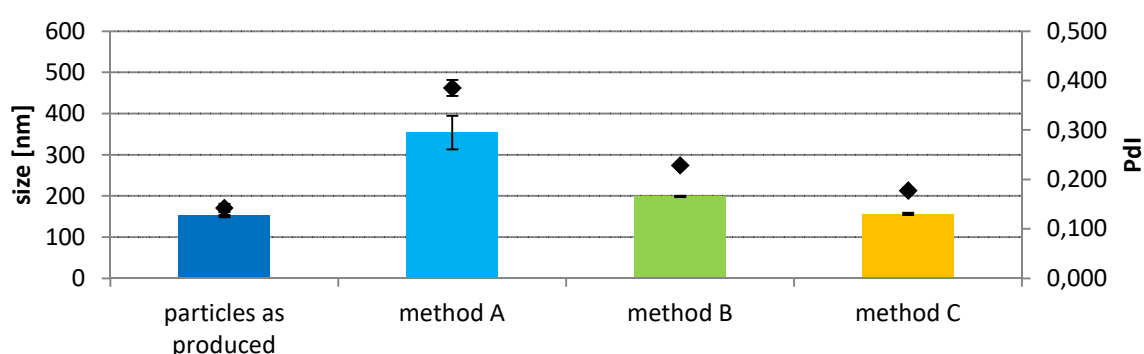


Figure 2.18 Overview of the impact of different purification methods on NP properties. [Method A = spin down and wash, method B = VivaSpin[®] and method C = VivaFlow[®].]

As expected, a harsh purification technique (in particular method A) resulted in large particle diameters and high Pdl values (equal to aggregation). A dropped ζ -potential

from 43.4 ± 0.5 mV to 6.5 ± 0.4 mV implies that even a portion of the Chitosan shell was sluced down. After Method B a slight aggregation was visible, and method C showed unchanged particle characteristics.

A colorimetric quantification [130] of residual and unbound amounts of the stabilizer was envisaged but declined due to the lack of accurate determination of the PVOH content in all purified NP suspensions. Later studies (see Chapter 5.2.1.2) show the insignificance of the presence of PVOH on cell viability in the applied dilutions.

Consequently, method A was only used if a complete removal of PVA was desired (e.g. for SEM images). In all other cases method C was applied to reduced the amount of PVA of the entire preparation bath without changing the colloidal characteristics of the nanoparticles.

2.4.4 Loading efficiency

Determining the loading efficiency [$\%LE = \left(\frac{\text{mass (siRNA)added} - \text{mass (siRNA)free}}{\text{mass (siRNA) added}} \right) * 100$]

or loading capacity [$\%LC = \left(\frac{\text{mass (siRNA)added} - \text{mass (siRNA)free}}{\text{mass NPs}} \right) * 100$] of a DDS the quantification of the cargo is one essential step to describe its potential performance. The amount of siRNA can easily be determined by indirect UV or fluorescence spectroscopy.

UV measurement

Following the thesis that all bound siRNA is fixed on the NPs and all unbound siRNA remains free in solution, the suspension of loaded PLGA-Cs NPs was centrifuged, and the supernatant was analyzed. An absorption spectrum of siRNA in the supernatant of PLGA-Cs NPs is imaged in Figure 23 and shows an independent absorption maximum of siRNA (nucleic acids) at 260 nm. Nether residual amounts of Chitosan nor the stabilizer PVOH seem to disturb this measurement. Additionally, it was shown that the absorption correlates with the amount of siRNA linearly (see Figure 2.20) at the utilized concentrations.

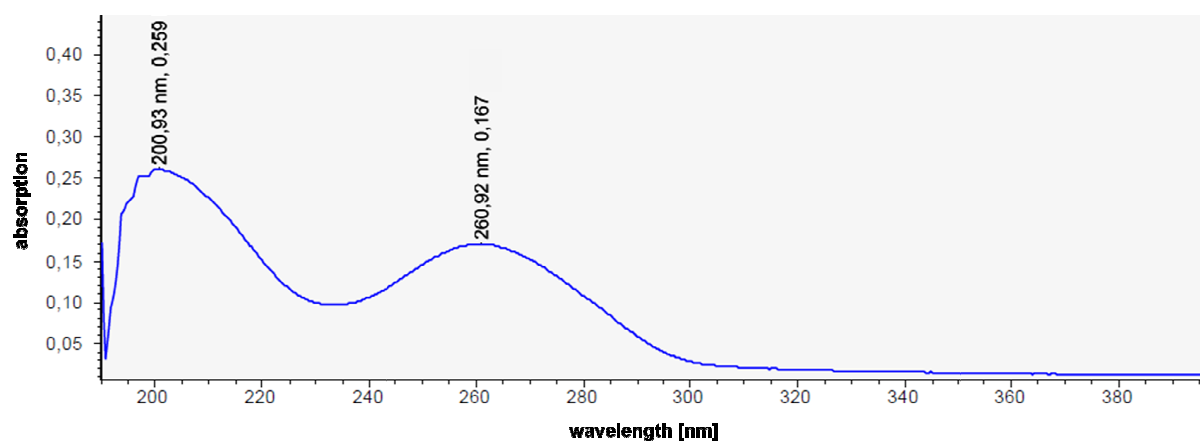


Figure 2.19 UV-spectroscopy: absorption spectrum of siRNA in PLGA-Cs NPs supernatant [20 mg/mL].

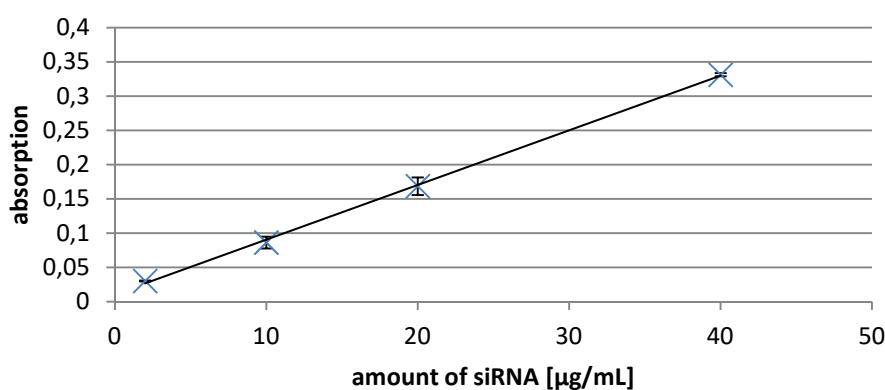


Figure 2.20 Linearity of the absorption in a concentration range between 2.5 and 40 µg/mL siRNA in the supernatant of PLGA-Cs NPs.

After the execution of these preliminary tests the quantification resulted in a %LE = 84.3 ± 0.5 % or a %LC = 0.843 ± 0.005 % [PLGA-Cs NP mass = 2 mg/mL; siRNA loading 1:100 = 20 µg/mL]. The coefficient of determination ($R^2 = 0.9993$) indicates this method as valid.

Fluorescence measurement

A quantification via fluorescence spectroscopy requires the assistance of a fluorescent dye (e.g. SYBR[®] Green II, Ribo Green or ethidium bromide). However, the observed system allowed no linear correlation between signal intensity and siRNA concentration in the desired concentration range. On the one hand

Figure 2.21 shows increased signal intensity when the fluorescent dye and blank PLGA-Cs NPs are brought together, but on the other hand, the signal intensity in general provides very low values.

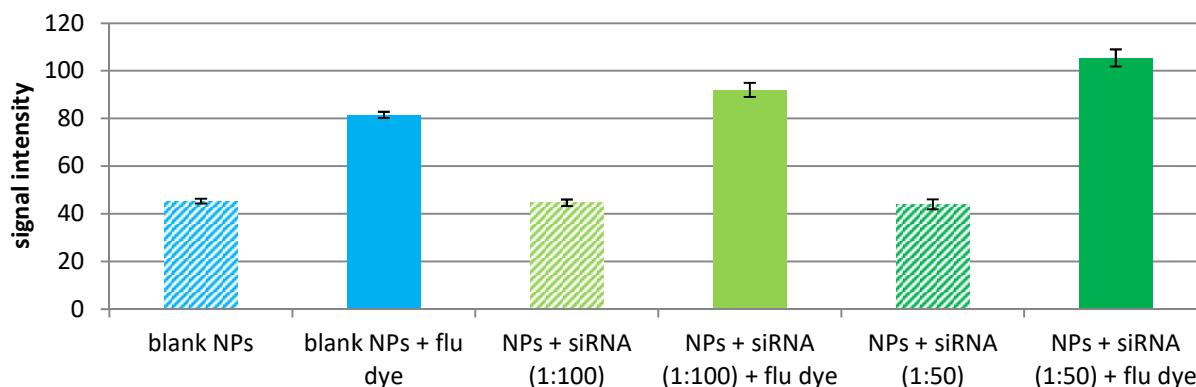


Figure 2.21 Fluorometric quantification of siRNA on PLGA-Cs NPs. Filled bars = stained samples (with SYBR[®] Green II); striped bars = unstained samples.

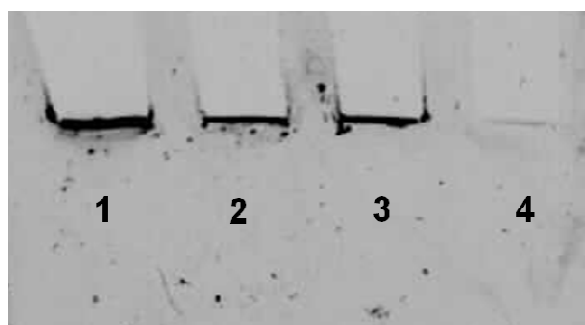


Figure 2.22 PAGE with 15 %-TBE Gel; inversed image. 1 = PLGA-Cs NPs:siRNA 50:1; 2 = PLGA-Cs NPs:siRNA 100:1; 3 = PLGA-Cs NPs; 4 = native PLGA-Cs NPs; sample 1-3 were stained with SYBR[®] green II RNA gel stain [1:1,000].

The inadequate quantification by fluorescence spectroscopy can be explained by an unspecific binding between dye (SYBR[®] Green II and ethidium bromide) and NPs (see Figure 2.22) and a quenching effect of the intercalated dye. Hence, a quantification of bound siRNA by the fluorescent signal is not indicated for this DDS.

2.5 Conclusion

Within this chapter, a preferable partial automatic preparation procedure for chitosan-coated PLGA nanoparticles was identified. Optimized preparation parameters will prospectively be maintained to compare particle characteristics when creating 2nd

generation formulations by using different cationic coating materials. Preparation in physiological PBS- and KRB buffer revealed a robust system against the presence of various ions and buffer substances. Here, the particle stability was mainly limited by high pH values. Above pH 7.0 the formally positive ζ -potential dropped to values around zero and caused a loss in stability towards aggregation.

The Emulsion-diffusion-evaporation technique functions as a resulting standard method to prepare flu-labeled and non-labeled NPs. Minor deviations in size and ζ -potential between labeled and non-labeled could be observed but do not limit any later applications of the samples. Hereafter, FA-PLGA NPs were primarily used compared with DiI-PLGA NPs because that the fluorescein amine was covalently coupled to the carboxyl group of the PLGA polymer and not only dispersed in the PLGA matrix.

A loading procedure of NPs with siRNA during the preparation step was tested but failed due to aggregation tendencies. This might be explained by the additional creation of polyplexes between siRNA and free solved chitosan. Furthermore, a possible contact of siRNA with organic solvents (here: ethyl acetate) may limit the cargo stability. Therefore, a post-loading technique resulted as a simple and safe method to bind siRNA on the NPs surface. A suitable quantification of bound siRNA could be achieved by an indirect UV-measurement at 260 nm. Resulting LE of ~84 % arises as a good starting point for later therapeutic applications. Fluorescent measurements show no benefit since blank PLGA-Cs NPs seem to interact unspecifically with fluorescent dyes, and bound siRNA showed minor fluorescent signals due to quenching effects.

Chapter 3 - Suitable coating materials for transfecting PLGA-based nanoparticles (2nd generation)

The author of this thesis made the following contribution to this chapter:

Planned and performed all experiments related to characterization of coating materials as well as particle preparation and characterization, analyzed all the data from the mentioned studies, interpreted all experimental data and wrote the chapter, it not stated otherwise.

Julia Müller, who did an internship at the institute and who was instructed by the author of the thesis, contributed by this chapter by performing some nanoparticle tracking analyzes.

Fluorescence correlation spectroscopy was performed by George Dandekar at Ghent University. He analyzed the data from the mentioned studies and interpreted the experimental data.

3.1 Introduction

Gene therapy is the therapeutic insertion of DNA- or RNA-based nucleic acids (NA) into a specific cell. For the intracellular delivery of different tools for down regulation of expressed genes (e.g. siRNA) or to insert new genes (e.g. plasmid DNA for transient expression vectors or carriers are needed. Hereafter, different transfection methods can be applied. Table 3.1 shows an overview of transfection reagents and methods.

Table 3.1 Overview of different reagents and methods for transfection.

<i>Method</i>	<i>Reagent/Vector</i>	<i>Transfection</i>
chemical or carrier-based	Calcium phosphate	stable/transient
	Cationic lipids	transient
	Cationic polymers	transient
	Dendrimers	transient
	DEAE-dextran	transient
	Magnetic beads	transient
physical or instrument-based	Micro-injection	stable
	Biolistic particle delivery	transient
	Laserfection	stable/transient
	Electroporation	transient
biological or virus-based	Retrovirus	stable
	Lentivirus	stable
	Adenovirus	transient
	Adenoassociated virus	stable
	Herpes simplex virus	transient
	Vacciniavirus	transient

The oldest chemical method represents the usage of calcium phosphate [131]. DNA mixed with calcium chloride (CaCl_2) in HEPES-buffered saline/phosphate solution creates a precipitate which can be taken up by phagocytosis/endocytosis. This inexpensive reagent is suitable and efficient for many cell types, however an application within RPMI medium (e.g. used to cultivate A549 cells) is not feasible. Because of the high concentration of phosphate a precipitation is impossible.

Moreover, this method suffers from inefficiency by slight pH changes, a limited reproducibility (due to the consistency of the reagent) and relatively high amounts of required DNA. Nowadays, a major use of cationic lipids (incl. liposomes [132] and lipoplexes) and polymers (e.g. PEI [133], dendrimers [134], Diethylaminoethyl (DEAE)-dextran [135]) can be explained by the easy handling and the possibility to perform high-throughput systems. Here, conjugations are created by electrostatic interactions of the negatively charged backbone of NAs (phosphate groups) and the positive part of a lipid or polymer. However, they are not equally efficient for all cell types and can cause toxic effects on cells when applied in high concentrations. A relatively new method is a magnet-mediated transfection [136-138]. NAs were associated to magnetic NPs (mostly magnetite). When applying a magnetic force, this complex is driven into adherent or fixed target cells. This technique benefits from a gentle treatment which causes less cytotoxicity and the possibility to perform experiments in the presence of serum.

A frequently used physical based transfection method is the Electroporation [139-141]. Transient membrane pores will be created by short electrical pulses; plus, small particles can pass. Electroporation, in general, is a robust and efficient transfection method. However, a compromise between efficiency and viability needs to be found, as a high efficiency causes higher cell mortality. Other instrument-based transfection methods like biolistic particle delivery [142] (also known as particle bombardment) via gene gun [143], laserfection (= opto-injection/photo-transfection) [144] or microinjection [145] play a minor part due to high instrumental costs, a laborious experimental setup or lower efficiencies.

Finally, vectors [146, 147] (e.g. lentivirus for stable transfection [148] and adenovirus for transient transfection) for *in vitro* and *in vivo* gene delivery need to be mentioned. They accomplish the highest efficiency (80-90% in primary cells) amongst all methods, but certain drawbacks limit their popularity. Next to a limited insert size of ~10 kb and biosafety issues (e.g. inflammatory response) this technique itself is challenging and laborious.

As mentioned before, many materials can be presented as potential non-viral vectors for gene delivery [149-152]. To draw up a shortlist three different biodegradable and biocompatible cationic polymers with promising vector-qualities were used to coat

PLGA-NPs, obtain a positive surface charge and thus enable delivery of siRNA through cellular membrane into the cytosol. Chitosan (Cs) [110, 153-156] (also see Chapter 2), Protamine (Prot) [156, 157] and CatStarch [158] represent the selected materials. Here, Cs-coated PLGA NPs (PLGA-Cs) constitutes the 1st generation formulation. Protamine-coated PLGA NPs (PLGA-Prot) and starch-coated PLGA-NPs with (PLGA-CatSt) belong to the 2nd generation of formulations with a retaining PLGA core and different cationic coating materials.

3.2 Materials and methods

3.2.1 Materials

For particle preparation Poly(D,L-lactide-co-glycolide) (PLGA, CAS No: 26780-50-7) Resomer[®] RG 752 H from Evonik Industries, Polyvinyl alcohol (PVOH, CAS No: 9002-89-5) Moviol[®] 4-88 from kuraray, Chitosan (Cs, CAS No: 9012-76-4) Protasan[®]UP CL 113 from Novamatrix (Sandvika, Norway), Protamine sulfate (CAS No: 9009-65-8) from Sigma-Aldrich and CatStarch (CatSt; in-house synthesis, detailed protocol see 3.2.2) was used. SiRNA was kindly provided from COMPACT project partner GlaxoSmithKline, UK. Fluorescein amine isomer I (FA, CAS No: 3326-34-9) to prepare flu-labeled particles was purchased from Sigma-Aldrich. For starch synthesis, partially hydrolyzed potato starch was provided from AVEBE, the Netherlands. The M_w is $\sim 1,300,000$ g/mol and the content of amylase is $\sim 33\%$. 2,2,6,6-Tetramethyl-1-piperidinyloxy (TEMPO; CAS No: 2564-83-2), tetraethylenepentamine (tEpA; CAS No: 112-57-2), 4-(4,6-Dimethoxy-1,3,5-triazin-2-yl)-4-methyl-morpholinium chloride (DMTMM; CAS No: 3945-69-5) and Sodium hypochlorite (NaClO; CAS No: 7681-52-9) were purchased from Sigma-Aldrich, Germany. Sodium borohydride (NaBH₄; CAS No: 16940-66-2) was purchased from Merck. Dialysis tubes Fisherbrand[®]; regenerated cellulose dialysis tubing 15 m roll; nominal MWCO 3,500; Fiat width: 46 mm * vol/cm: 6.74 mL; wall thickness: 28 μ m; dry cylinder diameter: 29.3 mm (21-152-9, T1 membrane 3500 Dalton MWCO 46 mm) from Fisher Scientific were used. Phosphotungstic acid hydrate (PTA; Tungstophosphoric acid; CAS No: 12501-23-4) from Sigma-Aldrich; was used in a 1% solution for TEM-staining.

For gel electrophoresis high-resolution Agarose (CAS No: 9012-36-6), Ammonium persulfate (APS; CAS No: 7727-54-0), Tris as Trizma[®] base (CAS No: 77-86-1) and Ethylenediaminetetraacetic acid (EDTA; CAS No: 60-00-4) from Sigma-Aldrich were used. Acrylamide, Rotiphorese[®] Gel 30 (37.5:1) and Tetramethylethylenediamine (TEMED; CAS No: 110-18-9) were purchased from Carl Roth GmbH + Co. KG. Gene Ruler Ultra Low Range DNA ladder, ready-to-use solution and DNA Loading Dye (6x) were bought from Thermo Scientific, Nuclease-free water was provided by Ambion by Thermo Scientific. Moreover, the following substances were purchased: boric acid (CAS No: 10043-35-3) from Merck Millipore, Germany; DNA LoBind Eppendorf Tubes[®] 1.5 mL, PCR clean from Eppendorf AG, Germany.

All other solvents, chemicals, and materials were of analytical grade and are designated in the related sections of this chapter.

3.2.2 Characterization of coating materials

3.2.2.1 Synthesis of a cationic starch derivative

Maintaining high transfection efficiencies an ideal vector for gene delivery keeps the viability of a treated cellular system. Regarding this Yamada et al. confirmed the benefit of some synthesized cationic starch derivatives [158] compared to utilized positive controls (e.g. jetPRIME). Hence, the coupling reaction of a biodegradable starch backbone with cationic side chains was transferred for coating (see chapter 3.1) PLGA NPs with this material.

Starch, in general, is a polysaccharide consisting of linear and helical amylose and a branched amylopectin. Biomaterials usually show a high individual variability. Therefore it is important to use a material with known and defined characterization parameters. For the synthesis of a cationic starch derivate, the starting material is a partially hydrolyzed potato starch. The entire synthesis consists of two steps: at first the oxidation of the starch to create a water soluble intermediate starch derivate (see Figure 3.1 A). After fractionation into different M_w s and the determination of the degree of substitution a second synthesis step includes the conjugation of the

oxidized starch with a short polyethyleneimine (PEI = 0.8 kDa) molecule (see Figure 3.1 B).

First of all 20 g of dried potato starch were dispersed in 800 mL Milli-Q water and stirred for at least 1 hour at 95 °C. After cooling down to RT the solution was dosed with 80 mg (= 4 mg/g starch) 2,2,6,6-Tetramethyl-1-piperidinyloxy (TEMPO). Under strict preservation of pH 8.5, 132 mL of a 12 percent solution of Sodium hypochlorite (NaClO) was slowly added followed by 8 g Sodium borohydride. After stirring overnight, the resulting water soluble and anionic starch derivative was divided into different fractions regarding its M_w . The fractionation was performed in the following order by ultrafiltration (Vivaflow[®]200 filtration units; from Sartorius Stedim Biotech GmbH, Germany): 5,000 MWCO, 30,000 MWCO and 100,000 MWCO (5 kDa and 30 kDa with a Hydrosart membrane and 100 kDa with a Polyether sulfone membrane). For washing Milli-Q water was used. The first cycle separated residual amounts of reagent material from starch - thus, the filtrate was discarded. The second cycle with 30,000 MWCO created a 'small' fraction of 5,000 – 30,000 Da. The last cycle with 100,000 MWCO created a 'medium' fraction of 30,000 – 100,000 Da (permeate) and a 'large' fraction of > 100,000 Da (retentate).

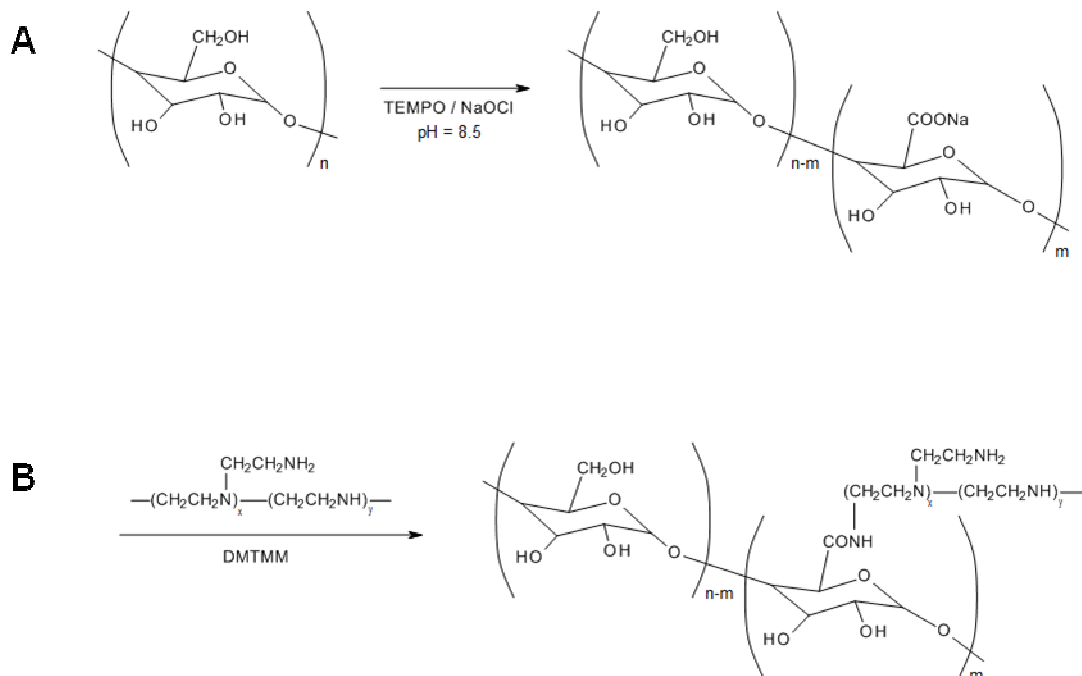


Figure 3.1 Full synthesis of starch-*graft*-PEI polymers according to Yamada et al. [158]. A: starch oxidation, B: conjugation reaction with PEI.

To receive oxidized starch as a dry material the separated solutions were concentrated with a rotary evaporator (Rotavapor R-215 from Büchi, Switzerland) followed by lyophilization (Alpha 2-4, Martin Christ GmbH, Osterode, Germany).

As the starch with the high M_w backbone (AnStarch) was expected to be the most promising derivative, it was applied as starting material for the following coupling reaction according to Kunishima et al. [159]. The degree of substitution (by sodium carboxylate = DS_{COONa}) was conducted via Blumenkrantz-assay [160], a colorimetric method which detects the content of uronic acid, following this equation:

$$\text{Degree of substitution [\%]} = \frac{\frac{A}{\varepsilon \times d} \times 1,000,000}{m(\text{AnStarch}) \text{ in } 50 \mu\text{l}} \times 100$$

A = absorbance; ε = extinction coefficient ($26\,700 \text{ l mol}^{-1} \text{ cm}^{-1}$), d = cuvette length (1 cm); m = mass in mg

This is essential for the calculation of required amounts of tetraethylenepentamine (tEpA) and 4-(4,6-Dimethoxy-1,3,5-triazin-2-yl)-4-methyl-morpholinium chloride (DMTMM). 500 mg of AnStarch (1.09 mmol NaCOO) were suspended in 10 mL Milli-Q water before 40 mL DMSO were added to solve the starch (at least 30 min.). The conjugation reagent (1.30 mmol DMTMM) needs to be added to activate the sodium carboxylate groups (stirring for 30 – 60 min.). The solution was then subsequently added to a mixture of 10 mL Milli-Q water, 40 mL DMSO and tEpA (27 mmol PEI) and left stirring for 72 hours. Hereafter, purification via dialysis (3,500 MWCO) against purified water was necessary. To concentrate the resulting mixture, a rotary evaporator (pressure set to 25 mbar, water bath temperature: max. 40 °C) was used and accrued precipitates (see Figure 3.2) were separated via centrifugation before lyophilization. This water insoluble byproduct is likely to consist of large starch conjugates and PEI [161] when a high degree of substitution is measured. Because of the steric hindrance of the molecule, the attainable degree of substitution is limited. A determination of the average molecular weight of the starch derivative was performed by gel permeation chromatography (GPC; HLC-8320 GPC, Tosoh, Japan) with an online viscometer (ETA-2010, PSS, Germany) in 1 % formic acid (1 mL/min at 35 °C) on SUPREMA-MAX 1000 and SUPREMA-MAX 30 columns (PSS, Germany).

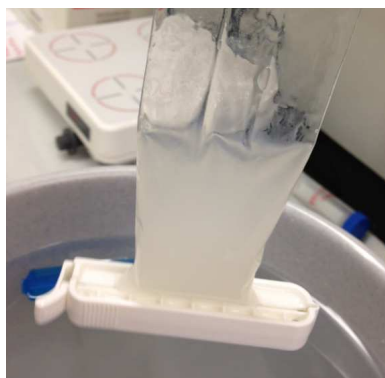


Figure 3.2 Resulting mixture of solved CatStarch and water-insoluble white precipitates of starch conjugate and PEI (byproduct) after extensive dialysis against purified water.

Universal calibration was executed with PSS Poly(2-vinylpyridine) standards (Mp 839 – 256,000 Da). Unfortunately, the evaluation was not feasible due to an irreparable malfunction of the device. The success of the coupling reaction with polyethyleneimine (see Figure 3.1 B) was confirmed by $^1\text{H-NMR}$ on a Bruker Biospin spectrometer NMR Magnet System 400 MHz Ultrashield plus (Bruker, USA) in D_2O ; δ_{H} CatStarch: (1H , 5.20 – 5.60), ($2\text{H}, 3\text{H}, 4\text{H}, 5\text{H}, 6\text{H}$, 3.30 – 4.22), PEI: ($\text{NH-CH}_2\text{-CH}_2$ 2.48 – 3.28 ppm) and FT-IR measurements in solid state with a Spectrum 400 FT-IR/FT-NIR spectrometer (PerkinElmer, UK) between 650 and 4,000 cm^{-1} of the synthesized material.

3.2.3.2 Buffering capacity of coating materials

Once nanoparticles are engulfed into endosomes/lysosomes via endocytosis (see Chapter 7.1) the delivery system needs to escape from degrading vesicles. Although partially controversial discussed the ‘proton sponge’ hypothesis [162] seems to be one meaningful explanation how a delivery system can reach its target compartment (e.g. cytosol). Having an entrapped substance that can neutralize the proton influx (e.g. cationic polyplex) causes actively relocated protons (by proton pumps = membrane bound $\text{H}^+\text{-ATPase}$) into the endosome to lower pH. Consequently, the substance become protonated (buffering effect) and more protons are pumped into, followed by a passive entry of chloride ions (see Figure 3.4 B). Due to the increasing ionic concentration an influx of water starts and the vesicle is

swelling up. Finally, the resulting osmotic pressure causes a rupture (see Figure 3.4 C) of the endosome and releases the inward into the cytosol.

As a strong buffering effect of a polymer lead to a fast endosomal escape an acidic titration [163] of the different coating materials helped to determine its buffering capacity (here: endosome buffering in a pH range between 7.4 and 5.1). For this purpose 10 mg of Protamine, Chitosan or CatStarch were dissolved in 10 mL 0.1 M NaCl and adjusted with 1 M NaOH to pH 11. The resulting solution was gradually titrated from pH 11 to pH 3 with 0.1 M HCl. Endosome buffering capacity was calculated as the percentage of amine groups becoming protonated within pH 7.4 – 5.1 according to the following equation:

$$\text{Buffering capacity [\%]} = \frac{\Delta V_{\text{HCl}} * 0.1 \text{ M}}{N_{\text{mol}}} * 100$$

ΔV_{HCl} = volume of 0.1 M HCl in μL to decrease the pH from 7.4 to 5.1

N_{mol} = total moles of protonable amine groups in 10 mg sample

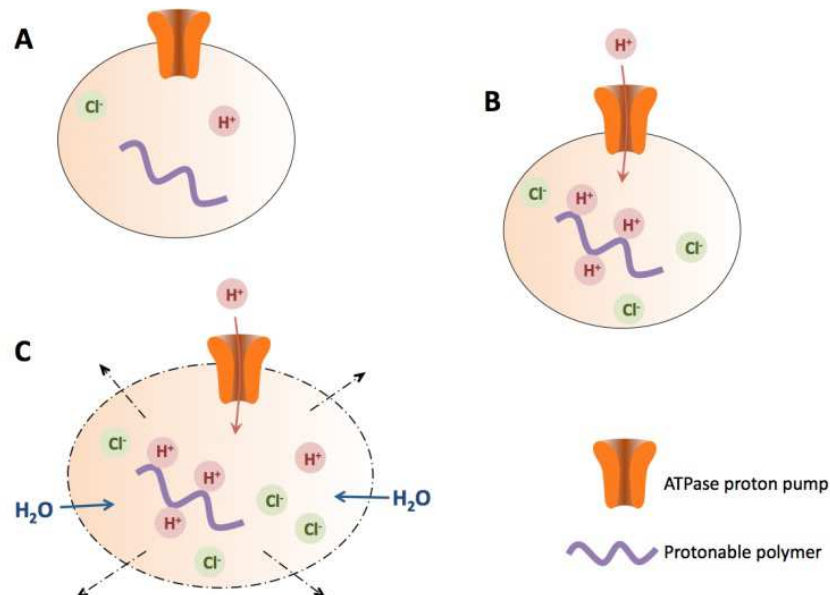


Figure 3.4 Endosomal escape of non-viral gene delivery vehicles (proton sponge hypothesis: pH buffering effect). A: entrapment in endosome, B: translocation of protons into the endosome to lower the pH, protonation of polymer (resistance against acidification), C: passive entry of chloride ions followed by water influx due to increased ionic concentration, swelling and rupture; adopted from Liang et al. [164].

3.2.3.3 Test of endotoxins in raw materials and NP suspensions

To confirm the validity of immunogenicity studies (see Chapter 5.3) an ELISA-based Endotoxin Detection Assay (EndoLISA[®] from hyglos GmbH, Germany) was used to exclude a potential immunogenic reaction due to endotoxin contamination. The assay was performed as recommended by the manufacturer. Protamine, Chitosan and CatStarch as raw materials were solved in endotoxin-free water to a final concentration of 1 mg/mL, respectively. A similar procedure was performed with PLGA and FA-PLGA and coated PLGA and FA-PLGA NPs but due to the lack of water solubility of PLGA the samples could only be dispersed in endotoxin-free water. A freshly prepared LPS (500 EU/mL) solution was diluted to create a standard curve containing: 0.05 EU/mL, 0.5 EU/mL, 5 EU/mL, 50 EU/mL and 500 EU/mL.

All samples were examined in duplicates.

3.2.3 Characterization of coated PLGA NPs

3.2.3.1 NP preparation

In chapter 2.2.2 the preparation procedure for PLGA-Chitosan-NPs was described. For the additional manufacture of PLGA-Protamine and PLGA-CatStarch NPs as 2nd generation formulations, the same modification of the emulsion-diffusion-evaporation technique was applied. PLGA (20 mg/mL) dissolved in ethyl acetate was slowly added to an aqueous solution of Protamine, Chitosan or CatStarch (3 mg/mL) in 2.5 % (w/w) PVOH and homogenized via ultra-turrax. The subsequent addition of water increased the amount of the aqueous phase and allowed the ethyl acetate to dissolve in water. This migration caused a hardening of the particles and the organic solvent was evaporated over night. As the cationic polymers were soluble in water, molecules could attach to the anionic surface of PLGA and created coated PLGA NPs. The yield or NP concentration in suspension was calculated by the mass of the pellet (nanoparticles) after centrifugation of a defined sample volume.

3.2.3.2 Colloidal characteristics of NPs

Photon correlation spectroscopy (PCS) was applied to analyze particle size. Zetasizer Nano Series ZSP (Malvern Instruments Inc., UK) was used with the following settings. Material: PLGA, RI: 5.500, Absorption: 0.010, dispersant: water, viscosity: 0.8872 CP, RI: 1.330, temperature: 25 °C, equilibration time: 120 sec., cell type: DTS 0012 disposable sizing cuvette, measurement/scattering angle: 173°, backscatter (NIBS default). Dilution: 1:10 diluted with Milli-Q water. Cumulants analysis was applied according to ISO13321 (1996) and ISO22412 (2008).

Results from the nanoparticle tracking analysis (NTA) implemented with the NanoSight LM10 (Malvern Instruments Inc., UK) confirmed prior colloidal characterizations in specific the size and distribution of the NP suspension. Here, a dilution of at least 1:200 was necessary.

All measurements were performed in triplicates as mean \pm SD. Additionally, mode \pm SD for NTA analysis.

3.2.3.3 Morphology of coated PLGA-NPs (SEM- and TEM-imaging)

Scanning electron microscopy (SEM) was conducted as previously described in section 2.3.4. For transmission electron microscopy (TEM) a JEOL JEM 2011 microscope from Oxford Instruments was used. For analyzing NPs loaded with flu-labeled ALEXA568-siRNA, no staining protocol was required. All other samples (1:10 dilution with MilliQ water) were incubated for 10 min. on a copper grid ('drop on grid' = dog), stained with a 1% (w/w) PTA solution for 45 sec. ('grid on drop' = god) and washed with water (god). After the removal of excess fluid with filter paper, the samples were dried overnight.

3.2.3.4 'Washing' study

Chapter 2.4.3 showed a declining ζ -potential (approaching neutral/zero) of PLGA-Cs NPs which led to a distinct aggregation tendency. This may be caused by a weak

binding of the Chitosan on the PLGA polymer. Implying this, a 'washing' study has the aim to show how strong the cationic coatings are bound on the surface. Following 'method A' (see Chapter 2.3.2) all coated NP samples were purified and analyzed after each stage, totaling three rounds.

3.2.3.5 Quantification and release of bound siRNA

For determining the loading efficiency of PLGA-Cs NPs (see Chapter 2.4.4) an indirect quantification via UV measurement was possible. Since this technique was inappropriate for PLGA-Prot and PLGA-CatSt NPs, gel electrophoresis with 10 % polyacrylamide or 5 % agarose gel containing 0.5 µg/mL ethidium bromide (CAS No:1239-45-8) running with 8V/cm in Tris-borate-EDTA (1xTBE) buffer (89 mM Tris (pH 7.6), 89 mM boric acid, 2 mM EDTA) or Tris-acetate-EDTA (1xTAE) buffer (40 mM Tris (pH 7.6), 20 mM acetic acid, 1mM EDTA) in) was used to investigate the process of siRNA-binding. Per lane 5 µL sample or Ladder mixed with 1 µL 6x loading buffer was applied. A release of bound siRNA on the particle surface was acquired through the addition of 1 µL heparin (as sodium salt from porcine mucosa from Sigma-Aldrich; CAS No: 9041-08-1) diluted in MilliQ water (10 U/µL) to each sample. RNA signal was analyzed by UV illuminator Fusion FX7 imaging systems from peqlab, Germany.

Fluorescence correlation spectroscopy is a specific fluorescent microscopy technique to measure the release of a particulate system by analyzing a fluctuation profile of the fluorescence signal without any physical separation processes. When a fluorescent molecule enters the focused spot (= 'detection volume') the fluorescent intensity increases and drops again when leaving the detection volume. The data of FCS analysis (referring to Braeckmans et al. [165]) was generated by George Dandekar, Ghent University, COMPACT WP 3 (P11). Stability and release efficacy of the DDS was analyzed in HEPES buffer and RPMI medium.

Samples were loaded with a siRNA-mixture, 1:5 (ALEXA647: GAPDH), by adding this solution in a ratio of 1:100 (siRNA: NP) to the nanoparticle suspension. Free siRNA-mixture in HEPES buffer measuring the free baseline (see Figure 3.5) and the

pure medium to measure the medium baseline were necessary controls for FCS analysis since some biological fluids tend to have autofluorescence.

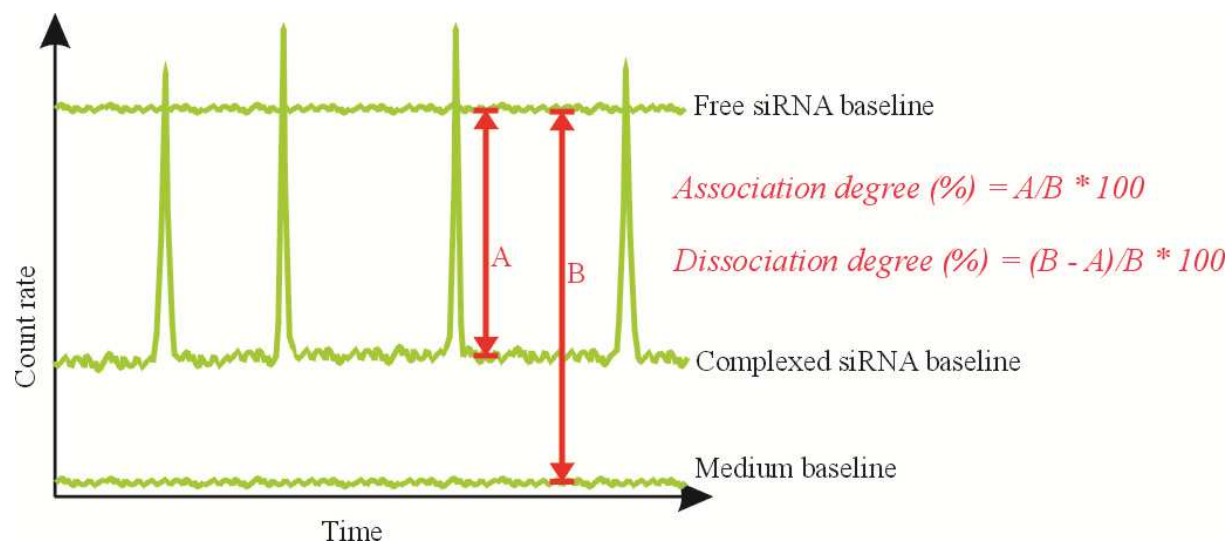


Figure 3.5 Scheme of fluorescence fluctuation profiles of a siRNA solution (free siRNA), a DDS dispersion (complexed siRNA) and the surrounded medium to calculate the degree of associated and dissociated siRNA. Adopted from Buyens et al. [166].

Directly before use loaded NPs were diluted with HEPES buffer or RPMI medium (final concentration of fluorescent molecule 5 - 20 nM). The laser beam of an inverted microscope (Eclipse TE300 from Nikon, Japan) equipped with a water immersion objective lens (Plan Apo 60x, NA 1.2, collar rim correction from Nikon, Japan) was focused to 50 μm above a sample containing black glass-bottom 96-well plate from Greiner Bio-one, Germany. NIS element software by Nikon allowed the implementation of a suitable laser. SymPhoTime by PicoQuant was applied to record fluorescent time trace (X-axis: time, Y-axis: fluorescent intensity) for 60 seconds.

All measurements were conducted in duplicates.

3.3 Results and discussion

3.3.1 Characterization of pure coating materials

One main distinction between the described cationic polymers can be made by the molecular weight (M_w). As a proper determination of the mean molecular weight via GPC was barred due to a persistent malfunction of the system, approximate values

from literature or preliminary studies were consulted: Protamine, as the smallest molecule with 5,100 Da, followed by Chitosan with 50,000-150,000 Da (estimated with $\sim 61,000$ Da [167]) and CatSt with an presumably molecular weight higher than 100,000 Da (limitation of smaller molecules due to tangential flow filtration of the starch derivative, see Chapter 3.2.2.1). Prior running GPC analyses (conducted by Hiroe Yamada, settings for CatStarch were used as described in section 3.2.2.1; notwithstanding the AnStarch sample was analyzed in 1 M Sodium nitrate at a flow-rate of 1 mg/mL at 35 °C on SUPREMA 1000 and 30 columns from PSS, Germany; for universal calibration Pullulan, Mp 342 – 708,000 Da standards were used) resulted in a mean M_w of about 580,000 g/mol for AnStarch and 830,000 g/mol for CatStarch polymer [161].

3.3.1.1 Chemical characterization of starch derivatives

Following the starch synthesis in Chapter 3.2.2.1 the oxidation of the starting material resulted in a water-soluble precursor material (AnStarch). The amount of sodium hypochlorite controlled the reaction and defined the degree of modification (objective of starch modification = 40 %). The degree of substitution was determined after fractionation by Blumenkrantz assay [160] and confirmed a DS_{COONa} of 36 %.

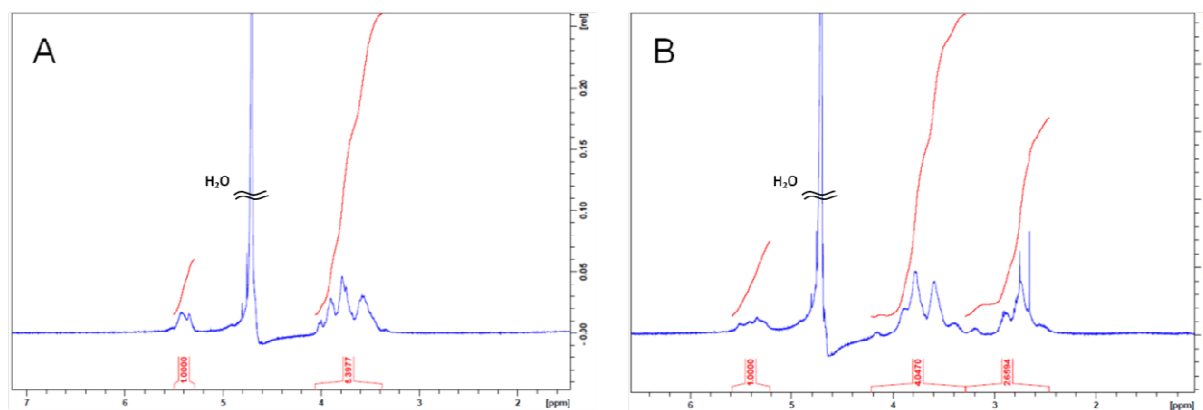


Figure 3.6 $^1\text{H-NMR}$ spectra of anionic starch (A) and cationic starch (B) derivatives in D_2O , A: oxidized starch, δ_{H} AnStarch: (1H , 5.30 ppm – 5.48 ppm), ($2\text{H}, 3\text{H}, 4\text{H}, 5\text{H}, 6\text{H}$, 3.38 ppm – 4.06 ppm); B: coupled starch with polyethyleneimine (PEI), δ_{H} CatStarch: (1H , 5.20 ppm – 5.60 ppm), ($2\text{H}, 3\text{H}, 4\text{H}, 5\text{H}, 6\text{H}$, 3.30 ppm – 4.22 ppm), PEI: ($\text{NH-CH}_2\text{-CH}_2$ 2.48 ppm – 3.28 ppm).

Based on these value synthesis with the large oxidized intermediate was preceded by conjugation of the C6 position of COONa group by the amino groups of PEI. The

amount of bound PEI was calculated from $^1\text{H-NMR}$ results, based on the integration ratio of 1H of starch (5.20 ppm – 5.60 ppm) and PEI protons (2.48 ppm – 3.28 ppm), see Figure 3.6 and resulted in a degree of substitution with PEI of approximately 15 %.

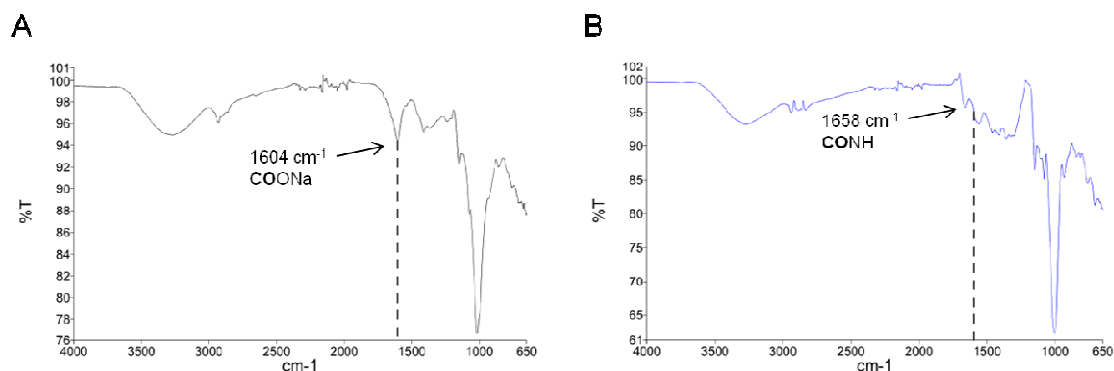


Figure 3.7 IR spectra of starch after oxidation = AnStarch (A, black) and after modification with PEI, CatStarch (B, blue).

As FT-IR measurements showed no absorbance of COONa (1604 cm^{-1}) from CatStarch (see Figure 3.7) all COONa groups seemed to be converted. However, the calculated result of $^1\text{H-NMR}$ was lower than expected. This deviation can be explained by the ability of starch and PEI for cross-linking as both species contain reactive sites (sodium carboxylate and amino groups).

3.3.1.2 Buffering capacity

A buffering capacity between pH 7.4 and 5.1 (endosomal pH-range) indicates the power of efficient endosomal escape. Hence, this parameter might be responsible for high transfection efficiencies. Through an acid-base titration, the endosomal buffering capacity was evaluated and visualized in Figure 3.8. Here, the rose colored area indicates the endosomal pH range. The required amount of HCl from pH 7.4 to pH 5.1 was determined and calculated according to Kim et al. [163].

Looking at the titration curve protamine shows a very weak buffering capacity. Only 25 μL of 0.1 M HCl ($\Delta_{\text{HCl}} = 25\ \mu\text{L}$) were used to cross the endosomal pH range and resulted in a buffering capacity of approximately 4 %.

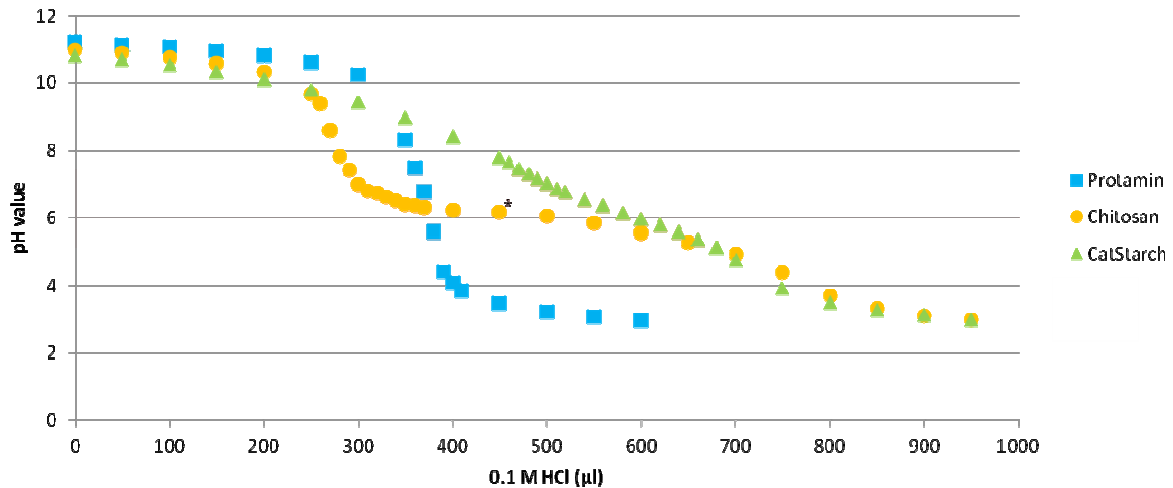


Figure 3.8 Buffering capacity by acidic titration of solved polymer: Protamine (blue), Chitosan (yellow) and CatStarch (green). * indicates a specific pH value: below pH 6.2 Chitosan is no longer soluble.

Whereas the two other polymers Chitosan ($\Delta V_{\text{HCl}} = 225^* - 400 \mu\text{L}$) and CatStarch ($\Delta V_{\text{HCl}} = 200 \mu\text{L}$) seem to have a higher ability to buffer the system between pH 7.4 and 5.1. Depending on the required amount of hydrogen chloride (acid) to decrease the pH from 7.4 to 5.1 a calculation of the buffering capacity is possible. Unfortunately, a proper evaluation of this value is not reliable (Buffering capacity: 7% - 12 %) since Chitosan is not soluble at a pH lower 6.2. The determination of CatStarch however, suffered from a precise analysis of the molecular weight. Consequently, a calculated buffering capacity between 6 and 34 % might be conceivable and is therefore contingent in meaning. Nevertheless, a possibly high endosomal buffering capacity might be one reason for sufficient transfection efficiencies.

3.3.1.3 EndoLISA

As the detection range of this assay ranges from 0.5 EU/mL to 500 EU/mL, all samples showed a lower content of endotoxins than 0.5 EU/mL with one exception. AnStarch revealed a slight endotoxin concentration of 0.15 EU/mL. As the reaction product (CatStarch) of this intermediate derivative contained no endotoxins, these results can be neglected. In conclusion, a possible immunogenic response of coated NPs cannot be explained by a contamination with endotoxins (see Chapter 5.2.29).

3.3.2 Characterization of coated PLGA NPs

3.3.2.1 Colloidal characteristics

For the sake of completeness coated and non-coated NPs, as well as flu-labeled and non-labeled NPs, were compared among each. Plain PLGA NPs show a mean size diameter of 130.4 ± 1.3 nm, a Pdl of 0.046 ± 0.005 and a negative ζ -potential of -32.6 ± 0.5 mV. Similar results were obtained for the labeled sample, but with a less strong ζ -potential of -21.1 ± 0.8 . These results can be explained by the presence of fluorescein which is covalently bound to the carboxyl group of the PLGA polymer.

Table 3.1 Colloidal characteristics (size, Pdl and ζ -potential) of non-labeled and flu-labeled (FA) coated (Prot, CS, CatSt) and non-coated PLGA NPs.

	PLGA NPs 			PLGA-Prot NPs 			PLGA-Cs NPs 			PLGA-CatSt NPs 		
	size [nm]	Pdl	ζ -potential [mV]	size [nm]	Pdl	ζ -potential [mV]	size [nm]	Pdl	ζ -potential [mV]	size [nm]	Pdl	ζ -potential [mV]
non-labeled	130.4 ± 1.28	0.046 ± 0.005	-32.6 ± 0.5	121.1 ± 1.1	0.046 ± 0.004	-13.7 ± 0.8	150.5 ± 1.2	0.092 ± 0.015	-32.2 ± 0.8	172.3 ± 2.7	0.072 ± 0.032	-37.0 ± 0.5
flu-labeled (FA)	126.0 ± 1.2	0.039 ± 0.008	-21.1 ± 0.8	122.9 ± 1.2	0.033 ± 0.018	-11.3 ± 0.4	145.3 ± 2.6	0.093 ± 0.014	-22.0 ± 0.3	136.0 ± 1.0	0.063 ± 0.021	-37.1 ± 0.5

As fluorescein occupies this functional group, it is no longer available to create a carboxylate. Hence, the surface charge of labeled NPs is less negative than of non-labeled NPs at a similar size and ζ -potential. A less charged PLGA-core and an associated increased hydrophobicity might also explain the decreased ζ -potential (from 32.2 ± 0.8 mV to 22.0 ± 0.3 mV) and a slightly varied aerodynamic diameter of PLGA-Cs NPs since fewer amounts of Chitosan bind to the PLGA. On the contrary, PLGA-CatStarch NPs showed a dropped mean diameter (from 172.3 ± 2.7 nm to 136.0 ± 1.0 nm) after the insertion of a fluorescent label. However, the surface charge of about 37 mV was retained.

Table 3.1 Colloidal characteristics of coated NPs in a dilution of 1:200 were measured via NTA analysis.

	PLGA-Prot	PLGA-Cs	PLGA-CatSt
mean [nm]	111.2 ± 3.2	117.0 ± 2.1	130.1 ± 5.6
mode [nm]	99.7 ± 5.0	106.0 ± 2.5	119 ± 8.8

Through steric hindrance the large starch derivative (see Chapter 3.3.1.1) may be associated differently to the PLGA-core, thus influenced the thickness of the coating and resulted in smaller particles. Colloidal characteristics of PLGA-Prot NPs, however, were hardly ever affected by the flu-labeled PLGA. Although showing a smaller diameter in general, the results (mean and mode) of the NTA analysis indicated the same trend: the higher the molecular weight of the coating material the larger the size of the coated NPs. Differences between mean and mode (mode value is approximately 10 nm smaller than mean) indicate a slight 'tailing' of the particle distribution which is typical for particle preparation methods which include a homogenization step. In conclusion, DLS is a fast and simple technique to analyze NPs, but the calculation is based on the hydrodynamic diameter which shows higher values than the 'real' state of NPs size.

3.3.2.2 SEM- and TEM imaging

Having a look at the morphology of the particles by a direct imaging technique, results of size measurements (DLS and NTA, see Chapter 3.3.2.1) shall be confirmed. Figure 3.9 shows a SEM micrograph of all three coated PLGA NPs. As expected PLGA-CatStarch NPs are larger than PLGA-Cs NPs and these are again larger than PLGA-Prot NPs. Considering the molecular weight of a coating material, the polymer with the higher molecular weight creates accordingly larger NPs. Despite the fact that the outer material of the NPs differs from another, all particles are approximately monodisperse and show a spherical shape with a smooth surface.

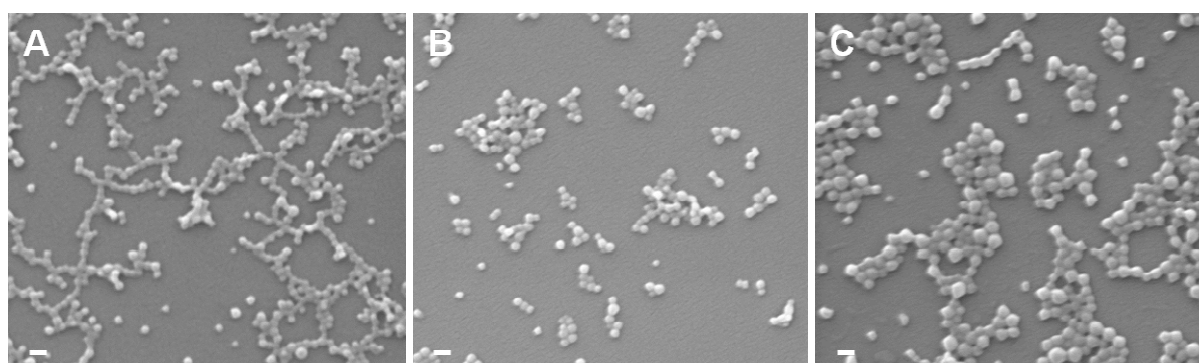


Figure 3.9 Scanning electron micrograph of Protamine-PLGA (A), Chitosan-PLGA (B) and CatStarch-PLGA nanoparticles (C). Scale bar: 200 nm.

Additional TEM images were made to indicate differences between flu-labeled and siRNA-loaded NPs. Having a look at Figure 3.10 Phosphotungstic acid worked well to visualize PLGA-based NPs (low electron density). Unfortunately, the staining created structural artifacts which impede a statement about the particle shape. Nevertheless, the particle size can be determined, and the largest diameter can be noticed for PLGA-CatSt NPs followed by PLGA-Cs and PLGA-Prot NPs (see Figure 3.10 A, B, and C).

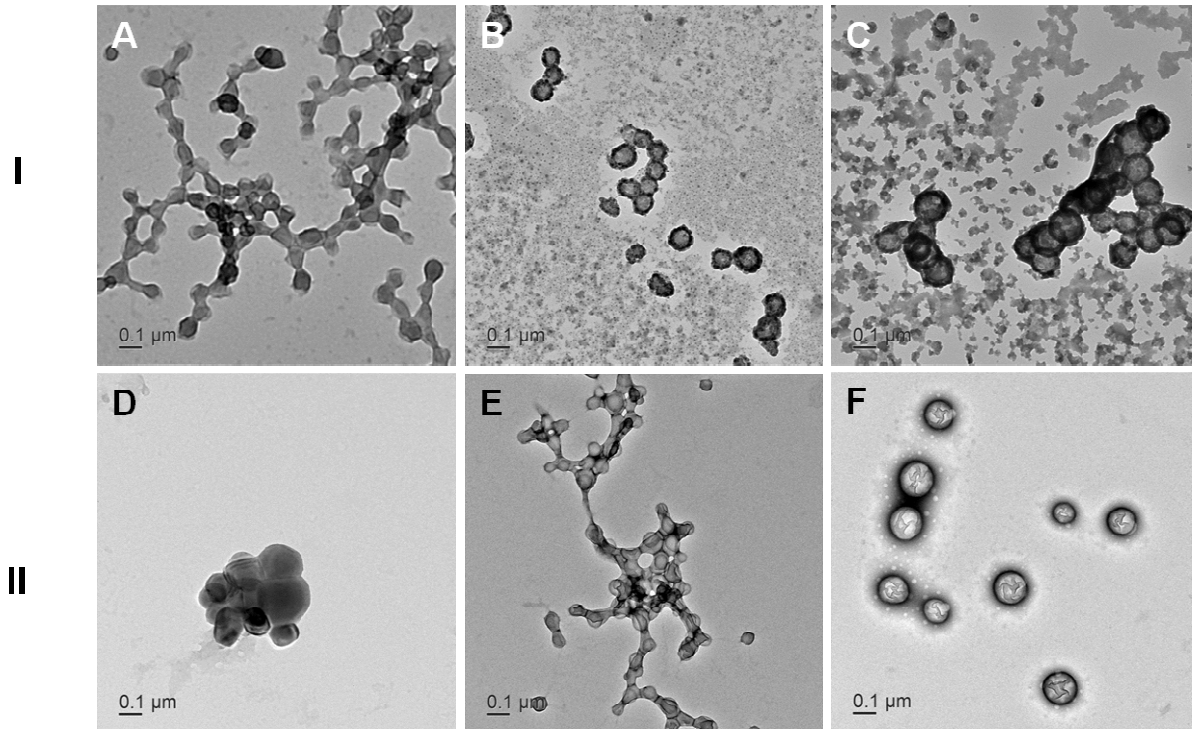


Figure 3.10 TEM-micrograph of non-labeled (I) and flu-labeled (II) PLGA NPs: Protamine-coated NPs (A/D), Chitosan-coated NPs (B/E) and CatStarch-coated NPs (C/F). Negative staining with 1% (w/w) Phosphotungstic acid.

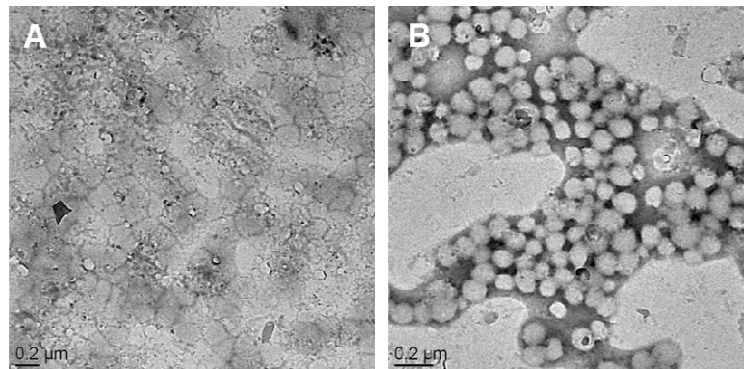


Figure 3.11 TEM-images of PLGA-CatSt (A) and ALEXA568-siRNA loaded (1:100) PLGA-CatSt NPs (B).

Interestingly, only PLGA-CatSt NPs could be depicted without a prior staining procedure (see Figure 3.11) by loading with ALEXA568siRNA in a ratio of 1:100 (siRNA: NPs). No PLGA-Prot and PLGA-Cs NPs particles could be detected.

3.3.2.3 'Washing' study

Based on previous examinations, where coated PLGA-Chitosan NPs seem to lose their cationic coating due to excessive washing, all three formulations were washed under harsh conditions and analyzed after each washing step. Chitosan-coated NPs showed the expected behavior of a gradually decreasing ζ -potential from 24.4 ± 0.5 mV to 1.2 ± 0.4 mV which was explained by a loss of Chitosan on the particle surface.

Table 3.2 Overview of colloidal characteristics of coated PLGA NPs after each washing step*

	PLGA-Protamine 			PLGA-Chitosan 			PLGA-CatStarch 		
	size [nm]	Pdl	ζ -pot. [mV]	size [nm]	Pdl	ζ -pot. [mV]	size [nm]	Pdl	ζ -pot. [mV]
as produced	122.3 ± 1.2	0.052 ± 0.012	16.3 ± 0.6	139.3 ± 1.1	0.125 ± 0.023	24.4 ± 0.5	177.9 ± 0.9	0.047 ± 0.027	38.4 ± 0.4
1 st washing step	153.5 ± 0.6	0.197 ± 0.008	30.3 ± 1.4	174.5 ± 1.1	0.235 ± 0.008	11.4 ± 0.3	182.3 ± 1.2	0.038 ± 0.025	45.3 ± 1.2
2 nd washing step	169.1 ± 0.7	0.218 ± 0.007	28.6 ± 0.1	207.0 ± 1.5	0.236 ± 0.011	6.5 ± 0.7	187.1 ± 0.8	0.040 ± 0.010	42.7 ± 1.1
3 rd washing step	133.9 ± 0.5	0.025 ± 0.012	23.9 ± 0.3	217.6 ± 2.0	0.293 ± 0.042	1.2 ± 0.4	191.5 ± 1.6	0.057 ± 0.014	39.1 ± 1.3

*one washing step: centrifugation of particle suspension (2 ml volume, 11000 rpm, 20 min, at 4^o C), throw supernatant and resuspension in 2 ml water

The almost neutral ζ -potential means a lack of stability and resulted in aggregation of the particles (Pdl: from 0.125 ± 0.023 to 0.293 ± 0.042). Interestingly, PLGA-Protamine and PLGA-CatStarch NPs showed a different behavior. Protamine-coated NPs showed an enlarged mean diameter due to aggregation after the first and second washing step but normalized again after the third one. Merely the surface charge remained at a higher level after washing. PLGA-CatStarch NPs seem to be a more robust carrier as colloidal characteristics did not change during all purification steps. Reason for that might be a stronger binding of the starch polymer on the PLGA. A rationale for the initial aggregation tendency of PLGA-Prot NPs followed by complete dispersal could not be found. Further investigations need to be conducted.

3.3.2.4 Quantification and release

With respect to Chapter 2.4.4, the loading efficiency of PLGA-Cs NPs could be investigated by an indirect UV-measurement of surface-bound siRNA. But trying to transfer this method to determine the amount of bound siRNA on of PLGA-Prot NPs and PLGA CatSt NPs failed.

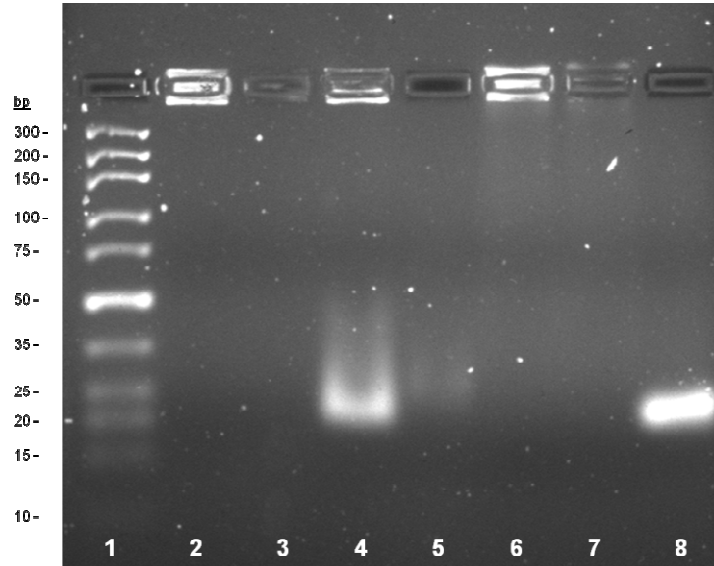


Figure 3.12 Agarose gel (5%) of loaded NPs and the corresponding supernatant; loading ration siRNA:NPs (1:50), 1 = Ultra Low range Ladder (300, 200, 150, 100, 75, 50, 35, 25, 20, 15, 10* bp), 2 = PLGA-Prot NPs, 3 = PLGA-Prot supernatant, 4 = PLGA-Cs NPs, 5 = PLGA-Cs supernatant, 6 = PLGA-CatSt NPs, 7 = PLGA-CatSt supernatant, 8 = 0.5 µg siRNA, stained with 0.5 µg/mL ethidium bromide. * band is not visible within this gel

With the help of gel electrophoresis, the binding behavior of siRNA on the carrier system was investigated. For this purpose nanoparticle suspensions and the corresponding supernatants were applied on a 5 % agarose gel (see Figure 3.12).

To begin with the employed siRNA contained 21bp. In Figure 3.12 the band could be found slightly above the 20 base pairs (bp) band (line 8: between 20 and 25 bp) and marked as an intact sample of nucleic acids. Having a look at the particles (line 2, 4, 6) all samples showed a signal inside the agarose pocket. When siRNA was bound on the particle, the applied potential for electrophoresis had no impact as particles were too large to penetrate through the gel and the cargo remained at the starting point. Merely the PLGA-Cs sample behaved slightly different: The observation that one relatively broad band was visible between 20 and 25 bp implied a weak binding

behavior of the cargo. Based on the applied potential siRNA was removed from the particles and pulled into the agarose gel. A minor bold particle signal at the pocket might be possible because of an unspecific binding of ethidium bromide (only Chitosan-coated NPs showed an unspecific binding with fluorescent dyes, see Chapter 2.4.4, Figure 2.22).

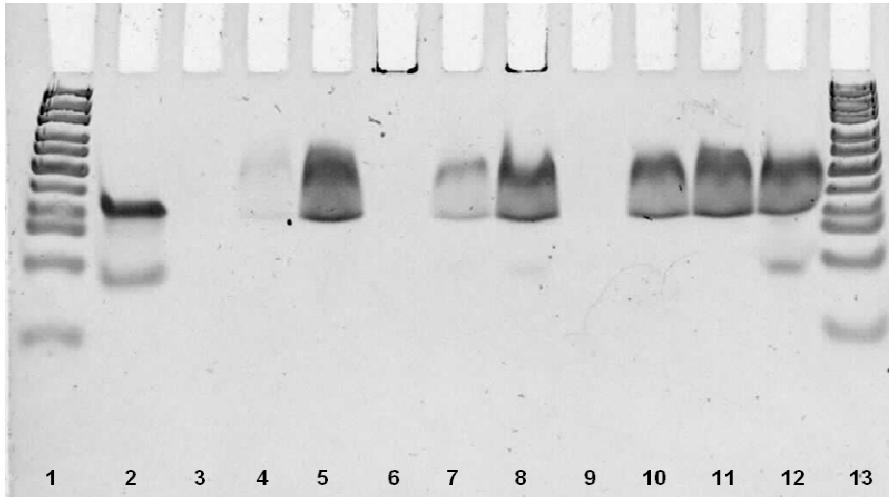


Figure 3.13 TBE gel (1x) of blank NPs, loaded NPs and the supernatant of loaded NPs treated with 10 U heparine (hep) per sample; loading ratio siRNA:NPs (1:50), 1 = Ultra-Low range Ladder (300, 200, 150, 100, 75, **50**, 35, 25, 20, 15, 10 bp), 2 = 0.2 µg siRNA, 3 = blank PLGA-Prot NPs + hep, 4 = PLGA-Prot supernatant + hep, 5 = loaded PLGA-Prot NPs + hep, 6 = blank PLGA-Cs NPs + hep, 7 = PLGA-Cs supernatant + hep, 8 = loaded PLGA-Cs NPs + hep, 9 = blank PLGA-CatSt NPs + hep, 10 = PLGA-CatSt supernatant + hep, 11 = loaded PLGA-CatSt NPs + hep, 12 = 0.2 µg siRNA + hep, 13 = Ultra Low range Ladder; stained with 0.5 µg/mL ethidium bromide.

The analysis of the PLGA-Cs supernatant showed a slight siRNA signal, so that an indirect quantification for this particle was feasible. The supernatant of PLGA-Prot and PLGA-CatSt NPs contained no measurable quantities of siRNA. For gel electrophoresis, 1 x TBE gels were used to obtain a higher resolution of the bands. To see if siRNA was bound on the particle surface, siRNA was released by the addition of 10 U heparin per sample (see Figure 3.13).

A comparison between line 2 and 12 showed an increased width of the siRNA signal (between 20 and 25 bp) after the addition of heparin. The second fainter band of these samples (< 15 bp) might be a signal of single-stranded molecules within the sample. As no siRNA occurred in the blank samples, no bands could be visualized in line 3, 6 and 9. Only blank PLGA-Cs NPs (line 6) showed an unspecific binding with

the ethidium bromide. Line 5, 8 and 11 indicated an almost complete release of the siRNA from the coated NPs. The signal intensity of all samples was located in the same range compared to the siRNA sample (line 12). Having a look at the supernatants of loaded NPs (line 4, 7, 10) PLGA-Prot seem to have bound the highest amount of siRNA on the particle surface. Hence, the band of the sample is the weakest one. Following this, most unbound siRNA could be found in the supernatant of PLGA-CatSt NPs which indicates that less siRNA is bound on PLGA-CatSt NPs compared to PLGA-Cs NPs and PLGA-Prot NPs. Further investigations by another quantification method need to confirm the results of the gel electrophoresis.

Fluorescence correlation spectroscopy was used to analyze the release profile of the DDSs in RPMI buffer (see Figure 3.14). In HEPES buffer all loaded carriers were stable and showed only a minor release of siRNA only (5 % - 9 %). As PLGA-Cs NPs and PLGA-CatSt NPs showed a burst release, which remained stable after 24 hours, a time dependent release from ~30 % after 1 hour to ~60 % after 24 hours and ~70 % after 48 hours at 37 °C was observed for PLGA-Prot NPs. Further investigations could be performed via single particle tracking technique to receive more information about the particulate system.

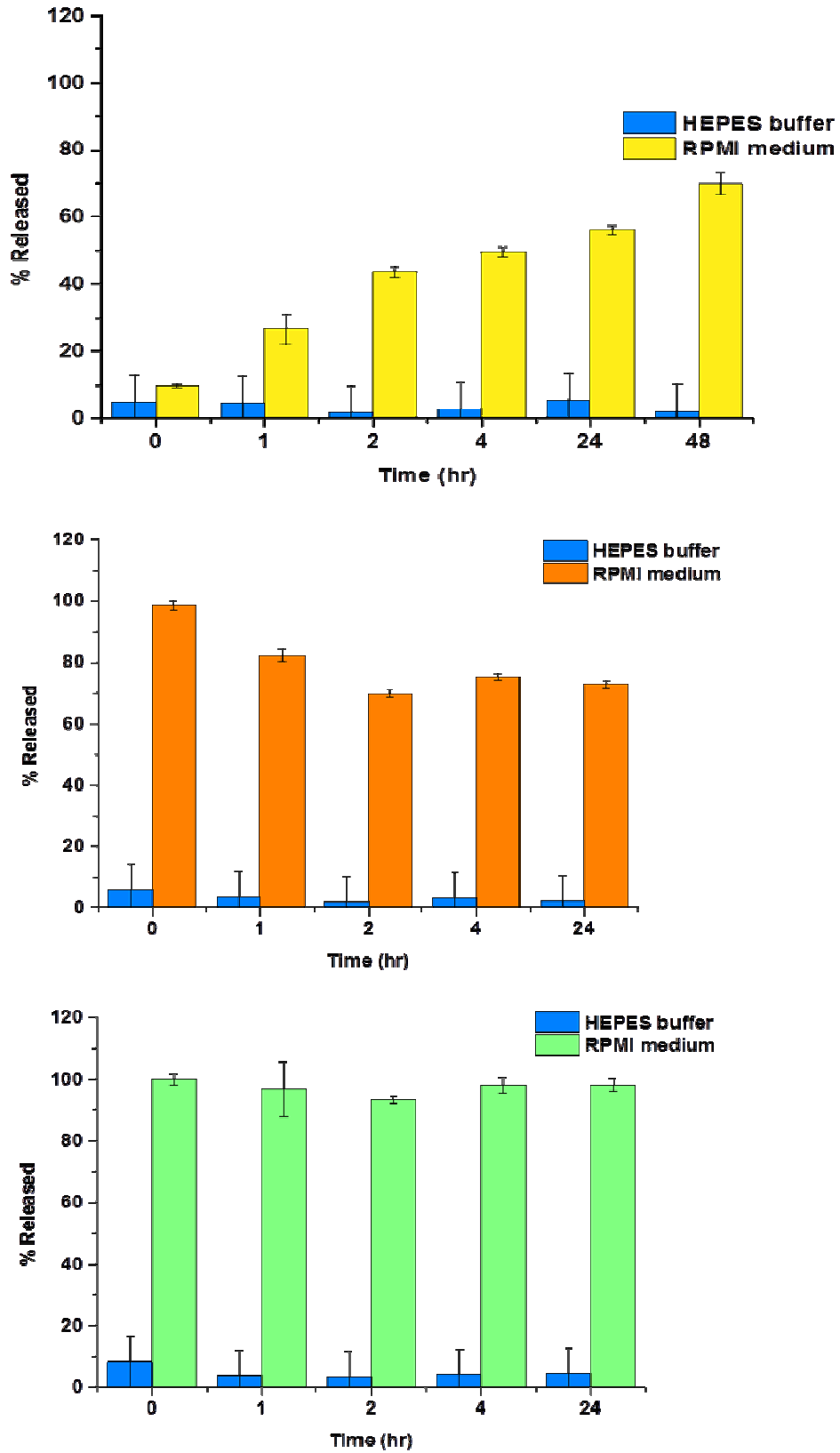


Figure 3.14 Release profile by FCS analysis of siRNA-loaded (siRNA:NP ratio = 1:100) PLGA-based NPs in RPMI medium: PLGA-Prot (yellow), PLGA-Cs (orange), PLGA-CatSt (green); Blue bars indicate the release in HEPES buffer as negative control.

3.3.2.5 Bleaching effect on flu-labeled NPs

After the preparation of coated FA-PLGA NPs, the resulting suspensions appeared obviously different from one another (see Figure 3.15). Especially PLGA-CatSt NPs showed an intense yellow color which was fading while increasing light exposure. This observation was less pronounced for PLGA-Prot NPs and hardly visible for PLGA-Cs NPs. As the flu-label is only bound on the PLGA a different color (absorption) of the NPs might be accomplished by a different binding behavior of the cationic polymers based on interactions with the covalently bound fluorescein.

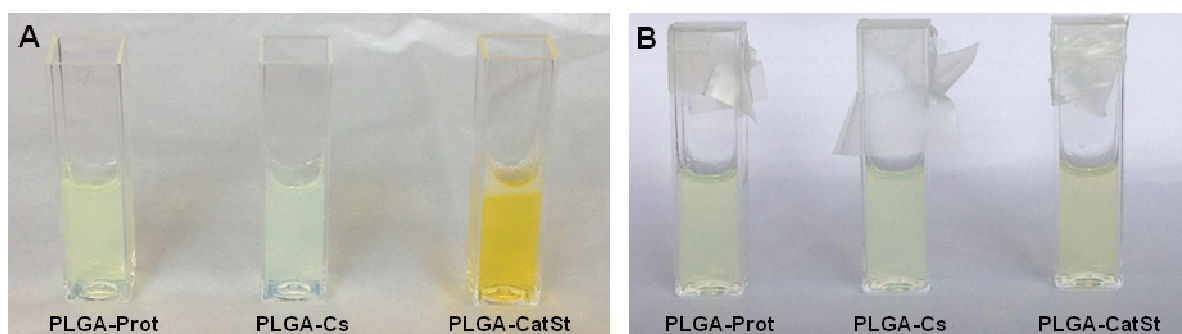


Figure 3.15 Bleaching effect of coated FA-PLGA NPs, A: freshly prepared NPs, B: NPs after 2 weeks of light exposure (full bleaching).

3.4 Conclusion

The emulsion-diffusion-evaporation technique to create PLGA-Cs NPs can be applied for the preparation of Protamine- and CatStarch-coated PLGA NPs. All resulting NPs showed suitable colloidal characteristics (particle size < 200 nm, a positive surface charge, Pdl < 0.2), which were preferable for the uptake of nanoparticles. Using the same amount of cationic polymer, respectively, allows a direct comparison of the different formulations. The higher the molecular weight of the coating material, the larger the resulting NPs (probably due to a thicker polymer shell). In the same order surface charges increase from PLGA-Prot NPs with the lowest ζ -potential of ~ 15 mV over PLGA-Cs NPs with ~ 30 mV to PLGA-CatSt NPs with the highest ζ -potential of 37 mV. Although the method for receiving a cationic coating remains the same, the binding of the cationic polymers differs depending on the applied material. In this context, it is possible to wash off certain amounts of

chitosan whereas Protamine and CatStach stay unaffected at the particle surface. Merely the rising ζ -potential of PLGA-Prot NPs after the first washing step remains undeclared.

Gel electrophoresis of siRNA-loaded and released (displaced by heparin) siRNA-loaded particles indicated that high loading efficiencies were not only based on possibly high surface charges. The interaction between siRNA and cationic polymer seemed to be one further influencing factor. Again a less strong binding of chitosan and consequently siRNA could be confirmed, as the electrical potential was able to drag the cargo off from the particles. However, PLGA-Prot and PLGA-CatSt NPs and the corresponding supernatants showed no siRNA signal. After the release of bound siRNA with heparin, all particles released approximately the same amount of applied siRNA. Analyzing the released samples of the particle supernatant, PLGA-CatSt NPs bound the highest amount of siRNA within the surrounded fluid followed by PLGA-Cs NPs and PLGA-Prot NPs. A formation of small siRNA-polyplexes with the available cationic polymer might be one possible explanation for the release of siRNA without the presence of the PLGA-based DDS.

Furthermore, a difference in buffering capacity for the three cationic polymers could be shown. Considering that gene delivery activity can be referred to a balance between the buffering capacity of a polymer (indicating the potential for endosomal escape) and the strength of interactions between polymer and nucleic acids [168] the transfection efficiency of a system is based on more than one attribute. If these differences in buffering capacity can also be seen in an endosomal escape assay, a direct correlation might be confirmed. Nonetheless, transfection studies on different lung specific cells are essential to prove the efficiency of a drug delivery system.

Chapter 4 - Stability of drug delivery systems for pulmonary application

The author of this thesis made the following contribution to this chapter:

Planned and performed all experiments related to particle stability, analyzed all the data from the mentioned studies, interpreted all experimental data and wrote the chapter, it not stated otherwise.

4.1 Introduction

Since the invention of first metered dose inhaler (MDI) in the 1950s [169] an application of drugs via the lung has become a feasible option. By now an inhalation therapy with anticholinergics [e.g. Tiotropium bromide (Spiriva[®]), Ipratropium bromide (Atrovent[®])] β_2 -adrenergic agonists [e.g. Fenoterol (Berotec[®] N), Salbutamol (Ventolin[™])] or glucocorticoids [e.g. Beclometasone dipropionate (Qvar[®])] belong to the standard therapeutic recommendation for diseases like COPD or asthma. Nevertheless, a successful pulmonary delivery of biomacromolecules (proteins, peptides, and nucleic acids; see Chapter 1.1.1) is still pending.

Depending on the drug or the employed carrier system and the potential patient group different inhalation devices may be suitable for a proper pulmonary application. Nowadays, four different main groups of therapeutic inhalation devices are available: dry powder inhaler (DPI), pressurized metered dose inhaler (MDI), Respimat[®] and nebulizer. DPIs (e.g. Breezhaler[®], Diskus[®], Easyhaler[®], Genuair[®], Handihaler[®], NEXThaler[®], Novolizer[®], Turbohaler[®]) are convenient and portable inhalation devices. The drug deposition occurs breath-actuated by a fast and deep breath. Consequently, less patient coordination is required [170]. However, additional excipients (e.g. lactose) are necessary, plus the delivery of high doses is difficult. MDIs, by contrast, use a propellant for aerosolization. Thus patient coordination is essential (non-breath actuated: simultaneous deep breath and triggering of the aerosol formation) and just like DPIs the delivery of high doses is limited. The Respimat[®] established the group of soft mist inhaler (SMI), which enlarges the dwelling time of the aerosol and minimizes the failure due to missing patient coordination. In general, it is an advanced MDI. With a nebulizer (e.g. Aeronex[®] Go, eFlow[®] rapid, I-neb[®], AKITA[®] jet, PARI Boy[®]) it is possible to inhale high doses completely without necessary patient coordination. They are particularly suitable for the therapy of children. But these devices are not handy and preferably made for domestic use.

Advanced inhalation devices produce an aerosol with a mean particle or droplet sizes of around a few μm to allow an efficient and precise aerosol deposition in the deep lungs (= pulmonary) for either topical or systemic delivery. Studies showed that the aerodynamic diameter determines the place of deposition in the human respiratory

tract [87, 171]. In Figure 4.1 the deposition fraction of inhaled aerosol is plotted against particle diameter and respiratory region (head airways, trachea-bronchial and pulmonary).

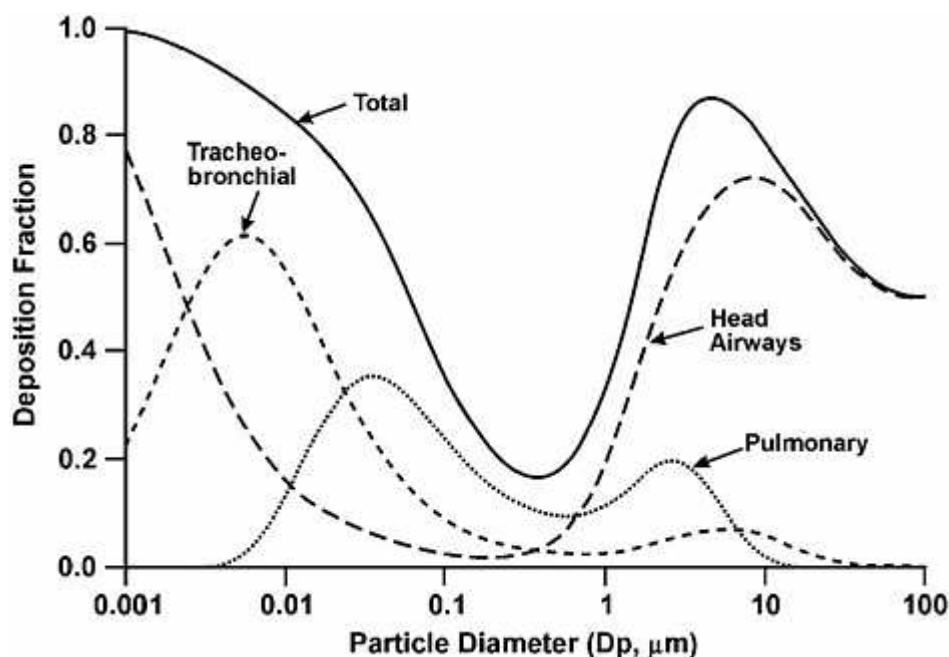


Figure 4.1 Fractional regional deposition of inhaled particles in the human respiratory tract (Snipes 1994). Reprinted with permission from Medical Physics Publishing, Madison, Wisconsin.”[171, 172]

As properties like particle size, the maximum amount of substances, microbial stability and storage stability may preclude a certain inhalation device, the focus in this chapter is put on the stability of the DDSs during storage, after lyophilization and after aerosolization via a nebulization device.

4.2 Materials and methods

Trehalose dihydrate (α,α -Trehalose; CAS No: 6138-23-4) was purchased from Sigma-Aldrich, USA; Ribonuclease A (RNase A) 17500U, 2.5 mL from Qiagen. Purified water was produced by Milli-Q water purification system from Merck Millipore, USA.

Colloidal characteristics of all NP suspensions before and after nebulization were measured concerning the described method in Chapter 2.3.1. and were conducted in triplicates.

4.2.1 Storage stability

For later applications, this carrier system needs possibly long storage stability due to the required post-loading mechanism. If a particulate carrier is not sufficiently stable for storage, this may limit the application of a whole DDS. In our case, the cargo can be stored separately freeze-dried apart from the carrier system and can be used directly before the loading step. Thus, a possible loss of cargo activity is limited. To investigate the storage stability of the particles at different storage conditions (4 °C, RT and 37 °C), prepared NPs suspension in a concentration of 2 mg/mL were observed. Samples were measured at different times up to 35 days (5 weeks). To ensure that variances are solely based on the storage temperature, samples were protected and sealed against light exposure, inadvertently shaking and contaminations.

4.2.2 Freeze dried NPs

As we know that PLGA-based NPs are not suitable to be stored at -20 °C (creation of solid aggregates), NP suspensions were freeze-dried (Alpha 2-4, Martin Christ GmbH, Germany) overnight with different amounts of trehalose as cryoprotectant to obtain a possible storage of the NPs as a dry powder. After lyophilization, an adequate amount of Milli-Q purified water was added to obtain the native sample concentration of redispersed particles. Particle characteristics were determined approximately 15 min. after water addition.

4.2.3 Nebulization

As the stability of a DDS after nebulization is mainly dependent on the applied nebulization method, three different devices were investigated. Here, one device for *in-vitro*, *in-vivo* and a therapeutic application was selected respectively. The Aeroneb[®] Lab Nebulizer from Aerogen (Figure 4.2) was chosen for its ability to deposit a defined volume of the DDS directly on an *in-vitro* cell culture model (nebulizer unit fits on a 12-well cell culture plate). An OnQ[®] Aerosol Generator creates a low-velocity aerosol with fine droplets by imbibing the liquid through a

vibrating (micro pumping action) domed aperture plate with precise holes. Here, the small volumetric mean diameter (VMD) nebulizer unit with a particle size between 2.5 and 4.0 μm , a flow rate $> 0.1 \text{ mL/min}$ and a residual volume $> 0.2 \text{ mL}$ was used (values taken from the instruction manual). As samples for *in-vitro* testing need to be filtered (Minisart[®] Syringe filter 0.2 μm from Sartorius Stedim Biotech GmbH, Germany) prior to usage, filtered and filtered+nebulized samples were measured. A total volume of 2 mL of each NP suspension (concentration: 2 mg/mL) was nebulized, and the resulting mist was collected with the help of a 50 mL falcon tube (from greiner bio-one GmbH, Germany).



Figure 4.2 Aeroneb[®] Lab Micropump Nebulizer (A) from Aerogen (www.aerogen.com), Small Volumetric Mean Diameter (VMD = 2.5 – 4.0 μm) Nebulizer Unit (B), OnQ[®] Aerosol Generator (C).

The second considered device was the MicroSprayer[®] from Penn-Century (see Figure XA). Within COMPACT *in-vivo* studies (in cooperation with our partner (P8) at University of Vienna) were planned as long as the DDS showed no significant deviations in size and surface charge after nebulization. To create an aerosol, the liquid (25 - 250 μL) is forced out air-free (with a high-pressure syringe) through the passageways and emerges as a fine mist at the very tip (inner diameter: 60 μm). This device is assigned for intratracheal (intrapulmonary) liquid application in mice (see Figure 4.3 B) and creates droplets with a mass mean diameter (MMD) between 16 and 22 μm . Again unfiltered, filtered (Steriflip[®]-GP filter unit 0.22 μm from Merck, Millipore) and filtered + nebulized samples (concentration: 2 mg/mL) were measured. Here, the total syringe volume of 250 μL was nebulized and collected into 15 mL

falcon tubes (from greiner bio-one GmbH, Germany). This procedure was repeated until a total volume of 2 mL was accrued.



Figure 4.3 MicroSprayer[®] (215) 753-6540 (FMJ-250 High Pressure syringe; Model IA-IC Intratracheal Aerolizer) from Penn-Century (www.penncentury.com); MicroSprayer[®] aerosol cloud (A) and in-vivo application in mice (B).

An established inhalation device for the therapeutic application of drugs or physiologic saline solution in humans (e.g. for a patient with cystic fibrosis/mucoviscidosis) is the eFlow[®] rapid nebulizer from PARI GmbH, Germany (see Figure 4.4). Referred to the technical data sheet a volume between 2.0 and 6.0 mL is converted into an aerosol with a MMD of 4.1 μm via a perforated oscillating membrane (aerosol head 30; oscillating frequency: 117 kHz) to reach the lower respiratory tract.

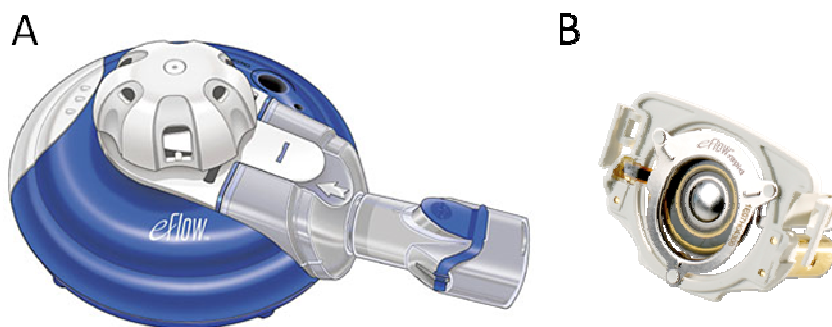


Figure 4.4 eFlow[®] rapid nebulizer system (A) from PARI (www.pari.com), aerosol head (B).

Aerosol heads with different perforated membranes (20, 30, 35 and 45; numbers describe the size of membrane perforations in μm) could be investigated. According to the manufacturer, the commercially available eFlow[®] rapid contains a 30 μm

aerosol head solely. Again 2 mL-samples (concentration: 2 mg/mL) were nebulized and collected into 50 mL falcon tubes (from greiner bio-one GmbH, Germany). Here, the same initial NP samples were used for stability studies with the Aeroneb[®] Lab and eFlow[®] rapid device.

4.3 Results and discussion

4.3.1 NPs stability at 4 °C, RT and 37 °C

Coated PLGA NPs were stored in suspension at 4 °C, RT, and 37 °C to investigate how far the coating material and thus the particle size and ζ -potential is affected by different storage conditions over time. Figure 4.5 shows changes in both parameters over a 35 day period after preparation. Comparing storage conditions at 4 °C and RT no significant changes in size or ζ -potential apart from the PLGA-Chitosan sample which shows a reduced ζ -potential from 25.7 ± 0.4 mV (day 28) to 17.8 ± 1.0 mV after 35 days could be revealed. Merely an enduring storage temperature of 37 °C has a coherent influence on particle stability. After 5 weeks a reduced surface charge could be noticed for all coated NPs: PLGA-Prot NPs from 13.8 ± 0.1 nm (day 1) to 8.1 ± 0.5 nm (day 35); PLGA-Cs NPs from 27.2 ± 0.2 nm (day 1) to 16.3 ± 3.7 nm (day 35); PLGA-CatStarch NPs from 37.2 ± 0.3 nm (day 1) to 26.8 ± 0.1 nm (day 35). Moreover, the hydrodynamic diameter of all three coated particle samples was decreased: PLGA-Prot NPs from 125.1 ± 0.6 nm (day 1) to 110.2 ± 0.3 nm (day 35); PLGA-Cs NPs from 141.5 ± 0.9 nm (day 1) to 111.8 ± 0.9 nm (day 35); PLGA-CatSt NPs from 163.8 ± 1.7 nm (day 1) to 147.2 ± 1.6 nm (day 35).

Noticeably, PLGA-Prot and PLGA-Cs NPs showed a similar particle size after 35 days. As uncoated PLGA NPs have a diameter of around 130 nm (see chapter 3.3.2) and the surface charge of these particles is still positive after 5 weeks, the reduced size of the coated NPs can not only be explained by a degraded coating. The presence of a sheer inner PLGA core covered with a gradually increasing concentration of the cationic material PLGA and PVOH (outer shell) seems to be likely.

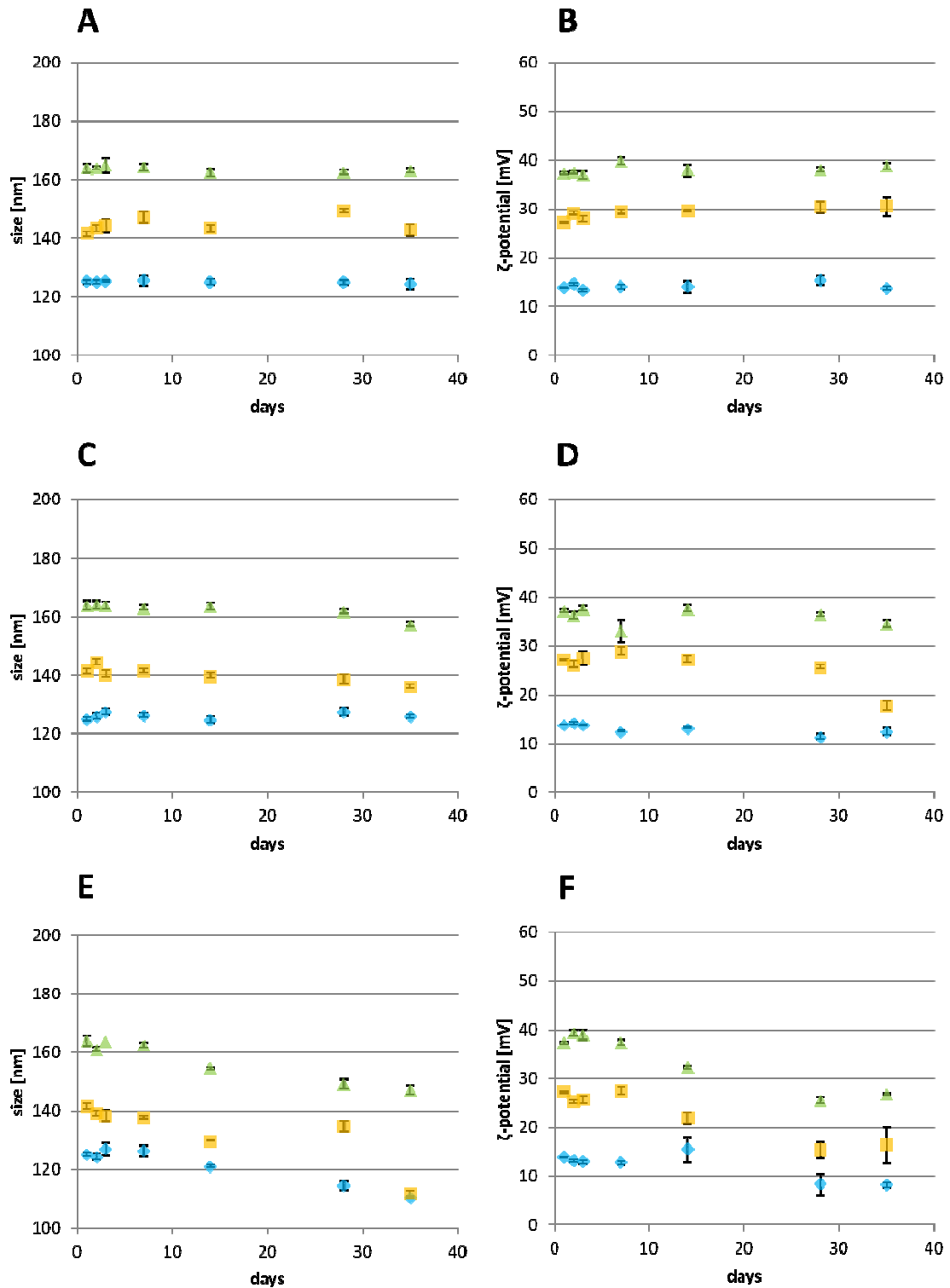


Figure 4.5 Storage stability: changes in size (A/C/E) and ζ -potential (B/D/F) of coated PLGA NPs at 4° C (A/B), RT (C/D) and 37 °C (E/F) over a 35 days' period. Blue = PLGA-Prot NPs, yellow = PLGA-Cs NPs, green = PLGA-CatSt NPs.

Figure 4.6 shows a SEM micrograph of coated PLGA NPs after preparation (I: A/B/C) and after 6 weeks at 37 °C (II: D/E/F). After storage, the surface of the particles appeared vague, less smooth and a little bit smaller. The reduced amount of particles resulted probably due to the sample preparation. The washing step to get rid of PVOH seemed to affect the stored particles more than the freshly prepared ones.

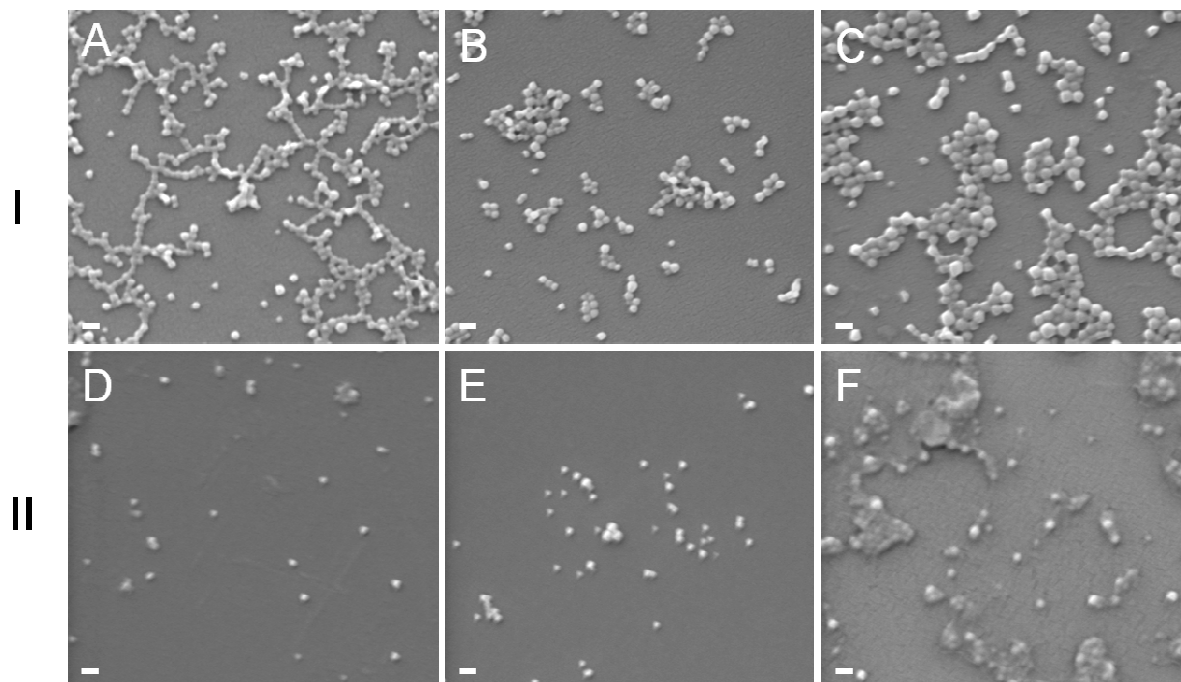


Figure 4.6 SEM micrographs of coated PLGA NPs as produced (I) and after storage for 6 weeks at 37 °C (II): PLGA-Prot NPs (A/D), PLGA-Cs NPs (B/E) and PLGA-CatSt NPs (C/F). Scale bar: 200 nm.

4.3.2 Re-dispersibility after lyophilization

To investigate whether freeze-drying affected NP characteristics native and coated PLGA NPs were analyzed. Here, different amounts of trehalose (up to 1.0%) were taken into consideration and the most favorable combination was marked by colored boxes (see Table 4.1). For PLGA and PLGA-CatSt NPs an addition of a cryoprotectant is not mandatory. Merely an increased negative ζ -potential of non-coated NP from -22.5 ± 0.6 mV to -35.7 ± 1.7 mV could be observed, but normalized when a little trehalose is present. For PLGA-Prot NP a minimum amount of 0.2% (w/w) trehalose is needed to prevent aggregation of the NPs from 122.3 ± 1.2 nm and a Pdl of 0.052 ± 0.012 to 149.0 ± 1.2 nm a Pdl of 0.182 ± 0.008 . It is more problematic to freeze-dry and re-disperse PLGA-Cs NPs. Even with 1.0% (w/w)

trehalose an increased mean particle size could admittedly be revised but not completely prevented.

Table 4.1 Properties of different NPs after lyophilization and re-dispersion with Milli-Q water. Colored frames mark the minimum quantity of trehalose in %(w/w) as cryoprotectant [grey = PLGA NPs; blue = PLGA-Prot NPs; orange = PLGA-Cs NPs; green = PLGA-CatSt NPs].

	PLGA NPs			PLGA-Protamine NPs			PLGA-Chitosan NPs			PLGA-CatStarch NPs		
	size [nm]	Pdl	ζ-potential [mV]	size [nm]	Pdl	ζ-potential [mV]	size [nm]	Pdl	ζ-potential [mV]	size [nm]	Pdl	ζ-potential [mV]
particles as produced	128.4 ± 1.0	0.049 ± 0.010	-22.5 ± 0.6	122.3 ± 1.2	0.052 ± 0.012	16.3 ± 0.6	139.3 ± 1.1	0.125 ± 0.023	24.4 ± 0.5	177.9 ± 0.9	0.047 ± 0.027	38.4 ± 0.4
without cryoprotectant	129.6 ± 1.1	0.043 ± 0.004	-35.7 ± 1.7	149.0 ± 1.7	0.182 ± 0.008	13.1 ± 1.7	192.1 ± 1.2	0.174 ± 0.020	51.2 ± 0.5	179.9 ± 1.7	0.038 ± 0.013	36.7 ± 0.9
+ 0.2% trehalose	129.2 ± 0.8	0.046 ± 0.024	-27.8 ± 0.4	125.6 ± 1.2	0.062 ± 0.015	18.7 ± 0.7	185.5 ± 0.6	0.158 ± 0.018	50.7 ± 1.2	179.5 ± 1.0	0.055 ± 0.015	33.7 ± 0.3
+ 0.5% trehalose	127.5 ± 1.2	0.062 ± 0.020	-25.6 ± 0.6	122.7 ± 0.2	0.050 ± 0.012	16.5 ± 0.6	173.8 ± 1.5	0.171 ± 0.005	49.0 ± 1.1	180.3 ± 0.7	0.055 ± 0.020	37.3 ± 0.7
+ 1.0% trehalose	129.0 ± 1.0	0.049 ± 0.010	-23.9 ± 0.8	122.6 ± 0.5	0.053 ± 0.003	15.6 ± 0.5	161.9 ± 0.7	0.170 ± 0.008	45.6 ± 0.6	180.4 ± 1.6	0.048 ± 0.014	37.3 ± 0.4

Furthermore, the lyophilization process itself seems to change the surface charge from 24.4 ± 0.5 mV for freshly prepared NPs to 51.2 ± 0.5 mV for treated NPs without cryoprotectant. Anyhow, the more trehalose is added, the more values for size and ζ-potential are brought closer to the results of untreated NPs.

4.3.3 Stability after nebulization

For later transfection studies on cell culture models under ALI (air-liquid interface) conditions NP stability after nebulization with the Aeronex[®] Lab was investigated (see Table 4.2). Beforehand a filtration step through a 0.2 μm cellulose acetate (surfactant-free) membrane did not affect a single one of the NP suspensions. This filterability indicates an adequate and complete preparation procedure (see Chapter 2.2.2 and 3.2.3) without forming bigger polymer aggregates. After atomization, only PLGA-CatSt NPs did not change and retained prior particle characteristics. Whereas PLGA-Prot NPs apparently aggregate from a mean diameter of $124.6 \text{ nm} \pm 1.3 \text{ nm}$ to $158.1 \text{ nm} \pm 0.7 \text{ nm}$ and a Pdl from 0.049 ± 0.030 to 0.154 ± 0.021 , PLGA-Cs NPs additionally showed an increased ζ-potential from 31.6 ± 0.4 mV to 53.2 ± 0.5 mV.

Table 4.2 Stability: NPs characteristics after nebulization via Aeroneb® Lab device. Filtration happened through a Minisart® syringe filter, 0.2 µm cellulose acetate (CA) membrane.

	PLGA-Prot NPs 			PLGA-Cs NPs 			PLGA-CatSt NPs 		
	size [nm]	Pdl	ζ-potential [mV]	size [nm]	Pdl	ζ-potential [mV]	size [nm]	Pdl	ζ-potential [mV]
as produced	126.0 ± 1.5	0.047 ± 0.023	16.7 ± 0.2	143.6 ± 3.6	0.129 ± 0.024	35.4 ± 2.2	157.6 ± 1.5	0.035 ± 0.012	54.1 ± 0.2
filtrated	124.6 ± 1.3	0.049 ± 0.030	16.1 ± 0.4	145.7 ± 1.2	0.081 ± 0.012	31.6 ± 0.4	156.9 ± 1.2	0.042 ± 0.022	53.3 ± 0.5
filtrated + nebulized	158.1 ± 0.7	0.154 ± 0.021	16.2 ± 0.6	160.9 ± 1.4	0.194 ± 0.008	53.2 ± 0.5	156.7 ± 1.8	0.012 ± 0.007	55.1 ± 0.9

For later *in-vivo* applications all coated PLGA NPs and blank PLGA NP seem to be suitable as no changes in size or surface charge could be observed (see Table 4.3). Merely the ζ-potential of PLGA-NPs shifted from -31.3 ± 0.8 mV to -19.3 ± 1.0 mV after filtration. This issue can be explained by possible binding processes of ions onto the filter membrane. Since the MicroSprayer® creates bigger droplets for intratracheal applications with a $MMD_{\text{MicroSprayer}}$ of 19 – 22 µm (compared to a VMD_{Aeroneb} of 2.5 - 4.0 µm and a $MMD_{\text{eFlow}} = 4.1$ µm) less distinct variances were expected. Furthermore, the atomization of the MicroSprayer® was subject to another method (see Chapter 4.2.3) and deviations became evident.

Table 4.3 Stability: NPs characteristics after nebulization via MicroSprayer® device. Filtration happened through a Steriflip®-GP filtration unit, 0.22 µm polyethersulfone (PES) membrane.

	PLGA NPs 			PLGA-Prot NPs 			PLGA-Cs NPs 			PLGA-CatSt NPs 		
	size [nm]	Pdl	ζ-potential [mV]	size [nm]	Pdl	ζ-potential [mV]	size [nm]	Pdl	ζ-potential [mV]	size [nm]	Pdl	ζ-potential [mV]
as produced	130.7 ± 1.2	0.054 ± 0.006	-31.3 ± 0.8	127.2 ± 0.7	0.047 ± 0.009	13.7 ± 0.7	150.4 ± 1.3	0.116 ± 0.012	25.0 ± 0.8	177.3 ± 2.0	0.054 ± 0.016	37.1 ± 0.9
filtrated	130.1 ± 1.4	0.038 ± 0.022	-19.3 ± 1.0	127.9 ± 1.9	0.025 ± 0.013	13.5 ± 0.5	149.5 ± 2.9	0.121 ± 0.029	24.2 ± 0.3	175.5 ± 2.5	0.036 ± 0.017	36.8 ± 0.6
filtrated + nebulized	129.1 ± 1.6	0.054 ± 0.005	-21.5 ± 0.9	128.0 ± 0.6	0.039 ± 0.012	12.2 ± 0.5	149.1 ± 3.4	0.116 ± 0.009	28.2 ± 3.4	175.8 ± 2.4	0.040 ± 0.009	34.4 ± 0.2

Exact results of freshly produced and filtrated NPs are displayed in Table 4.2 (same NP batch was used for studies with Aeroneb® Lab and eFlow®). Figure 4.7 shows a bar chart of coated PLGA NP: the mean particle size diameter and Pdl were plotted against the utilized aerosol head. As expected the membrane with the smallest

perforations ('25') showed the biggest impact on the particles. Nevertheless, the used aerosol head PLGA-CatSt NPs remain its initial size and Pdl around 157 nm and a Pdl of ~ 0.040 . PLGA-Prot NPs, however, showed a remarkable increase in size and Pdl from ~ 125 nm, Pdl ~ 0.050 to 160 – 230 nm, Pdl > 0.2). A nebulization of PLGA-Cs NPs is only acceptable (152.0 ± 1.2 nm, Pdl: 0.147 ± 0.021) when using a '45' aerosol head. Smaller perforated membranes resulted in NP aggregates of ~ 145 nm with a Pdl ~ 0.100 . Results of the surface charge were not shown since no change of the ζ -potential was apparent.

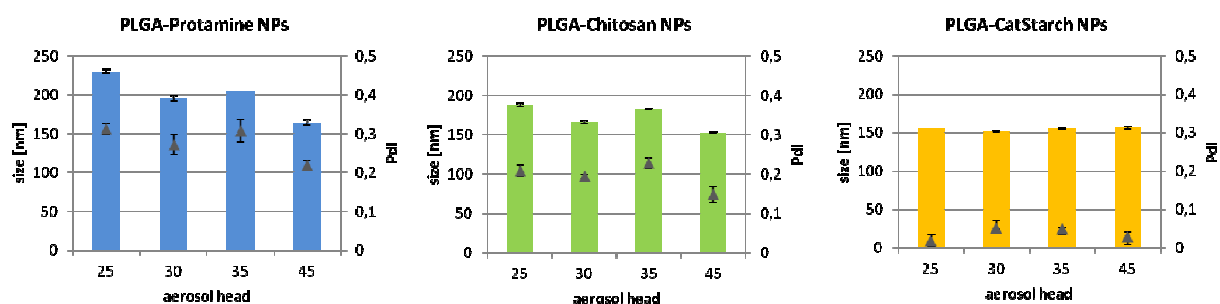


Figure 4.7 Comparison of nebulization stability (mean size and size distribution) depending on aerosol head (low number = small droplets) of PARI eFlow[®] rapid device and particle type. PLGA-Protamine (blue), PLGA-Chitosan (green), PLGA-CatStarch (yellow).

4.4 Conclusion

PLGA NPs were coated with cationic and water-soluble substances (protamine, chitosan, and starch). Although having the same PLGA basis in the inner core the material on the surface of the delivery system determines the stability properties. The storage of a nanoparticle suspension is limited due to starting aging or aggregation processes at 37 °C after two weeks. However, retaining the samples at 4 °C or RT for at least 35 days is feasible without any concerns. The storage stability is an important aspect thus particle suspensions show (apart from CatStarch coated samples) a limited re-dispersibility after lyophilization. Maybe the freeze-drying process is not optimally designed for proteins. It is known, that the addition of 0.2% (w/w) trehalose as a bioprotectant [173] can prevent aggregation. This treatment was less favorable for chitosan-coated NPs. As chitosan NPs are known to have a gel-like character [174] this behavior might be partially adopted for chitosan-coated NPs. Due

to lyophilization, the structure might be damaged, and a re-dispersion ends up in aggregates.

Nebulizers are preferred devices in line for later therapeutic applications of the investigated DDSs. The Aeroneb[®] Lab and the eFlow[®] devices use an oscillating membrane to create an aerosol. As the atomization technique means a high mechanic stress for the particles, it is comprehensible that stability can be affected. The use of different aerosolization heads divergent in size of the perforations showed a stronger aggregation the smaller the holes in the membrane are. Again, CatStarch-coated NPs indicate a better resistance. A more robust binding of the starch derivative on the PLGA particle compared to chitosan or protamine might be one explanation. This aspect can be partially substantiated by the washing procedure (see Chapter 3.3.3.4): it was possible to wash off amounts of the chitosan coating (dropped ζ -potential) due to harsh centrifugation and re-dispersion. A filtration of all NP samples through a 0.2 μm filter is viable. Very low (protein) binding membranes for aqueous solutions (Minisart[®]: cellulose acetate and Steriflip[®]: polyethersulfone) do not interfere with the cationic coating of the NPs, and no difference between both membrane materials is present. Only the comparison of both membranes with uncoated PLGA NPs is not yet confirmed. As the evaporation of ethyl acetate during NPs preparation proceeded completely, it is not necessary to take the incompatibility of these membranes with the organic solvent (ester) into account.

Prospective, detailed experiments concerning the cargo stability need to be analyzed. The stability of the siRNA, after nebulization of the complete drug delivery system (e.g. via gel electrophoresis) followed by transfection studies of aerosolized loaded carriers is one idea. The resistance of bound siRNA against degradation (RNase A) is another important parameter to investigate. Preliminary studies were already conducted and showed certain stability against mechanical stress (= nebulization) and resistance against RNase A (see Figure 4.8). But as this data results merely from preliminary studies and should be repeated with a high quality siRNA (only one visible band) and with additional released samples and different loadings to allow a substantiated statement (especially since no signal of siRNA on PLGA-Prot NPs could be found).

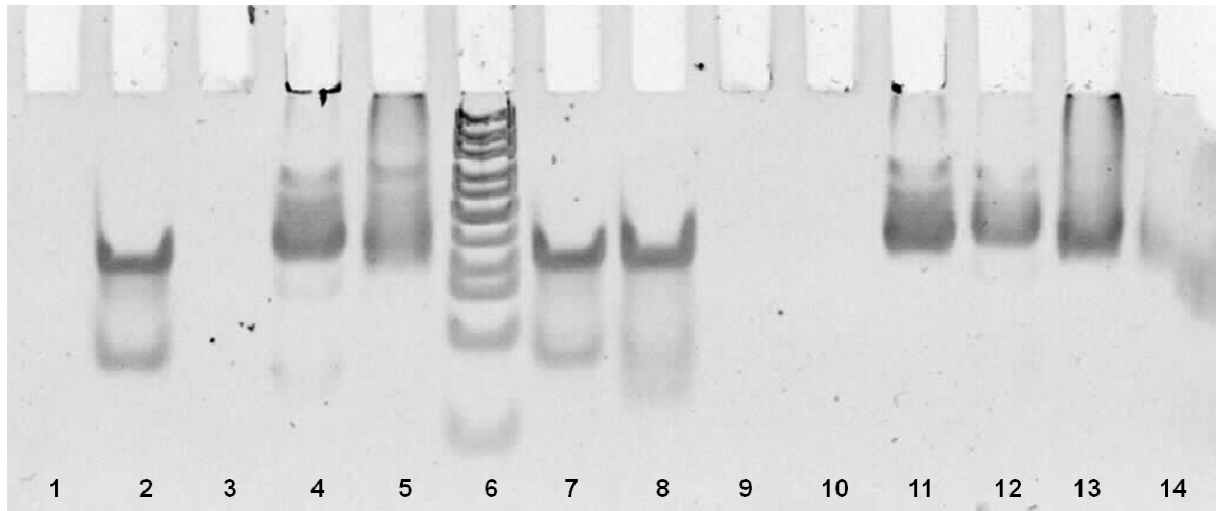


Figure 4.8 TBE gel (1x) of loaded NPs and GAPDH siRNA incubated with RNase A (70 U/sample) for 30 min. at 37°C or loaded NPs and siRNA after nebulization via PARI e-Flow rapid device. loading ratio siRNA:NPs (1:50), 1 = 0.2 µg siRNA + RNase A, 2 = 0.2 µg siRNA, 3 = loaded PLGA-Prot NPs + RNase A, 4 = loaded PLGA-Cs NPs + RNase A, 5 = loaded PLGA-CatSt NPs + RNase A, 6 = Ultra-Low range Ladder (300, 200, 150, 100, 75, **50**, 35, 25, 20, 15, 10 bp), 7 = 0.2 µg siRNA, 8 = 0.2 µg siRNA neb., 9 = loaded PLGA-Prot NPs, 10 = loaded PLGA-Prot NPs neb., 11 = loaded PLGA-Cs NPs, 12 = loaded PLGA-Cs NPs neb., 13 = loaded PLGA-CatSt NPs, 14 = loaded PLGA-CatSt NPs neb; stained with 0.5 µg/mL ethidium bromide.

Chapter 5 - Cell viability and immunogenicity

The author of this thesis made the following contribution to this chapter:

Planned, designed and performed all experiments related to cytotoxicity by MTT assays and MTS/PMS on THP-1 cells, analyzed all the data from the mentioned studies, interpreted all experimental data and wrote the chapter, it not stated otherwise.

Cell culture of hAELVi cells was performed by Stephanie Kletting.

MTS/PMS assay und ViaLight™ assay were implemented and analyzed by Stine Rønholt at University of Copenhagen.

The immunogenicity studies were performed by Anne Marit de Groot at Utrecht University. She analyzed the data from the mentioned studies and interpreted the experimental data.

NF- κ B activation assays were performed by Pharmacoidea under the direction of Tamás Letoha. He analyzed the data from the mentioned studies and interpreted the experimental data.

5.1 Introduction

The preparation of nanoparticles or the term nanotechnology in general implies more and more the question concerning nanotoxicology [175]. Not only in association with medical applications a prediction of the toxic potential of the utilized materials and formulations is indispensable. A database of GRAS materials (Generally Recognized as Safe) may be applied as well as the NCS (Nanotoxicology Classification System) for final formulations [176]. Here, a comparison of nano and non-nano formulations is crucial. Regarding this, Lehr and Groß described a safety classification system (modification see Figure 5.1) for nano-products and materials [177].

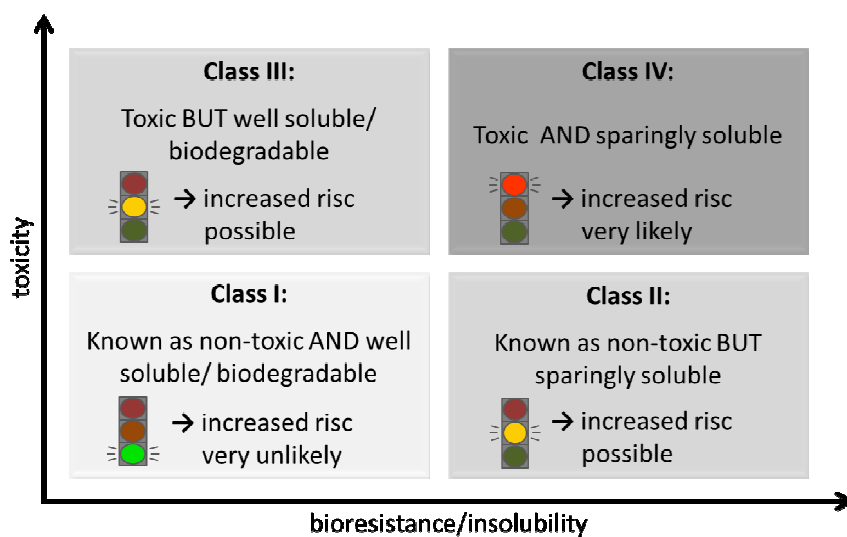


Figure 5.1 Safety classification-system for nano-products and materials in comparison to their non-nano-forms [178] (adopted and modified from Lehr and Groß [177]).

Despite these preliminary theoretical considerations *in vitro* evaluations of developed nanoparticulate systems are essential before getting permission for *in vivo* studies. These include, inter alia, the assessment of cytotoxicity and immunogenicity on target cells. As the designed nanoparticulate system (see chapter 2 and 3) is intended for pulmonary applications studies need to include lung specific cell models. First, monocultures of epithelial lung cells (main barrier for particles to overcome) of the upper and lower respiratory tract were evaluated. For the alveolar region A459 cells and for the bronchial region Calu-3 cells represent well-established and commonly used epithelial cell lines. Later on more advanced systems like co-cultures

[179, 180] or triple-culture [181, 182] may show more reliable results due to a better accordance with the conditions in the human body.

Within this chapter established cell viability and immunogenicity tests were performed to receive a first impression about the safety profile of applied formulations and DDSs. Although a direct correlation between *in-vitro* and *in-vivo* results is limited to preliminary studies on cell culture models before going into animals are still obligatory.

5.2 Materials and methods

5.2.1 Cell viability

Within COMPACT viability studies were implemented by Stine Rønholt (P3, WP3) through MTS/PMS assay und ViaLight™ assay. Furthermore, apart from COMPACT, MTT assays were performed.

5.2.1.1 Cell culture

Macrophages

Human monocyte-derived cell line (THP-1; DSMZ No. ACC 16) [183-185] from an acute monocytic leukemia patient were obtained from the Leibnitz-Institute DSMZ-Deutsche Sammlung von Mikroorganismen und Zellkulturen in Braunschweig and cultivated in Roswell Park Memorial Institute (RPMI) 1640 medium (from Gibco by Life Technologies, USA) supplemented with 10 % FBS. Cells were applied as suspension cells (non-stimulated) and as adherent macrophage-like cells (stimulated, see Figure 5.2).

The differentiation process was implied by the addition of 7.5 ng/mL Phorbol 12-myristate 13-acetate (PMA; CAS No.: 16561-29-8) [186] followed by 24 h incubation under standard cell culture conditions (37 °C with a humidified 95 % atmosphere containing 5 % CO₂). For viability assessment of adherent cells 1 x 10⁵ cells/well were seeded in a 96-well plate; the same amount was used for suspended cells (not stimulated).

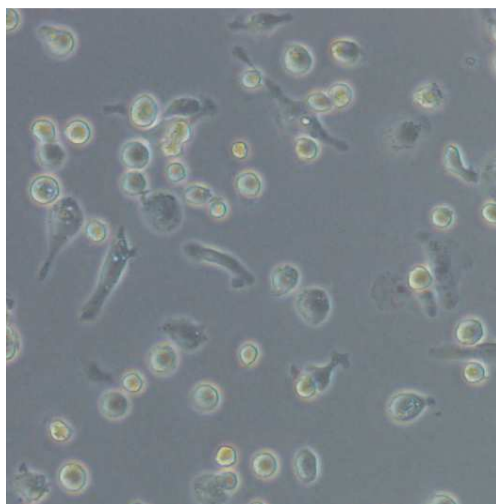


Figure 5.2 THP-1 cells (100,000 cells/well; in 24-well cell culture plate) 24 h after differentiation with PMA. Some adherent macrophage-like and spherical suspension cells are visible in parallel.

Epithelial cells

Adenocarcinomic human alveolar epithelial cells (A549; ATCC[®] No. CCL-185[™]) [187] from 'American Type Culture Collection' (ATCC) represent AT II-like epithelial cells [188, 189] and were cultivated in RPMI 1640 medium + 10% FBS under standard conditions (see above). For the MTT assay 10,000 cells/well and for MTS/PMS and Vialight assay 9,000 cells/well were seeded in 96-well plates.

Calu-3 (ATCC[®] No. HTB-55[™]) [190], a adenocarcinoma-derived human bronchial epithelial cell line was purchased from 'American Type Culture Collection' (ATCC). Cells were cultivated under standard conditions in Minimum Essential Medium (MEM) supplemented with 1% Non-Essential Amino Acids (NEAA: Glycine 750 mg/l, L-Alanine 890 mg/l, L-Asparagine 1320 mg/l, L-Aspartic Acid 1320 mg/l, L-Glutamic Acid 1470 mg/l, L-Proline 1150 mg/l, L-Serine 1050 mg/l and 1% sodium pyruvate).

5.2.1.2 MTT assay

MTT 3-(4,5-dimethylthiazol-2-yl)-2,5-diphenyltetrazolium bromide is an intracellular colorimetric assay [191] to detect the metabolic activity by the amount of NAD(P)H-dependent cellular oxidoreductase enzyme (only present in living cells). MTT (yellow color) is reduced into insoluble (purple color) formazan which is located in the cytosol (see Figure 5.3).

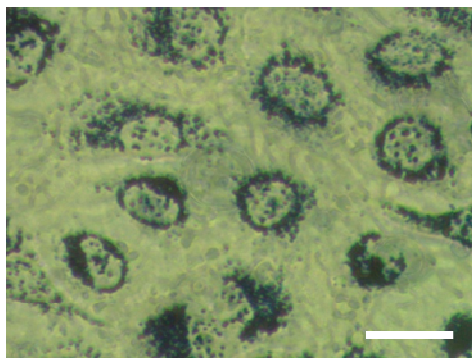


Figure 5.3 Light microscope: Image of A549 cells (positive control in HBSS) with intracellular purple formazan crystals after the treatment with MTT reagent (tetrazole). Scale bar 20 μm .

Hence, dimethyl sulfoxide (DMSO) needs to be added to dissolve the crystals and to measure the amount of formazan. The assay was performed with the following protocol: A549 cells were seeded at 10,000 cells per well (0.2 μL) in a 96-well cell culture plate and incubated for two days at 37 $^{\circ}\text{C}$, 5 % CO_2 95 % humidified atmosphere. The medium was removed, and cells were washed twice with pre-warmed (at 37 $^{\circ}\text{C}$) HBSS (pH 7.4, + CaCl_2 , + MgCl_2 , without phenol red from Gibco by Life technologies, USA). 200 μL sample volume (sterile nanoparticles were filtrated with Steriflip[®], 0.22 μm in concentrations between 0.05 mg/mL and 1.0 mg/mL), 1% TritonX-100 in HBSS as a positive control and pure HBSS as negative control were added and incubated for 6 h at 37 $^{\circ}\text{C}$ standard conditions. Afterward the supernatant was removed and washed with HBSS once. A MTT (from Sigma M5655-1g) stock solution (5 mg/mL PBS) was diluted at a ratio of 1:10 with HBSS and 100 μL were applied on cells for 4 h under gentle shaking and protection against light exposure respectively. The liquid was removed followed by the addition of 100 μL dimethyl sulfoxide (DMSO) for 20 min. again at 37 $^{\circ}\text{C}$ and gentle shaking in the dark. The absorption of the resulting colored solution was quantified by measuring at 550 nm with Tecan i-control. The relative viability was calculated as follows:

$$viability [\%] = \frac{A - S}{CM - S} \times 100$$

A: absorption sample, S: absorption positive control; 1% Triton-X 100, CM: negative control; HBSS

LD_{50} values were calculated to obtain the resulting standard curve.

5.2.1.3 MTS/PMS assay

The main principle of the MTT and MTS/PMS assay [192] is basically the same. The MTS/PMS is often described as a 'one-step' MTT assay. Here, the tetrazolium dye 3-(4,5-dimethylthiazol-2-yl)-5-(3-carboxymethoxyphenyl)-2-(4-sulfophenyl)-2*H*-tetrazolium (MTS; reagent powder CellTiter 96[®] AQueous from Promega) is used in conjunction with the intermediate electron acceptor 1-methoxy phenazine methosulfate (PMS; < 90% (UV) from Sigma (P9625-500MG)) to produce a formazan product absorbance maximum at 490 nm intracellularly. Project partner conducted this assay concerning the following protocol: cells (A549) were seeded at 9,000 cells/well (96-well plate) in 100 μ L medium; cultured under standard conditions at 37 °C in a 5 % CO₂ 95 % humidified atmosphere for 24 h and incubated for 6 h. Sodium dodecyl sulfate (SDS; 10,000 μ M) was used as positive control and buffer treated cells as negative control. Formulations and controls were prepared in 10 mM HEPES HBSS buffer instead of DMEM media. Growth medium was removed from cells and samples (predetermined concentrations) were added. After 6h incubation, samples and controls were discarded and cells were washed two times with HBSS. Then MTS/PMS (final concentration: MTS 240 μ g/mL, PMS: 2.4 μ g/mL) solution was added and incubated for 1.5 h at 37 °C with mechanical shaking and light protection. Absorbance was measured at 492 nm. The relative viability was calculated as described in section 5.2.1.3.

5.2.1.4 ViaLight™ assay

As a second method, to confirm previous cytotoxicity results from the MTT or MTS/PMS assay, the ViaLight™ Plus Cell Proliferation and Cytotoxicity BioAssay Kit from Lonza was used. Here, the amount of ATP (present in all viable and metabolically active cells) was measured via bioluminescence [193]. The enzyme luciferase catalyzes the formation of light from luciferin (both contained in ATP monitoring reagent) and ATP. Such a luciferase-based assay provides a sensitive and direct measurement of cell viability without distorting effects which might occur due to washing or medium removal steps.

The assay was performed on the following protocol: A549 cells were seeded at 9,000 cells/well (in 100 μ L, 96-well plates) and cultured under standard conditions at 37 °C in a 5 % CO₂ 95 % humidified atmosphere for 24 h. Sodium dodecyl sulfate (SDS; 10,000 μ M) treated cells were used as positive control and buffer treated ones as negative control. Formulations and controls were prepared in 10 mM HEPES HBSS buffer. The growth medium was removed from cells and samples (predetermined concentrations) were placed on the cells and incubated for 6 h. After incubation, 50 μ L cell lysis reagent were added and incubated for additional 10 min. Afterward, 100 μ L cell lysate were transferred in a white-walled luminometer plate and 100 μ L ATP monitoring reagent were added. After 2 min. of incubation at RT luminescence was measured.

5.2.2 Immunogenicity

Nowadays, the development of novel vectors for gene delivery focuses mainly on non-viral vectors because of safety issues. An often mentioned bottleneck of viral vectors is the arising immune response [194, 195] and an induction of inflammatory response which leads to degenerated tissue or cells [196]. Nevertheless, immunogenicity is a major concern of therapeutic biomacromolecular products. Hence non-viral vectors need to be tested for any possible immunogenic potential. Thus, these results may limit later necessary *in vivo* applications. Different assays are available which predict the immunogenicity of a delivery system. Within COMPACT two preliminary NF- κ B dependent *in vitro* assays (dendritic cell maturation and toll-like receptor assay) were selected to interpret the activation data appropriately. All results were performed in cooperation with Marit deGroot, University of Utrecht, COMPACT partner in WP3 (P2b) according to Zeng et al. [197].

Deviations in data analysis (e.g. applied particle concentrations) occurred due to two different measurement series (1st and 2nd generation formulations). For PLGA-Cs NPs additional NF- κ B and Hsp70 activation assays were executed by Pharmacoidea.

5.2.2.1 Dendritic cell maturation assay

Dendritic cells (DCs) belong to one group of antigen-presenting cells in our immune system [198]. Mature and activated DCs can stimulate naive T-lymphocytes (“T” for *thymus* = place of maturation) and thus initiate and modulate the immune response of the human body [199, 200]. As the distinction of subtypes among murine bone marrow-derived dendritic cells (mBMDC) is initially more apparent than among human DCs [201] mBMDCs will be used in both assays. Here, mBMDCs were cultured for one week, and the DDS plus controls [PBS buffer, LPS (lipopolysaccharide) and siRNA solutions] were added (partially in different concentrations: 1st generation 50 – 410 µg/mL and 2nd generation 5 – 150 µg/mL) and incubated overnight. DCs were separated from other bone marrow derived immune cells by their high expression of the membrane proteins CD11c (Integrin type I; transmembrane protein) and major histocompatibility complex class II (MHCII). The maturation of mBMDC was assessed by up-regulated CD40 and CD86 expression (co-receptors in T-cell activation). The cells needed to be stained the next day with antibodies against all these proteins (CD11, MHCII, CD40 and CD86) and measured by flow cytometry. The percentage of the matured DC is then calculated by the following formula:

$$DC [\%] = \frac{CD11c^+MHCII^+CD49^+CD86^+ \text{ cells} * 100}{CD11c^+MHCII^+ \text{ cells}}$$

Living cells were gated using forward scatter (FSC) and side scatter (SSC). In this gate the dendritic cells were selected by CD11c (Allophycocyanin = APC, Ex_{max} 650 nm/ Em_{max} 660 nm; red laser: 640 nm) and MHCII (Horizon-V450; Ex_{max} 404 nm/ Em_{max} 448 nm; violet laser: 405 nm). The maturation of these dendritic cells was then assessed by gating the double positives for both CD40 (R-phycoerythrin = PE, Ex_{max} 496 nm/ Em_{max} 578 nm; yellow-green laser: 561 nm) and CD86 (Fluorescein isothiocyanate = FITC; Ex_{max} 494 nm/ Em_{max} 520 nm, blue laser: 488 nm).

5.2.2.2 Toll-like receptor assay

As part of the pattern recognition receptor (PRR) family, toll-like receptors (TLRs) [202] belong to the innate immune system and recognize specific pathogen-associated molecular patterns (PAMPs) to differentiate between host and foreign structures.

Table 5.1 Overview of human TLRs and their associated recognized antigens; blue: tested in TLR assay; extracellular = location on cell membrane, intracellular = location on endosomal or endolysosomal membrane.

Pam3CSK = triacylated polypeptide (cell-wall component), activator of the proinflammatory transcription factor NF κ B; HKLM: heat-killed bacteria, *Listeria monocytogenes*; FSL1: synthetic diacylated lipoprotein (from *Mycoplasma salivarium*); Poly I:C = Polyinosinic:polycytidylic acid; LPS: lipopolysaccharide (from *e. coli*); FLA-ST (Pam2CGDPKHPKSF): flagellin (from *S. typhimurium*); ODN = oligodeoxynucleotide; CL264: 9-benzyl-8 hydroxyadenine derivative (in para position it contains a glycine on the benzyl group); CpG = cytosine-phosphate-guanine.

	recognized antigen	agonist(s)	Location
TLR1	Bacterial lipoproteins and peptidoglycans	Pam3CSK	Extracellular
TLR2	Bacterial peptidoglycans (lipoproteins etc.)	Pam3CSK, HKLM, FSL1	Extracellular
TLR3	dsRNA	Poly I:C	Intracellular
TLR4	Lipopolysaccharides (etc.)	LPS	Extracellular
TLR5	Bacterial flagella	FLA-ST	Extracellular
TLR6	Bacterial lipoprotein	FSL1	Extracellular
TLR7	ssRNA, bacterial and viral	CL264, Imiquimod, Gardiquimod	Intracellular
TLR8	ssRNA, bacterial and viral, phagocytized bacterial RNA	ssRNA40, ssPolyU	Intracellular
TLR9	CpG DNA	ODN2006	Intracellular
TLR10	Unknown	-	?
TLR11	Flagellin / Profilin	-	no functional protein found in humans

They are a class of several proteins (TLR1 to TLR11 in humans) and are expressed on the membrane of leukocytes (DCs, macrophages, natural killer cells, T- and B-cells), epithelial cells, endothelial cells and fibroblasts [203] or occur intracellularly. To measure human TLR activation TLR reporter cell lines, Human Embryonic Kidney 293 cells (HEK-Blue™ hTLR2, 3, 4, 7 and 9; InvivoGen, France) were cultured and incubated with loaded and unloaded particles in concentrations between 72 – 575 µg/mL (1st generation) and 11.25 – 370 µg/mL (2nd generation).

5.2.2.3 NF-κB activation

As part of the COMPACT project NF-κB activation assays were performed by Pharmacoidea (P18) under the direction of Tamás Letoha to investigate if PLGA-Cs NPs inhibit LPS- and TNF (tumor necrosis factor) -induced activation. L929 (mouse fibroblasts), SHSY-5Y (human neuroblastoma cells) and RAW264.7 (mouse leukemic monocyte-macrophages) cells were transformed respectively with pNF-κB-luc4 and pSV-2/neo plasmids [204]. Culturing each cell line for 24 h on luminoplates (3 x 10⁴ cells/well) in DMEM + 10 % FBS cells were incubated with NP samples in concentrations between 0.0625 mg/mL and 2.0 mg/mL for 30 min. 6 h or 16 h later the medium was removed. After washing and lysis of the cells (with 20 µL/well Reporter Lysis Buffer from Promega) for 10 min. at RT. 20 µL/well from the substrate (from Promega) was added to measure luciferase activity (with a Luminoskan™ Ascent microplate luminometer from Thermo Scientific). Cells were treated 30 min. after the peptide treatment with TNFα (CAS No.: 94948-59-1, 100 µg/mL); for TNF stimulation, with LPS (CAS No: 297-473-0; 100 ng/mL) for LPS stimulation and with PMA (Phorbol 12-myristate 13-acetate; CAS No.: 16561-29-8; 100 nM) for PMA stimulation.

Hsp70 activation assay: Transformed RAW264.7 macrophages with pNF-κB-luc4 and pSV-2/neo plasmids were incubated for 30 min. at 40 °C followed by the same treatment as NF-κB activation assay (see above).

All assays were performed in triplicates as mean ± SD.

5.3 Results and discussion

5.3.1 Cytotoxicity

5.3.1.1 MTT

Within this chapter coated PLGA-based NPs were analyzed to determine toxic effects of the nanoparticulate system on lung cells. Figure 5.4 shows the evaluation of PLGA-Prot, PLGA-Cs and PLGA-CatSt NPs on A549 and Calu-3 cells.

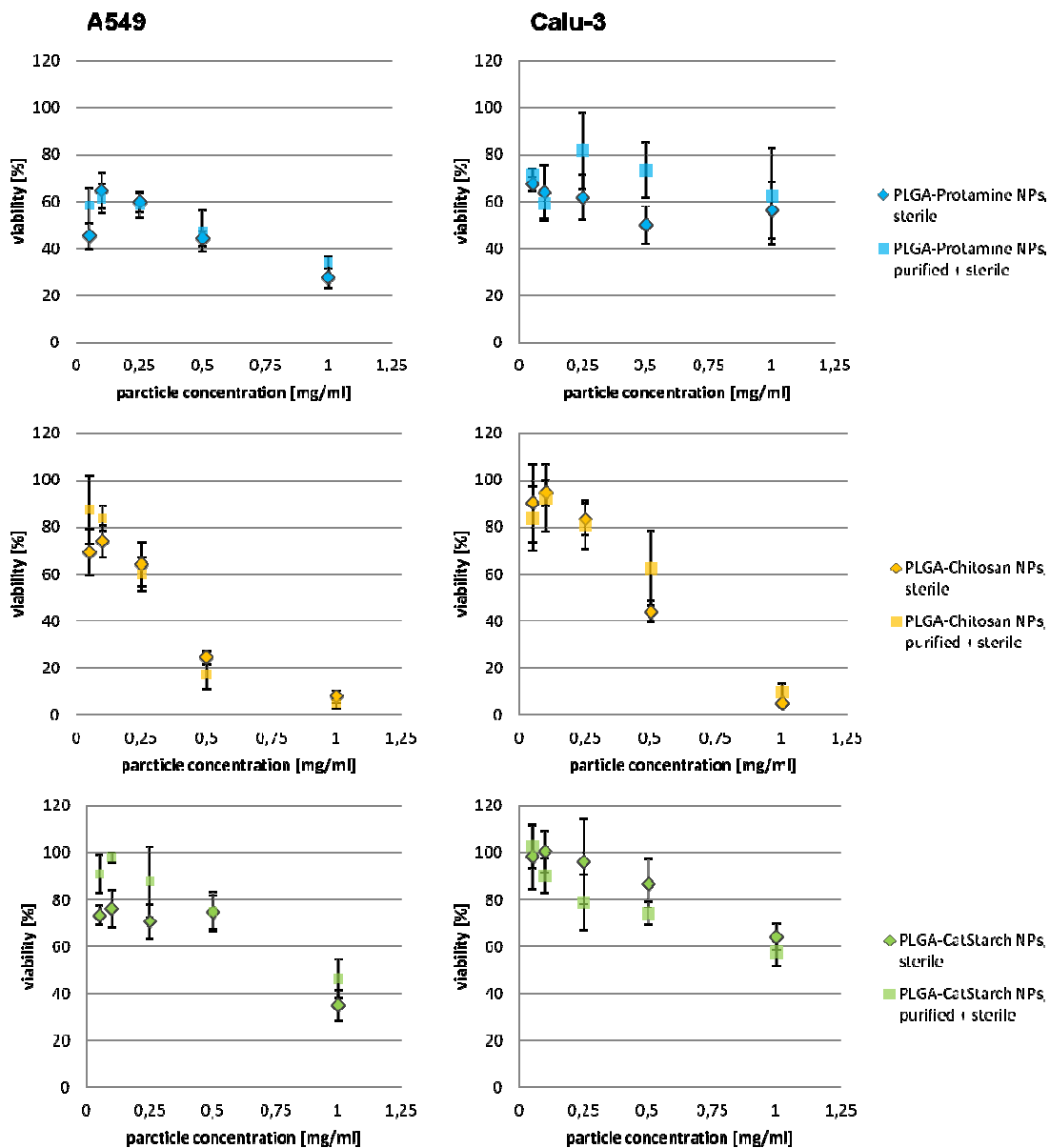


Figure 5.4 Evaluation of MTT assay from coated PLGA NPs in concentrations between 0.05 mg/mL and 1.0 mg/mL on lung epithelial cells (A549 and Calu-3).

Initially, a benefit regarding cell viability due to a prior purification procedure of the particles was not apparent. In the comparison between both cell lines, Calu-3 cells showed a better resistance against high particle concentrations. As a result, the calculation of LD₅₀ values suffered from missing viability rates lower than 50 % (see Table 5.2). Both cell lines tolerate relatively high particle concentrations. Starting with concentrations between 0.05 mg/mL and 0.25 mg/mL no toxic effects could be observed. Applying concentrations higher than 0.5 mg/mL first effects of PLGA-Prot NPs and PLGA-CatSt on A549 cells became visible. For PLGA-Cs NPs, however, viability was limited to A549 and Calu-3 cells. Only 20% of viable cells survived, after applying more than 0.5 mg/mL of particle suspension. At the latest after raising concentrations up to 1 mg/mL, all cells showed strong toxic effects.

These results are not based on an influence of the pure cationic material only. Considering that the particle samples were diluted with buffer, to obtain necessary concentrations, a consequence for higher particle contents is the presence of less buffer and thus less salts. Consequently, a different pH (NPs suspensions: pH ~ 5) or varying osmotic pressures may occur and affect the cells.

Table 5.2 Overview of LD₅₀ values for purified (Vivaflow®50) and non-purified coated PLGA NPs calculated from MTT-assay on A549 and Calu-3 cells. All samples were filtrated (Minisart®, 0.22 µm). n/a: poor fit due to low/no toxicity

<i>carrier system</i>	<i>A459</i>	<i>Calu-3</i>
	<i>LD₅₀ [mg/ml]</i>	<i>LD₅₀ [mg/ml]</i>
PLGA-Prot	0.438	n/a (*1.363)
PLGA-Prot_{purified}	0.472	n/a (*1.462)
PLGA-Cs	0.253	0.528
PLGA Cs_{purified}	0.246	0.585
PLGA-CatSt	0.710	n/a (*1.361)
PLGA-CatSt_{purified}	0.885	n/a (*1.209)

*values calculated from trend of progress on < 1.0 mg/ml

In conclusion, PLGA-Cs NPs seem to have the highest toxic effect on A549 and Calu-3 cells. LD₅₀ values around 0.25 mg/mL confirm a stronger limitation in contrast to PLGA-Prot NPs with LD₅₀ = 0.438 mg/mL – 0.472 mg/mL and PLGA CatSt NPs with LD₅₀ = 0.710 mg/mL – 0.885 mg/mL.

5.3.1.2 MTS/PMS assay

Divergent from the experimental setup in section 5.3.1.1 siRNA-loaded NPs were applied on A549 cells additionally. As MTT and MTS/PMS assays follow the same mechanism, results of prior studies should be comparable. Having a look at Figure 5.5 independent of the particle coating, the presence of bound cargo has no significant impact on cell viability.

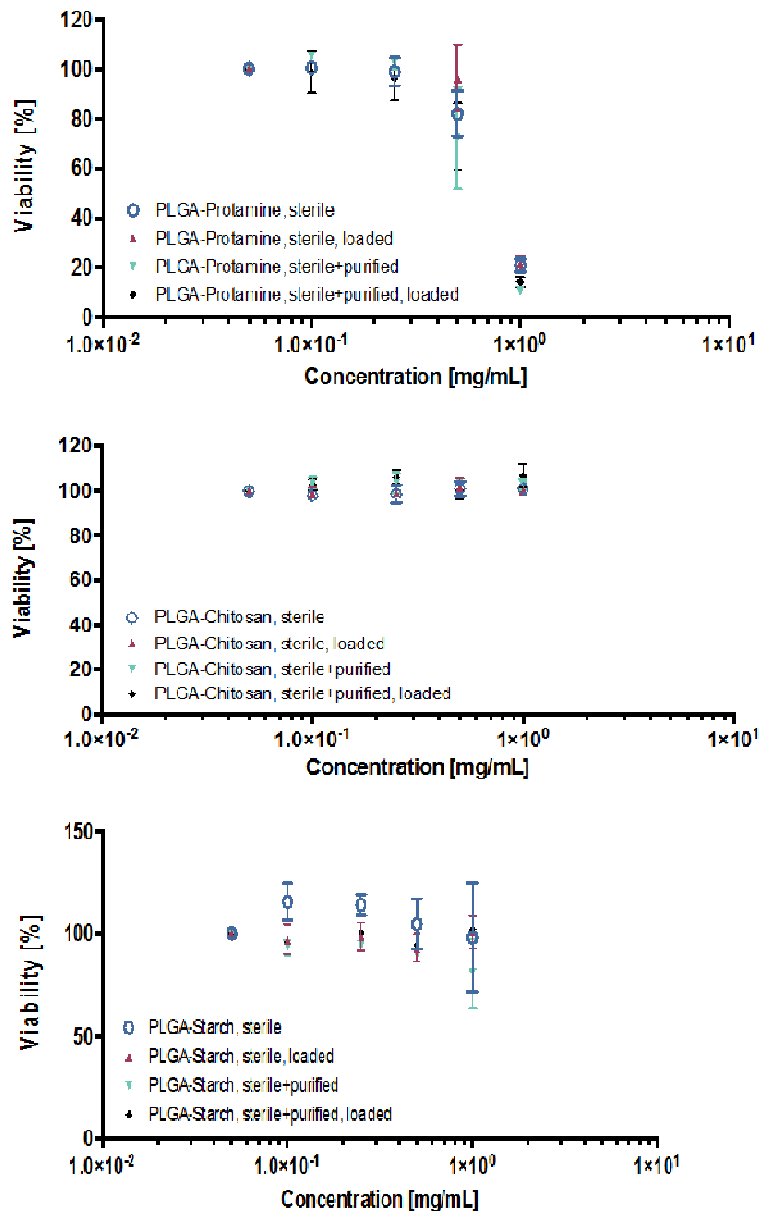


Figure 5.5 Evaluation of MTS/PMS assays: coated PLGA NPs (in concentrations between 0.05 mg/mL and 1.0 mg/mL) on A549 cells. Non-purified + non-loaded, Purified, loaded and purified + loaded NPs samples were applied.

Additionally, as already seen in MTT assays, purified NPs showed roughly the same results as non-purified samples. Differing from prior MTT assays, PLGA-Prot NPs seem to be the most harmful type of coated nanoparticles and not PLGA-Cs NPs. After incubation with PLGA-Prot-NPs, cell viability dropped from 80 % for 0.5 mg/mL to 20 % at a concentration of 1 mg/mL whereas cells kept viable (approximately 100 %) over the entire dilution series of PLGA-Cs NPs. For PLGA-CatSt NPs no damaging effect at particle concentrations < 0.5 mg/mL could be observed; merely a broader standard deviation at the highest of all tested concentrations.

Concerning later planned studies on co-culture models consisting of epithelial cells with macrophages on top, preliminary studies with PLGA-Cs NPs were conducted to investigate differences between stimulated and non-stimulated THP-1 cells (see Figure 5.6).

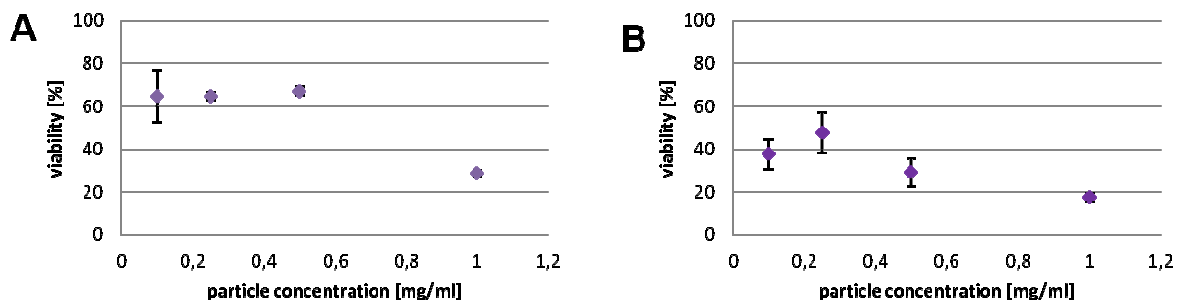


Figure 5.6 Evaluation of MTS/PMS assay: PLGA-Chitosan NPs (in concentrations between 0.1 mg/mL and 1.0 mg/mL) A: stimulated (p71) and B: non-stimulated (p72) THP-1 cells.

Although using the MTS/PMS assay with a reduced amount of washing steps, cells were influenced by the analytical procedure and showed a generally reduced viability level of ~ 60 % for stimulated and ~ 40 % for non-stimulated cells for concentrations up to 0.5 mg/mL. The Viability of both types of THP-1 cells became reduced by 50 % applying a particle concentration of 1 mg/mL. Consequently, THP-1 cells as macrophage-like cells were less robust than epithelial cells. Moreover, activated THP-1 cells were even more affected by particles. This result is comprehensible considering the activation process which means additional stress for treated cells.

5.3.1.3 ViaLight™ assay

As ViaLight™ assays are known to be more sensitive than colorimetric viability assays higher standard deviations (especially with increasing particle concentrations) need to be mentioned. For PLGA-Prot NPs the same trend of viability was observed: a slight reduction of viability by 0.5 mg/mL particles and a dropping viability by 1.0 mg/mL.

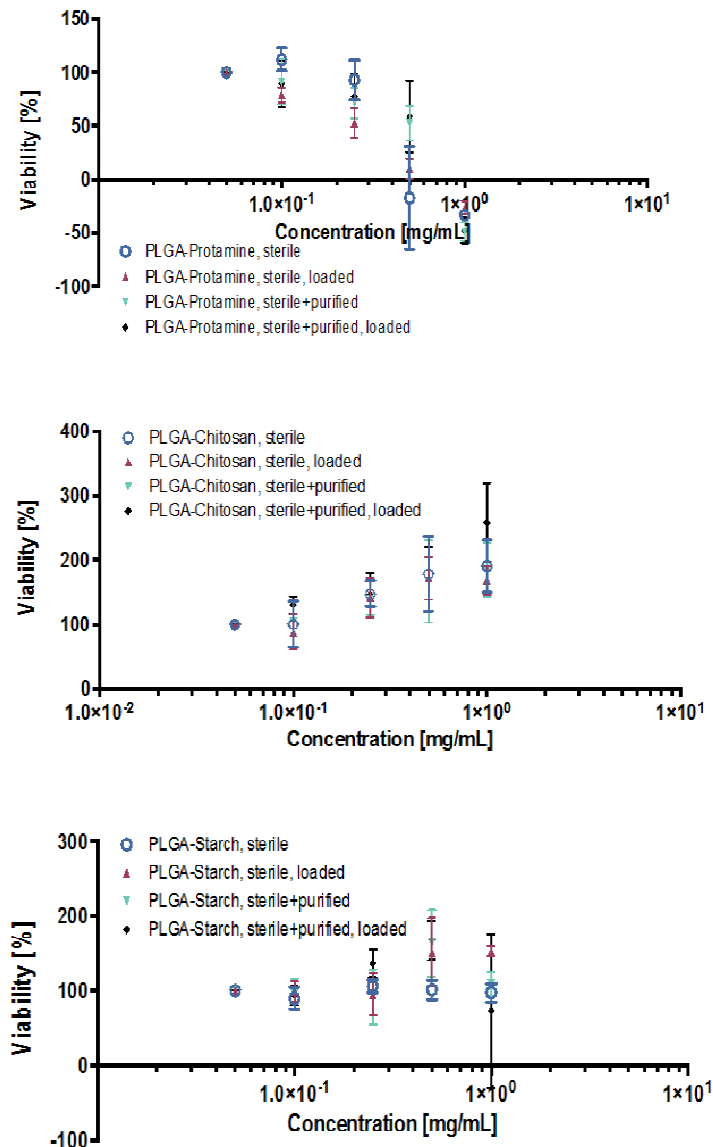


Figure 5.7 Evaluation of the ViaLight™ assay: coated PLGA NPs (in concentrations between 0.1 mg/mL and 1.0 mg/mL) on A549 cells. Non-purified + non-loaded, purified, loaded and purified + loaded NP samples were applied.

At first sight, a gradually increased cell viability of A549 cells after incubation with rising PLGA-Cs NP concentrations was not expected. However, these results can be explained by toxic effects which occur when cells react with an increased metabolism. Hence, higher values were a result of cellular stress against external factors. The same tendency could be observed for PLGA-CatSt NPs even though less pronounced.

5.3.2 Immunogenicity

5.3.2.1 DC maturation assay

Within the COMPACT consortium PLGA-Cs NPs as 1st generation formulation, as well as 2nd generation formulations (PLGA-Prot and PLGA-CatSt NPs) were tested independently from another which caused a different evaluation of the obtained results. In the series of 2nd generation test different particle concentrations and buffers as negative control were applied. Activation results measured as fluorescent intensity or amounts of cells on y-axis; see Figure 5.8 and 5.9, respectively). A direct comparison of all results was not possible, but a relative description of the tendency from changing particle concentrations was sufficient.

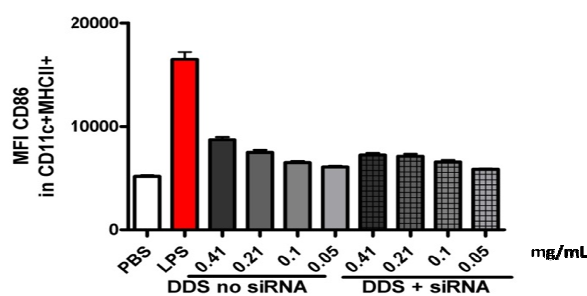


Figure 5.8 Evaluation of dendritic cell maturation assay; mean fluorescent intensity (MFI) is plotted against applied PLGA-Cs samples; PBS as negative control and LPS as positive control.

This assay (see Figure 5.7) showed a minor up-regulation of co-stimulatory factors CD86 (protein on antigen-presenting cells, which provides co-stimulatory signals for t-cell activation) and CD40 (co-stimulatory protein on antigen-presenting cells) on bone marrow derived dendritic cells in a dose-dependent manner for PLGA-Cs NPs. The assay testing 2nd generation formulations showed a minimal DC activation of

PLGA-Prot NPs and a minor activation of PLGA-CatSt NPs at highest concentrations, respectively. Thus, results of PLGA-CatSt NPs directly correlated with cell growth and cell viability.

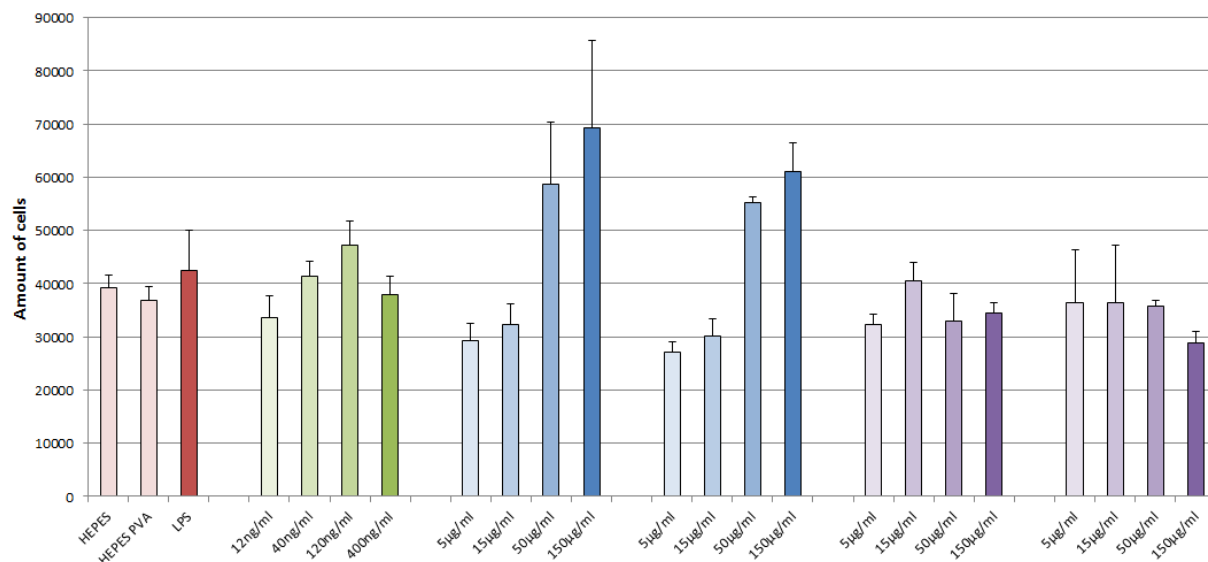


Figure 5.9 Evaluation of dendritic cell maturation assay; amount of cells is plotted against applied 2nd generation formulations; HEPES and HEPES+PVA as negative control and LPS as positive control. PLGA-Prot NPs (purple, left), PLGA-Prot NPs + siRNA (purple, right), PLGA-CatSt NPs (blue, left), PLGA-CatSt (blue, right) and siRNA (green); SEAP = Secreted Alkaline Phosphatase.

5.3.2.2 TLR assay

Within this chapter, human TLR activation of different subtypes was tested. PLGA-Cs NPs (see Figure 5.10) showed no TLR2, 4 and 9 activation. A possible effect of TLR3 was not assessable as controls showed a lower activation than by the positive ligand (false negative results were possible). The analysis of the first generation formulation did not include TLR7 (endosomal ssRNA), which was available for the following developed formulations. Hence, a later evaluation of the activation of TLR7 by PLGA-Cs NPs needs to be performed to complete this data set.

Having a look at the results of the TLR2 (see Figure 5.11) and TLR4 (data not shown) activation assay, no significant results from PLGA-CatSt and PLGA-Prot NPs were observed.

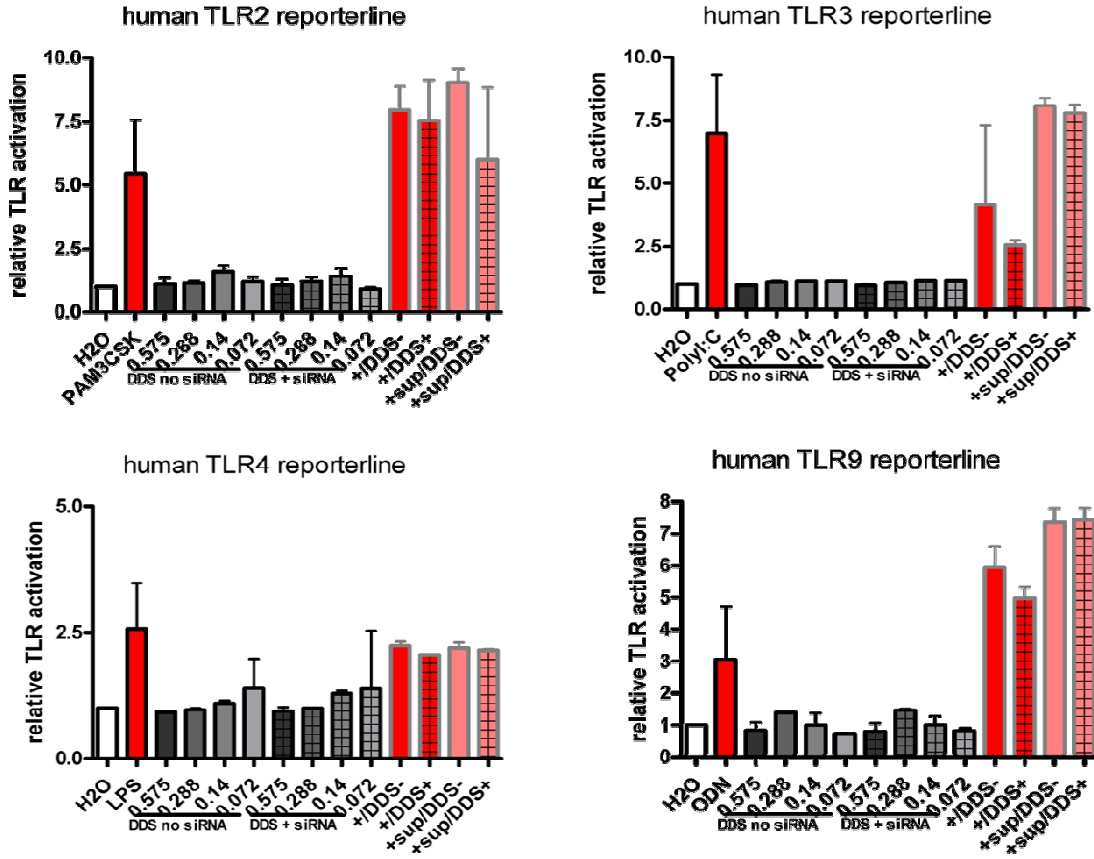


Figure 5.10 Evaluation of TLR assays; relative TLR activation is plotted against applied PLGA-Cs samples; water as negative control

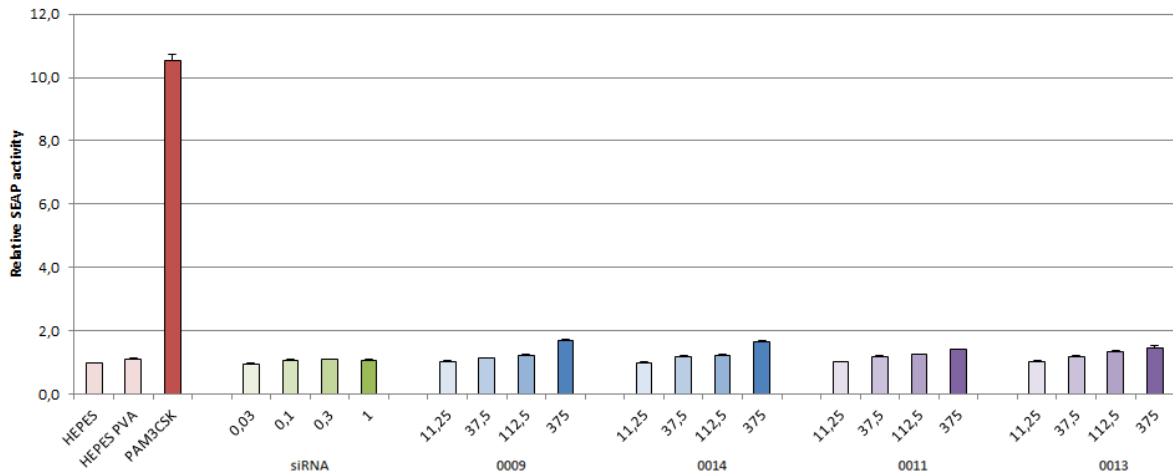


Figure 5.11 Evaluation of TLR2 activation assay; activity is plotted against applied 2nd generation formulations in μg/mL; HEPES and HEPES+PVA as negative control and PAM3CSK as positive control. PLGA-Prot NPs (purple), PLGA-CatSt NPs (blue) and siRNA (green). SEAP = Secreted Alkaline Phosphatase

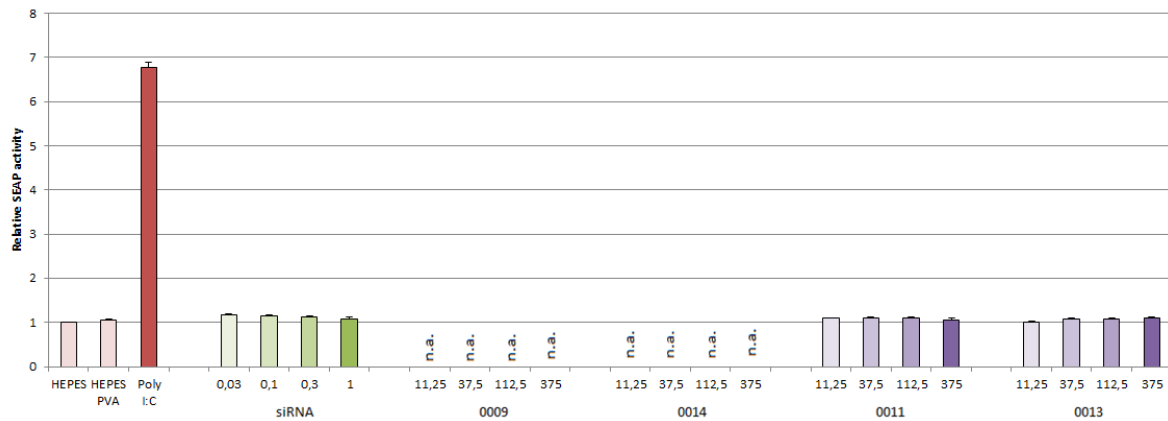


Figure 5.12 Evaluation of TLR3 activation assay; activity is plotted against applied 2nd generation formulations in $\mu\text{g/mL}$; HEPES and HEPES+PVA as negative control and Poly l:C as positive control. PLGA-Prot NPs (purple), PLGA-CatSt NPs (blue) and siRNA (green). SEAP = Secreted Alkaline Phosphatase. n.a. = not available because false negatives failed

A similar observation was made for TLR3 (see Figure 5.12), TLR7 and TLR9 (data not shown): no activation of TLR 3 and 7 by PLGA-Prot NPs was found, whereas no assessable results for TLR9 (both particles) and TLR3, 7 and 9 activation (PLGA-CatSt NPs) were obtained (see above). Table 5.3 shows an overview about obtained immunogenicity results. In conclusion, PLGA-Prot and PLGA-CatSt marginally activated DCs at higher concentrations ($> 150 \text{ mg/mL}$). This activation was not caused by TLR2, 3, 4, 7 or 9 activation and was independent of siRNA loading. As PLGA-CatSt particles induced excessive growth of cells, an activating effect may be caused by other factors as immunogenicity.

Table 5.3 Overview of DC maturation and human TLR activation results. x = result is not available; o = negative result without verification (system may bind to TLR3, TLR7 and TLR9 control); plus (+) = human TLR activation; minus (-) = no human TLR activation.

	<i>mDC</i>	<i>hTLR2</i>	<i>hTLR3</i>	<i>hTLR4</i>	<i>hTLR7</i>	<i>hTLR9</i>
siRNA	-	-	-	-	-	-
PLGA-Prot	-	-	-	-	-	O
PLGA-Prot-siRNA	-	-	-	-	-	O
PLGA-Cs	(+)	-	o	-	X	-
PLGA-Cs-siRNA	(+)	-	o	-	X	-
PLGA-CatSt	+	-	o	-	O	O
PLGA-CatSt-siRNA	+	-	o	-	O	O

5.3.2.3 NF- κ B and Hsp70 activation assay

PLGA-Cs NPs and free Chitosan showed a modest NF κ B activation in L929 fibroblasts, SHSY-SY neuroblastoma cells, and RAW264.7 macrophages. The cellular response towards proinflammatory stimuli (TNF α , LPS, PMA) was reduced when cells were pretreated with PLGA-Cs NPs. However, this effect was based on a partly dose-dependent manner. Here, the highest reduction was observed at RAW264.7 cells followed by L929 and SHSY-SY cells. The lower impact on SHSY-SY cells might be caused due to lower uptake rates. Additionally, Hsp70 was only activated at the highest particle concentration of 2 mg/mL. As some inconclusive results were measured (rather low LPS effect on RAW264.7 cells and a decreased NF κ B signal without prior proinflammatory stimuli) these results need to be repeated to exclude possible implementation errors.

5.4 Conclusion

As MTT assays are prone to interference due to culture condition changes, the COMPACT consortium decided to use MTS/PMS due to its increased sensitivity [205, 206] and fewer required steps (to avoid additional cell stress). However, MTT was very robust and metabolized by most cell lines [207]. The ViaLight™ as an ATP detection assay is by far the most sensitive one [208], but results suffered from high standard deviations and rising viabilities for PLGA-Cs and PLGA-CatSt NPs. Considering all viability assays, all three types of delivery systems showed no or merely less cytotoxic effects at applied concentrations.

All three types of coated PLGA NPs slightly activated BMDCs (see section 5.3.2.1) at concentrations above 150 μ g/mL. This activation was not caused by TLR2 and TLR4 activation and was independent of siRNA loading. The coated PLGA NPs also did not activate the TLR3, 7 and 9 reporter cell lines. But as they reduced agonist-mediated activation, this observed lack of activation of TLR3, 7 and 9 (detection of double-stranded RNA, single-stranded RNA, and CpG DNA) may be explained by the desired ability of the DDS to bind and deliver nucleic acids in general. As PLGA-CatSt caused excessive cell growth, CatStarch seemed to be a 'self-adjuvant' polymer.

PLGA-Cs NPs showed merely marginal NF κ B and Hsp70 activation. Clearer results need to be acquired from further investigations. Nonetheless, *in-vivo* biodistribution studies of loaded DDSs using ALEXA750-labeled siRNA in mice have been planned and will be conducted soon.

Chapter 6 - Transfection efficiency of drug delivery systems

The author of this thesis made the following contribution to this chapter:

Planned, designed and performed all experiments related to transfection, analyzed all the data from the mentioned studies, interpreted all experimental data and wrote the chapter, if not stated otherwise.

Cell culture of hAELVi cells was performed by Stephanie Kletting.

6.1 Introduction

Within this chapter, the ability of coated cationic polymer-based DDS as a vector to transfect cell culture cells was investigated. A Luciferase assay is a commonly used technique to show the efficacy of a potential transfecting agent or a gene delivery system. Here, pGL3 plasmid DNA (pDNA; plasmid which encodes the production of Luciferase protein) will be internalized into eukaryotic culture cells. After applying a matching siRNA, the measurement of the luminescence should show a knock-down of the luminescence signal. As transiently transfected cells are known to lose their foreign genetic information from the plasmid (usually within 24 - 96 hours) due to proliferation processes (cell division and other factors) a stably transfected cell line is necessary for valid knock-down results. Such a cell line with a remaining pDNA construct can be created by a transient transfection followed by serendipitous integration of the gene into its genome for its replication. A co-expression of a selection marker (e.g. antibiotic resistance) ensures the cultivation of desired clones. However, hard-to-transfect cell lines, especially primary cells, require viral methods (e.g. transduction). These methods suffer from time-consuming production of necessary vectors and safety concerns [209].

As part of the COMPACT consortium stably transfected BHK (baby hamster kidney fibroblasts; EGFP-transfected) cells and HeLa (immortal cervical cancer; eGFP and Luciferase-transfected) cells were provided by project partners. Here, plasmid DNA (pGL3 = pDNA: plasmid which encodes production of Luciferase protein and/or eGFP (enhanced green fluorescent protein) has been integrated into cell culture cells. Unfortunately, the signal intensity when the cells were cultivated in-house was not evolved sufficiently. Therefore, and due to the lack of time the development of a new experimental setup to show a knock-down after transfection without the availability of a stably transfected cell line was necessary. Additionally, a proper transfer of results from BHK or HeLa cells to human lung cell models (cell line or primary cells) is vague.

6.2 Materials and methods

In the following section different transfection agents were applied to identify the most suitable positive control for later studies on lung specific cells. Lipofectamine[®] RNAiMAX reagent (from Invitrogen by Life Technologies, USA), siPORT[™] NeoFX[™], a lipid-based transfection agent (from Ambion by Life Technologies, USA), jetPRIME[™] and INTERFERin[™] (from Polyplus transfection, France), and HighPerFect, a blend of cationic and neutral lipids for transient transfection, (from Qiagen) were considered. Furthermore, all RNase sensitive samples were bottled into DNA LoBind Eppendorf Tubes[®] 1.5 and 5 mL from Eppendorf AG, Germany. For normalization a quantification of the protein amount was conducted via Microplate BCA[™] Protein Assay Kit – Reducing Agent Compatible from Thermo Scientific and pGL3 plasmid was extracted and purified using Plasmid Mega-Kit from QIAGEN from an *E.coli* DHA-alpha culture strain. Luciferase 1000 assay system was purchased from Promega. Transwell[®] (12-well Transwell[®] plates 3460 with polyester membrane Transwell[®]-inserts, pore size: 0.4 μm , growth surface area: 1.12 cm^2 were used to measure TEER values in $\Omega^* \text{cm}^2$ (e.g. hAELVi B/15 p 36 20.4.15; blanc = 110; barrier > 300). Luciferase plasmid pGL3 was extracted and purified in-house (see section 6.2.2) and siRNAs (negative control and pGL3 matching sequence) were provided from COMPACT partner GSK and Luciferase GL3 duplex (target sequence: CUUACGCUGAGUACUUGA) was purchased from Dharmacon.

Additional materials, chemicals and media are listed in the related sections. All experiments were conducted in triplicates

6.2.1 Cultivation of A549 and hAELVi cells

Epithelial cell line

Adenocarcinomic human alveolar epithelial cells (A549; ATCC[®] No. CCL-185[™]) [187] from 'American Type Culture Collection' (ATCC) were cultivated as previously described in section 5.2.1.1.

Immortalized lung epithelial cells

hAELVi.B (human alveolar epithelial lentivirus immortalized, clone B) [210] cells were cultivated in small airway epithelial cell basal media (Clonetics® SABM™ medium from Lonza, Walkersville, USA); with 1 % Penicillin-Streptomycin (PenStrep: Penicillin 10,000 U/mL, Streptomycin 10,000 µg/mL; Gibco by Life Technologies, USA), 1% fetal bovine serum (FBS; from Lifetechnologies, Germany), supplied with growth factors (Clonetics® SABM™ SingleQuots® from Lonza, Walkersville, US) to convert SABM™ Basal Medium to SAGM™ Growth Medium (small airway growth medium). 500 mL contain BPE (bovine pituitary extract), 2.0 mL; Hydrocortisone, 0.5 mL; rhEGF (recombinant human epidermal growth factor), 0.5 mL; Epinephrine, 0.5 mL; Transferrin, 0.5 mL; Insulin, 0.5 mL; Retinoic Acid, 0.5 mL; Triiodothyronine, 0.5 mL; GA (gentamicin 30mg/mL, amphotericin 15 µg/mL), 0.5 mL; BSA-FAF (bovine serum albumin, fatty acid free), 5.0 mL at 37 °C in 95 % humidified air (5 % CO₂). To enable cell attachment Cellstar® T75 standard cell culture flasks, Cellstar® 24-well cell culture plates (both from greiner bio-one) and Transwell® polyester membranes (Corning 3460 with a pore size of 0.4 µm) were coated with 1 % (v/v) fibronectin (Corning, USA) and 1 % (v/v) collagen (from bovine skin; Sigma, Germany).

In contrast to A549 cells which are incapable of forming a functional barrier *hAELVi* cells express tight junctions. These barrier properties roughly correspond to the situation *in-vivo*. Measurements of the transepithelial electrical resistance (TEER) were conducted by a heating plate at 37 °C to avoid temperature-dependant influences using a chopstick electrode coupled with an epithelial Volt/Ohm meter (EVOM, from World Precision Instruments, USA) and describe the integrity of a cell layer [54]. For this purpose, cells were seeded at a density of 100,000 cells/cm² on Transwell® membranes and cultivated under liquid covered conditions (LCC: 500 µL apical compartment and 1.5 mL basolateral compartment) and measured on day 4, 6, 8, 11 and 12. TEER values were calculated by consideration of resistance values (110 Ω) of cell-free inserts containing only medium with a cultivation area of 1.12 cm².

6.2.2 Extraction of pGL3 plasmid from *E.coli*

Bacterial cells from the culture strain *E.coli* DHA-alpha (genotype: F⁻ Φ 80/*lacZ*ΔM15 Δ(*lacZ*YA-*argF*) U169 *recA1 endA1 hsdR17* (rK⁻, mK⁺) *phoA supE44 λ⁻ thi-1 gyrA96 relA1*) containing pGL3 plasmid were used as starting material to extract the pGL3 vector. To purify the amount of plasmid DNA the Plasmid Mega-Kit from QIAGEN was used as recommended in the associated protocol. The DNA concentration was determined by UV spectrophotometry at 260 nm (Eppendorf BioPhotometer) and diluted with TE-buffer (10 mM Tris, 1 mM EDTA; pH 8.0) to a final concentration of 1 μg/mL, aliquoted and stored at – 20 °C (- 80 °C for long term storage).

6.2.3 Simultaneous co-transfection

As the application of a stably pGL3-transfected cell line was not applicable, a simultaneous co-transfection was used to analyze transfection efficiencies of the investigated DDSs. Performing this experiment attention should be paid to the fact that pGL3 plasmid (200 ng/well) and siRNA (600 ng/well) solutions (diluted with medium to obtain a final sample volume of 100 μL/well) were separately incubated with 1 μL/well of transfection agent (Lipofectamine[®] RNAiMAX from Invitrogen by Life Technologies, USA) to ensure a proper polyplex formation. Afterward a mixture of plasmid- and siRNA-complexes was feasible. To exclude a possible source of error by deficient siRNA a Luciferase GL3 duplex (from Dharmacon, Inc., USA) was tested next to the provided COMPACT pGL3 siRNA (from GSK).

Prior studies (see section 6.2.4) confirmed sufficient transfection experiments when FBS is present in cell culture medium. Thus, A549 cells were seeded in RPMI medium containing 10 % FBS at a density of 30,000 cells/well and hAELVi cells in SAGM containing 1 % FBS at a density of 50,000 cells/well (both in 24-well cell culture plates). After reaching a confluence of 80 – 90 % cell culture medium was replaced and 100 μL/well sample solution were applied followed by 24 h of incubation at standard conditions. Here, 100 μL sample solution contained 200 ng pGL3 plasmid + 1 μL transfecting agent and 600 ng siRNA + 1 μL transfecting agent as a positive control or bound on coated PLGA NPs in a ratio of 1:50 (siRNA:NP), see section

2.3.3. For negative controls, the volume of transfecting agents was replaced by medium or only pGL3 plasmid. Additionally, a transfecting agent was applied. After incubation sample solutions were discarded, cells were washed with PBS buffer and 100 μL /well lysis buffer were added (incubation for 10 min. at RT). BCA-RAC assay and Luciferase assay were conducted as described in section 6.2.5 (BCA-RAC assay) and 6.2.6 (Luciferase assay).

6.2.4 Screening of transfection reagents

Depending on the experimental setup of transfection trials and the chosen cell line different commercially available transfection reagents may be suitable as a positive control. In this connection, a positive control has to show a possibly high impact on applied cells which is commonly evaluated by the respective manufacturer for standard cell lines. As in this chapter co-transfection experiments on A549 and hAELVi.B cells were performed, a prior screening of competing transfecting agents on both introduced cell lines was necessary.

A549 cells were seeded in RPMI medium with 10 % FBS and without FBS at a density of 30,000 cells/well (24-well cell culture plate) and hAELVi cells in SAGM with 1 % FBS in a density of 50,000 cells/well (24-well cell culture plate). After reaching a confluency of 80 - 90 % (incubation under standard culture conditions for approximately 3 days) transfection experiments could be initiated: medium was replaced and plasmid (200 ng/well) and siRNA (600 ng/well) were mixed separately with respectively 1 μL /well transfection reagent. After incubation for 15 min. at RT (formation of complexes) both mixtures were combined and medium or reagent buffer was added to obtain a final volume of 100 μL /well. For controls transfection reagent was substituted by medium. 100 μL /well transfecting mixture were added and cells were incubated for 24 h under standard conditions. Subsequently, cells were washed with PBS buffer, 100 μL /well lysis buffer were added and cells were incubated for 10 min. at RT. BCA-RAC assay and Luciferase assay were conducted as described in section 6.2.5 (BCA-RAC assay) and 6.2.6 (Luciferase assay).

6.2.5 BCA vs. BCA-RAC for normalization

To analyze a Luciferase assay accurately a normalization of the luminescence signal = relative light units (RLU) to the total amounts of cells is indicated. A commonly used method for normalization is the determination of the entire amount of protein via bicinchoninic acid assay (BCA; Pierce™ BCA assay kit; from Thermo Scientific). To create a Luciferase assay compatible cell lysate the Cell Culture 5 x Lysis reagent (CCLR; from Promega) was used after dilution with Milli-Q purified water.

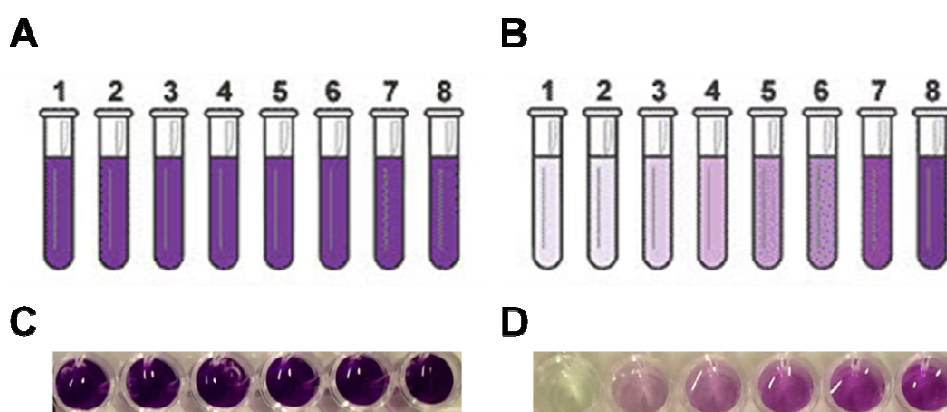


Figure 6.1 Comparison of the effect of reducing agents on standard BCA (A/C) and BCA-RAC (B/D) protein assays; A/B: samples contain 5 mM DTT and bsa standards at the following concentrations in $\mu\text{g/mL}$ from tube 1 to 8: 0, 125, 250, 500, 750, 1000, 1500, 2000. C/D samples contain 1 x promega lysis buffer (among others 2 mM DTT and 1 % Triton X-100) and bsa standards at the following concentrations in $\mu\text{g/mL}$ from left to right: 0, 100, 400, 600, 800, 1000. (A/B were adopted from www.thermoscientific.com/order/catalog/product/23252, 16.02.2015).

The composition of this (1x) buffer according to the Promega Luciferase Assay System – Technical Bulletin No. 281 is as follows: 25 mM Tris-phosphate (pH 7.8), 2 mM DTT, 2 mM 1,2-diaminocyclohexane-N,N,N',N'-tetraacetic acid, 10 % glycerol, 1 % Triton® X-100. The high concentration of dithiothreitol (DTT) and detergent (Triton® X-100), however, precludes the usage of the BCA assay and most other protein quantification assays (see Figure 6.1). Therefore, an BCA-RAC assay (Pierce™ Microplate BCA Protein Assay Kit - Reducing Agent Compatible from Thermo Scientific) was used. This specific assay is compatible with concentrations of DTT up to 5 mM and Triton® X-100 up to 10 % to quantify the total amount of protein. Here, after 24 h of incubation sample solutions were discarded and cells were washed with PBS buffer. After the addition of 100 μL /well cell lysis buffer followed by

10 min. of incubation, 9 μL cell lysate were transferred in a 96-well plate and incubated again with 4 μL compatibility reagent solution for 15 min. at 37 °C. Afterwards 260 μL BCA-reagent were added and the 96-well plate was covered and incubated for 30 min. at 37 °C. Using the standard control as blank the absorbance rates of cool (RT) sample controls and standards (bsa: 0 – 2,000 $\mu\text{g}/\text{mL}$) were measured at 562 nm with a Tecan[®] Infinite 200 PRO multimode microplate reader (using i-control[™] software; Tecan Deutschland GmbH, Germany).

6.2.6 Luciferase assay

Here, the Luciferase 1000 assay system from promega was used. After 24 h sample incubation cells (in 24-well cell culture plate) were washed with 500 μL PBS buffer. As much waste as possible was removed followed by the addition of 100 μL lysis buffer (incubation 15 min. at RT). Cell lysate (20 $\mu\text{L}/\text{well}$) was transferred into an OptiPlate[™]-96 white (from PerkinElmer, USA). 100 μL of Luciferase reagent (protected from light exposure) were added via auto-injector, and the emitted light (as relative light units = RLU) was immediately measured via Tecan[®] Infinite 200 PRO multimode microplate reader (using i-control[™] software; Tecan Deutschland GmbH, Germany). This step was repeated for the remaining wells.

6.3 Results and discussion

6.3.1 Reagent screening

Depending on the deployed transfection agent and the selected cell type results of co-transfection experiments with Luciferase (pGL3) plasmid and siRNA showed enormous differences. Within this study, agents needed to be capable of transfecting plasmid DNA and siRNA at the same time. Differences between (-) non-matching siRNA and (+) pGL3-matching siRNA were evaluated and indicated the knock-down ability of the reagent, which was the determining value identifying a positive control.

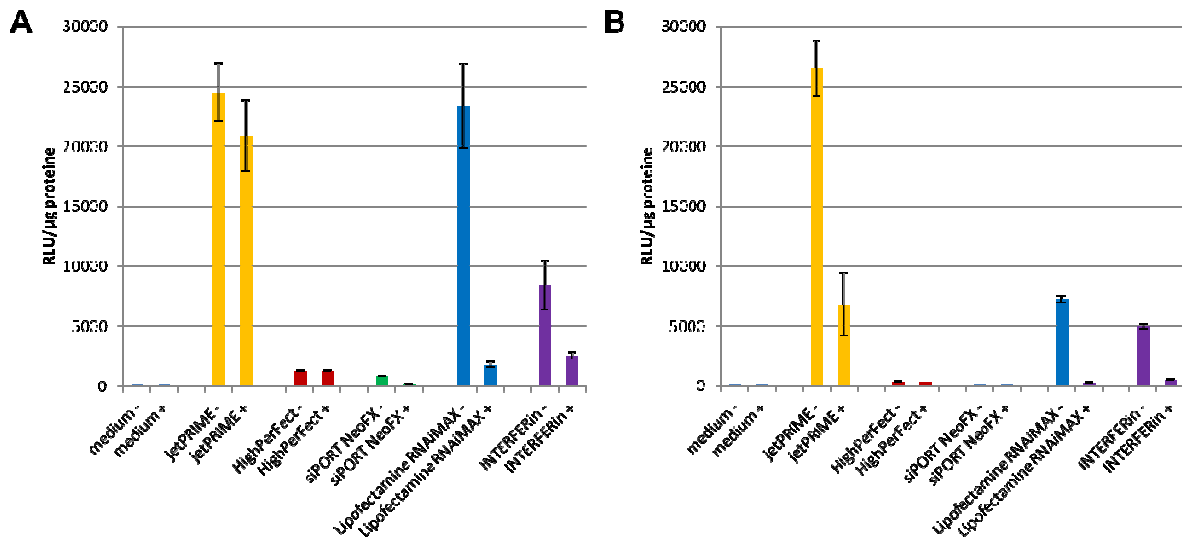


Figure 6.2 Screening of different transfection reagents on A549 cells cultivated without FBS (A) and with 10% FBS (B). Minus (-) indicates a transfection with a negative control siRNA and plus (+) indicates a transfection with a Luciferase (pGL3) knock-down siRNA (both provided by COMPACT partner gsk).

Within this study (see Figure 6.2) HighPerFect showed only a weak light emission by the transfected Luciferase plasmid and almost no knock-down by the + siRNA on A549 cells. Similar results could be obtained for siPORT NeoFX transfection agent. First knock-down tendencies showed INTERFERin with a moderate light emission from the (-) siRNA control and a slightly reduced signal from pGL3 matching (+) siRNA. On A549 cells (Figure 6.2 A: without FBS) jetPRIME and Lipofectamine RNAiMAX were sufficient in transfecting pGL3 Luciferase plasmid into the cells, whereas only Lipofectamine RNAiMAX could induce knock-down of the light exposure. In FBS containing RPMI medium (Figure 6.2 B) both reagents achieved a significant reduction of the Luciferase signal. However, Lipofectamine RNAiMAX failed in inducing high amounts of l'Luciferase plasmid compared to jetPRIME. As the efficiency of a transfection agent is dependent on the selected cell line, differences between A549 and hAELVi cells were expected. Here, only Lipofectamine RNAiMAX was able to show an adequate knock-down of emitted light (see Figure 6.3).

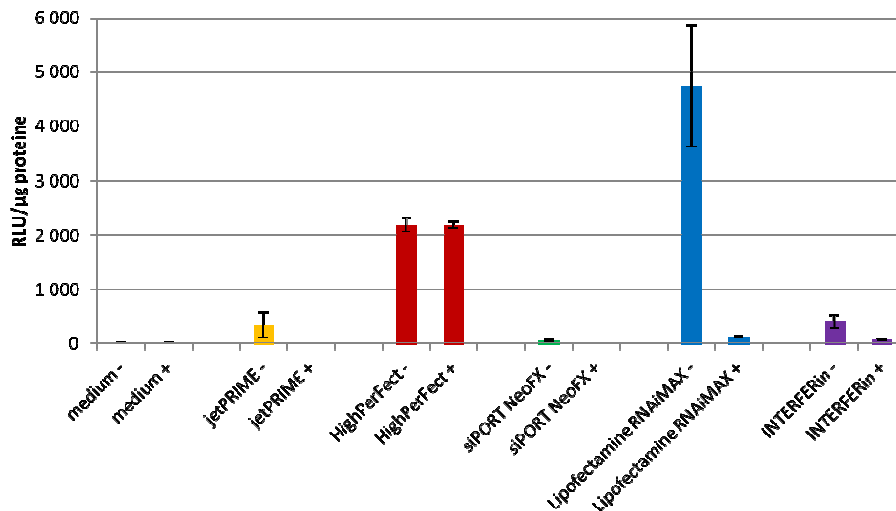


Figure 6.3 Screening of different transfection reagents on hAELVi cells cultivated with 1% FBS (B). Minus (-) indicates a transfection with a negative control siRNA and plus (+) indicates a transfection with a Luciferase (pGL3) knock-down siRNA.

All other reagents showed very weak effects in general. Merely HighPerFect apparently transfected the Luciferase plasmid, but not siRNA (no knock-down visible). In conclusion, Lipofectamine RNAiMAX had the best accordance with co-transfection results on A549 and hAELVi cells. Thus, Lipofectamine RNAiMAX represents the positive control for later transfection studies with DDSs.

6.3.2 Transfection experiments on A549 cells

The transfection efficiency of a developed carrier is one essential parameter when comparing several drug delivery systems. Figure 6.4 gives an overview of all three coated PLGA-based particulate systems loaded (siRNA:NP, 1:50) with project-internal Luciferase siRNA (+) and a commercially available pGL3-matching siRNA (Dha +; Luciferase duplex from Dharmacon).

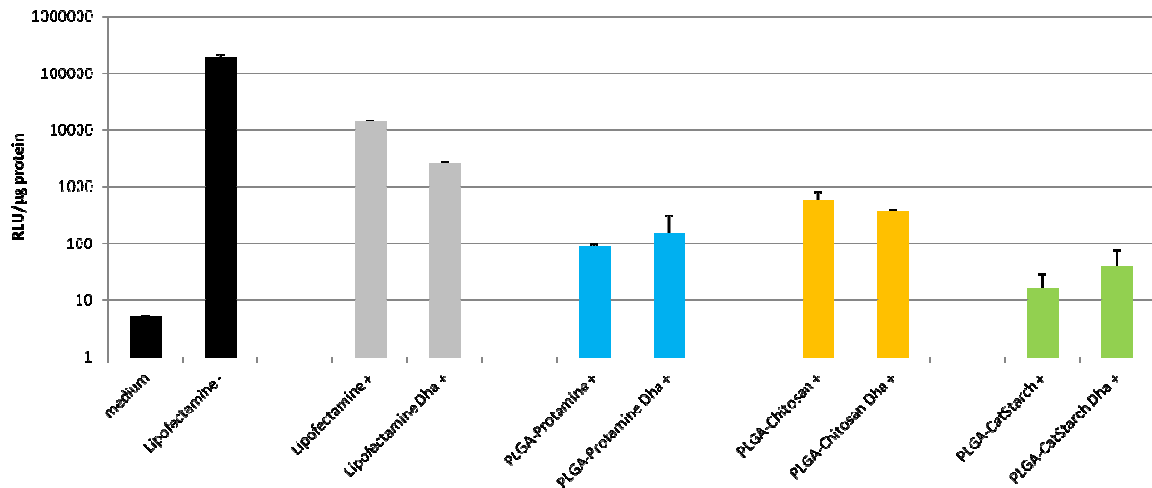


Figure 6.4 Evaluation of simultaneous co-transfection experiments of DDSs on A549 cells. Plus (+) indicates a transfection with a COMPACT internal Luciferase (pGL3) siRNA and Dha + a Luciferase pGL3 duplex from Dharmacon. Minus (-) indicated a transfection with a non-coding siRNA. Particles: PLGA-Prot (blue), PLGA-Cs (yellow) and PLGA-CatSt (green) NPs were compared with Lipofectamine as a positive control.

Following previous results (see section 6.3.1) Lipofectamine RNAiMAX was applied as a positive control and complexed with pGL3 plasmid DNA and siRNA (-, + and Dha +). As the addition of Lipofectamine plus non-matching (-) siRNA reached almost the same RLU level, results of NPs with non-matching siRNA were not shown to obtain a coherent evaluation. Some but non-significant differences between the commercial Dharmacon duplex and COMPACT siRNA occurred. Thus, both nucleic acids were intact and efficient. All investigated particulate systems seemed to show a better knock-down ability than the positive control. Nevertheless, differences could be observed depending on the particle coating. Although Protamine showed a minimal buffering capacity (see section 3.2.3.2) and PLGA-Prot NPs the slightest surface charge (see, section 3.3.2.1), transfection efficiency was determined by additional factors (e.g. loading efficiency). In this context, the co-influence of various characteristics of the DDS and the applied materials may explain a reduced knock-down of PLGA-Cs NPs and an increased down-regulation of PLGA-CatSt NPs within this study. As a result, simultaneous co-transfection with pGL3 plasmid DNA and siRNA worked even though the efficiency could not be predicted by prior determined characteristics.

6.3.3 Transfection of hAELVi cells

hAELVi cells show enlarged generation times compared to cancer cell lines, thus more cells (50,000 cells/well) were initially seeded to obtain a final sufficient confluence of ~ 80 %. Apart from this, the same experimental setup on A549 cells was applied to investigate transfection efficiencies on hAELVi cells (see Figure 6.5). Here, all obtained values (RLU/ μg protein) showed a lower level which confirmed improved barrier properties of hAELVi cells compared to A549 cells. Regarding differences within applied samples the positive control, PLGA-Prot NPs and PLGA-Cs NPs showed similar transfection efficiencies. However, PLGA-CatSt NPs could induce an enhanced knock-down of the Luciferase signal. Again, confirming prior assumptions more than one parameter seemed to be responsible for an improved transfection as observed deviations on A549 and hAELVi were solely cell specific.

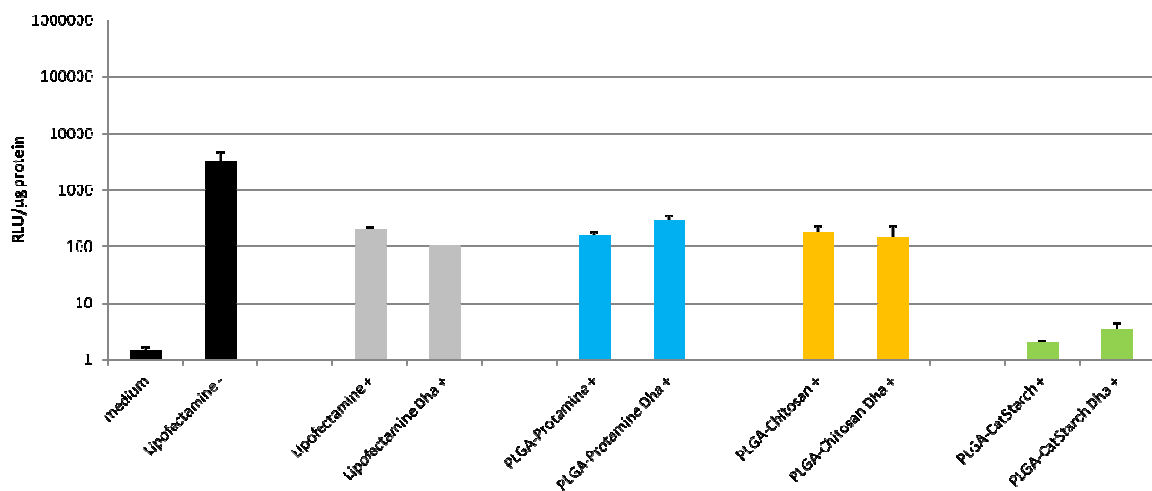


Figure 6.5 Evaluation of simultaneous co-transfection experiments of DDSs on hAELVi cells. Plus (+) indicates a transfection with a COMPACT internal Luciferase (pGL3) siRNA and Dha + a Luciferase pGL3 duplex from Dharmacon. Minus (-) indicated a transfection with a non-coding siRNA. Particles: PLGA-Prot (blue), PLGA-Cs (yellow) and PLGA-CatSt (green) NPs were compared with Lipofectamine as a positive control.

Based on previous results, possible transfection efficiencies of hAELVi cells with functional barrier properties were evaluated. For this purpose cells needed to be cultivated on Transwell[®] membranes to enable TEER measurements (see Figure 6.6). After cultivating cells for 11 days increased TEER values indicated an intact

cellular monolayer and represented the starting point for additional transfection studies. Unfortunately, no significant luminescence signal by pGL3 plasmid could be measured. In conclusion, a simultaneous co-transfection is not suitable for this system with barrier performing cells.

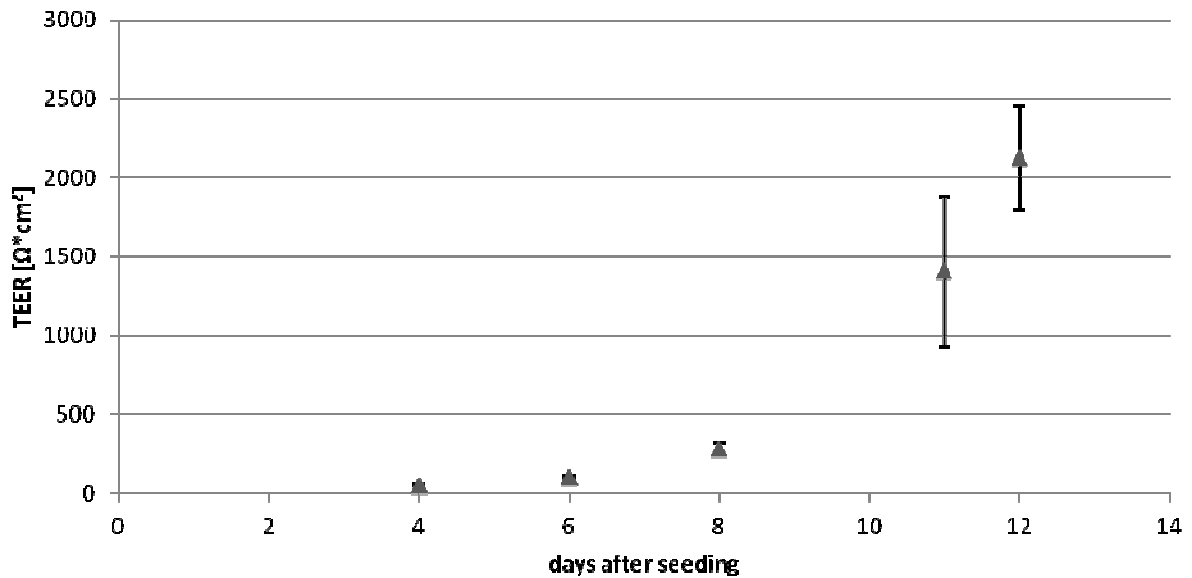


Figure 6.6 Barrier properties of hAELVi cells. TEER measurements were performed over a period of 12 days.

6.4 Conclusion

Within this chapter, the ability of a nanoparticulate system to transfect lung-specific cells was investigated. After identifying Lipofectamine RNAiMAX as a suitable positive control and BCA-RAC assay as a sufficient normalization method, a functioning simultaneous transfection with pGL3 plasmid and siRNA on A549 and partly on hAELVi cells (no transfection efficiency measurable on monolayer hAELVi cells) was shown. However, A549 cells were easier to transfect than hAELVi cells. These cell-specific differences can be explained by poor epithelial barrier function [211, 212] of A549, whereas hAELVi cells deploy functional tight junctions. As co-transfection experiments required a transfection agent to transfect a Luciferase plasmid, all samples contain this reagent (with an unknown composition). Hence, possible interactions between cells, applied materials and transfection agent can never be excluded.

Consequently, initial results need to be verified by other transfection studies. One possibility would be measuring the knock-down of an endogenous gene via GAPDH siRNA, followed by qPCR analysis. Another approach could be the investigation of stable Luciferase/eGFP transfected A549 and hAELVi cells, as transfection studies on BHK1 and HeLa cells showed merely limited effects. Furthermore, the combination of Luciferase and eGFP shows the advantage of holding two comparable knock-down parameters within one cell line. Following this, a transfection of hAELVi cells under air-liquid interface (ALI) or LLC as well as on co-culture models (hAELVi plus THP-1 cells) needs to be performed (in co-operation with COMPACT partners in WP 6).

In-vivo transfection studies with transgenic mice needed to be postponed, as murine TNF α antisense was not available and the animal model needed to be established first, at that time.

Chapter 7 - Uptake and localization of nanoparticles on cells (*in-vitro*)

The author of this thesis made the following contribution to this chapter:

Planned, designed and performed all experiments related to localization and uptake studies, analyzed all the data from the mentioned studies, interpreted all experimental data and wrote the chapter, if not stated otherwise.

Cell culture of hAELVi cells was performed by Stephanie Kletting.

FCS analyses were performed by Edward Sayers at Cardiff University. He analyzed data from the mentioned studies and interpreted the experimental data.

7.1 Introduction

Different transport mechanisms on how substances or particles can reach their target are known. A distinction is made between paracellular transport between cells and through their tight junctions, transcellular transport through cells (including receptor-mediated transcytosis) and intracellular transport into cells. The paracellular transport is restricted to solutes with a maximum diameter of 6 nm [213] and the transcellular transport usually to macromolecules like transferrin, insulin, IgA or lipophilic NPs [214]. The primary transport mechanism for our polymeric carrier systems seems to be the latter one, the intracellular transport, which is also described as endocytosis.

When a particle hits the cell surface, it cannot simply pass through the cell membrane. But an energy-using process can be initiated. Depending on the properties or characteristics of a particulate system (size, shape, hydrophobicity of applied materials and ligand attachments) [215] the cellular internalization can be classified into different submechanisms: phagocytosis, macropinocytosis, clathrin-mediated and caveolae-mediated endocytosis. The last three pathways belong to the umbrella term pinocytosis. Pinocytosis in general, also known as “cell drinking”, is describing the uptake of extracellular fluids and the substances it contained.

After engulfing the particulate system, endosomal vesicles (or primary vesicles) will be formed, and the endocytic pathway starts by routing them to early endosomes. This organelle is mainly located in the cell periphery and can be described as a cargo-sorting station [216]. The lumen of an early endosome is slightly acidic (~ pH 6.0 - 6.8) [217, 218] where ligands dissociate from their receptors. The material from the early endosome will be delivered to a late endosome with an acidic pH of 5.5 and finally to the lysosome, the last compartment of the endocytic pathway where ligands are degraded by the lower pH of 4.5 – 5.0 [219]. In the following section, the terms endosome and lysosome (here, a differentiation via CLSM is not possible) will be used interchangeably.

7.2 Materials and methods

7.2.1 Cell culture

Different lung-specific cells of human origin and other non-pulmonary cells were available and seeded at 20,000 cells/well (19,600 cells/cm²) in 8-well cell culture slides (No. 30118 from SPL life technologies, Chosun) for uptake and localization studies.

7.2.1.1 Lung cells

Human monocyte-derived cells (THP-1), adenocarcinomic human alveolar epithelial cells (A549) and adenocarcinoma-derived human bronchial epithelial cells (Calu-3) were cultivated as described previously in section 5.2.1.1. For FCS analysis A549 cells were seeded at 200,000 cells (270,000 for initial uptake studies) per imaging dish (from MatTek Corporation, USA) and incubated for 24 h. Detailed information about cultivating hAELVi cells can be found in section 6.2.1.

7.2.1.2 Non-pulmonary cells

Prior experiments indicated cell specific transfection efficiencies particularly due to their specific uptake behavior. Although studies within this work were focused on lung-specific cells, a varying particle uptake depending on the applied cell line was investigated. Briefly, Normal Human Dermal Fibroblasts (NHDF-p) as proliferating cells, next to immortalized Human Skin keratinocytes (both cultivated in Dulbecco's Modified Eagle Medium, DMEM; plus 10 % FBS) and HeLa cells, the oldest immortalized human cell line taken from cervical cancer from Henrietta Lacks (cultivated in Eagle's Minimum Essential Medium, EMEM from Lonza; plus 10 % FBS and 1 % PenStrep), were evaluated.

7.2.2 Uptake and localization

Confocal laser scanning microscopy (CLSM) was used to visualize different cell compartments and engulfed NPs. For fixation, cells were washed with PBS first, followed by the addition of 200 μ L MeOH (ice chilled) for 15 min. at 4 °C. Hereafter, MeOH was removed and cells were washed again with PBS. To stain the cellular membrane 200 μ L Rhodamine-labeled *Ricinus Communis* Agglutinin I (RCA I from Vector Laboratories; diluted 1:1,000 in PBS) were incubated for 10 min. at RT. After washing with PBS, cells were counterstained with 200 μ L 4',6-diamidino-2-phenylindole (DAPI; CAS No.: 28718-90-3; nuclei stock: 1 mg/mL from Life Technologies™, Germany; diluted 1: 50,000 in PBS) for 20 min. at RT. Finally, cells were washed again with PBS. Fixed and stained cells were analyzed by CLSM (Zeiss LSM710, Zeiss, Germany) equipped with a 63 x water immersion object lens. Obtained images were edited by Zen2012 software (Carl Zeiss Microscopy GmbH, Germany). Settings were optimized to each sample except for correlative microscopy. Here, settings were kept the same for all samples to enable comparability.

To confirm a particulate uptake into cellular endosomes a lysosomal staining (of selective accumulated weakly basic amines into organelles with a low pH [220]) was applied. Therefore, living cells were incubated with FA-labeled NPs (30 μ g/mL) for 24 h at 37 °C, followed by 200 μ L LysoTracker® Red (DND-99; Abs: 577 nm; Em: 590 nm; 1 μ L in 5 mL PBS) for 2 h at 37 °C.

For initial uptake studies on viable THP-1 cells loaded (1:5 ratio of ALEXA-labeled siRNA and non-labeled siRNA in a total ratio of 1:100 siRNA:particles) FA-PLGA-Cs NPs (0.1 μ g/mL) were incubated for 24 h in FBS-free medium.

7.2.4 Fluorescent correlation spectroscopy

In cooperation with Edward Sayers, Cardiff University, a COMPACT partner in WP3 (P5) the particulate systems were tested regarding particulate binding and uptake into cells. Here, A549 cells were exemplarily used for a pulmonary alveolar epithelial cell model. After determining the suitability of the flu-labeled particles (coated FA-PLGA NPs) for microscopy and fluorometry FA-labeled PLGA NPs were loaded

by adding an aqueous solution of siRNA (1:5 ratio of ALEXA-labeled siRNA and non-labeled siRNA) in a ratio of 1:100 (siRNA:particles) and subsequently diluted with serum containing medium (SCM) down to 100 µg/mL. For initial uptake studies samples were immediately added to the cells and incubated for 1 h at 37 °C. Binding experiments, however, were performed on pre-chilled (on ice for 15 min.) cells and samples were incubated for 15 min. at 4 °C. Following this, cells were washed with imaging medium (DMEM, 20 mM HEPES and 10 % FBS) and imaged by CLSM (SP5 from Leica, Germany) at 37 °C.

A lysosomal co-localization of the flu-labeled carrier (FA-PLGA NPs) and cargo (ALEXA647siRNA) was determined by an overlay of lysosomal dextran. To label the lysosome cells were loaded with 50 µg/mL Dextran-A546 for 2 h. Afterward, cells were washed with imaging medium and chased overnight. Between different time points, cells were incubated at 37 °C and all settings were kept for all measurements within a sample.

7.2.5 Correlative microscopy

Adenocarcinomic human alveolar basal epithelial cells (A549) were seeded on an 8-well chamber slide (from SPL) in a density of 30,000 cells/well (= 25,000 cells/cm²) in Roswell Park Memorial Institute (RPMI) 1640 medium (from Gibco by Life Technologies, USA) supplemented with 10 % FBS. After incubation with FA-labeled particles for 24 h the cells were washed with PBS. To fix the cells on the slide, it is possible to use 2.5 % glutaraldehyde for 2 h. But because of the relatively strong resulting auto-fluorescence the cells were fixed with 3 % para-formaldehyde (PFA; prepared by diluting a 16 % stock solution with Milli-Q purified water) for 30 min. Here, the creation of a rougher or broken cell surface needs to be considered. After the removal of the fixing agent, the cells were washed with PBS buffer, followed by a drying sequence with ethanol: 50 % (30 min.) → 60 % (30 min.) → 70 % (30 min.) → 80 % (30 min.) → 90 % (10 min.) → pure EtOH (10 min.). Finally, 20 µL/well Hexamethyldisilazane (HDMS) were applied on the cells and let to evaporate the solution.

For SEM analysis (for CLSM, see section 7.2.2) the prepared cells need to be sputtered on the slide with a very thin gold layer (Quorum Q150R ES, profile: QT Timed Gold; Quorum Technologies, UK) and examined using a scanning electron microscope (Zeiss EVO HD 15, Carl Zeiss AG, Germany) with the associated Zeiss SmartSEM[®] software.

7.3 Results and discussion

7.3.1 Uptake by different cell culture cells

7.3.1.1 Uptake by human lung cells

Initial uptake studies of ALEXA647siRNA-loaded FA-PLGA-Cs NPs on viable THP-1 cells showed NPs engulfed into the cytosol and accumulated siRNA in or around the nucleus (see Figure 7.1 A). Some cells seemed to have only ALEXA647 siRNA inside and no FA-labeled NPs. However, an incubation of labeled siRNA without a carrier system also resulted in accumulating siRNA into the nuclear region (see Figure 7.1 B).

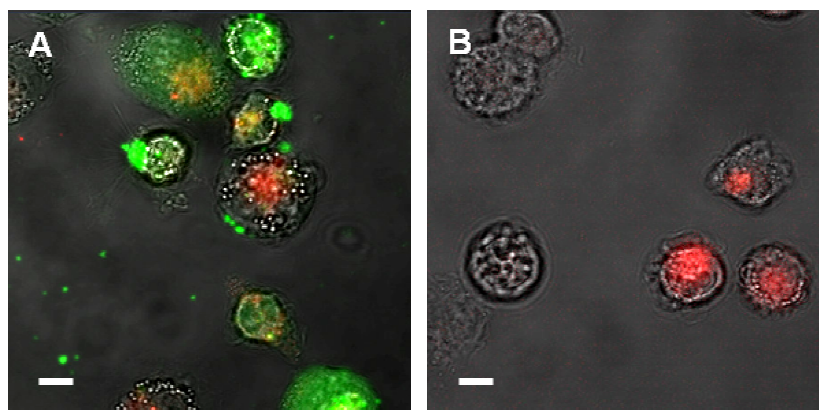


Figure 7.1 A: FA-PLGA-Cs NPs (green, 0.1 mg/mL) loaded (siRNA:NP in a ratio of 1:100) with spiked siRNA (red, ALEXA647:negative siRNA in a ratio of 1:5) in B: spiked siRNA (red, ALEXA647:negative siRNA in a ratio of 1:5) in FBS-free medium on viable THP-1 cells (without fixation). Scale bar 10 μ m

This means that ALEXA647-labeled siRNA was incorporated by THP-1 cells even without the necessity of a carrier system. The ALEXA dye seemed to cause an aggregation of labeled siRNA, as cells were able to take up these precipitates. That the ALEXA647-label was only visible near the nucleus indicated presumably intact

molecules of nucleic acids or antisense strands. As a result, succeeding uptake studies (besides FCS analysis) used only unloaded FA-PLGA NPs to prevent false conclusions based on a fluorescent ALEXA647 signal.

CLSM images (see Figure 7.2) show the particulate uptake of FA-labeled PLGA NPs (A/D/G: FA-PLGA-Prot, B/E/H: FA-PLGA-Cs, C/F/I: FA-PLGA-CatSt; z-stack of G was not available) depending on their cationic coating and the applied cell type (I: A549; II: Calu-3; III: hAELVi).

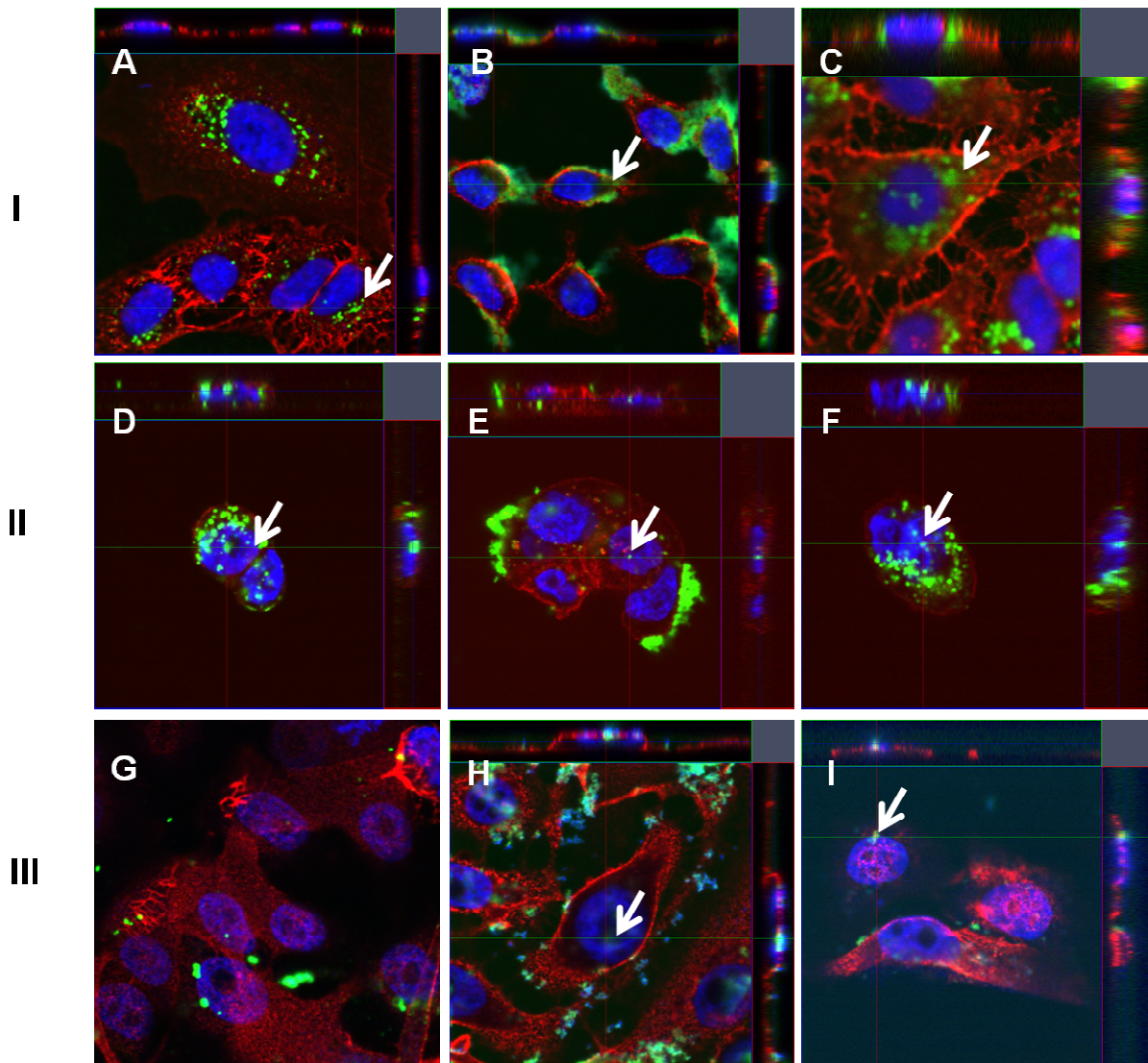


Figure 7.2 CLSM image of the cellular uptake after 24 h on A549 (I) and Calu-3 (II) and hAELVi (III) cells: FA-PLGÁ-Protamine NPs (A/D/G), FA-PLGA-Chitosan NPs (B/E/H) and FA-PLGA-CatStarch NPs (C/F/I). white arrow marks the point of z-x and z-y stacks (for G N/A).

Here, both human cancer cell lines (A549 and Calu-3) showed a comparable uptake pattern: a distinct internalization of FA-PLGA-Prot NPs and FA-PLGA-CatSt NPs into

spherical vehicles within the cytosol. However, FA-PLGA-Cs NPs were merely found as some fluorescent spots inside the cells. Most of the flu-labeled NPs stuck as large aggregates onto the cell membrane and showed high fluorescent signal intensity. Having a look at especially hAELVi cells, Chitosan-coated NPs created again aggregates which were attached to the cell membrane. An uptake of FA-PLGA-Prot and FA-PLGA-CatSt NPs was limited and showed only a few internalized particles.

Within every sample, single cells showed absolutely no uptake of the particulate system which might be caused by the current stage of the cells. Particle uptake seems to be an active transport into the cell and might be limited when cells stay at a quiescent phase or at imminent apoptosis.

7.3.1.2 Uptake on non-pulmonary human cells

Comparative uptake studies on human skin cells (see Figure 7.3, IV: HaCat; V: NHDF-p) showed again engulfed FA-PLGA-based NPs (J/K: FA-PLGA-Prot, M/N: FA-PLGA-Cs, P/Q: FA-PLGA-CatSt; z-stack of K was not available).

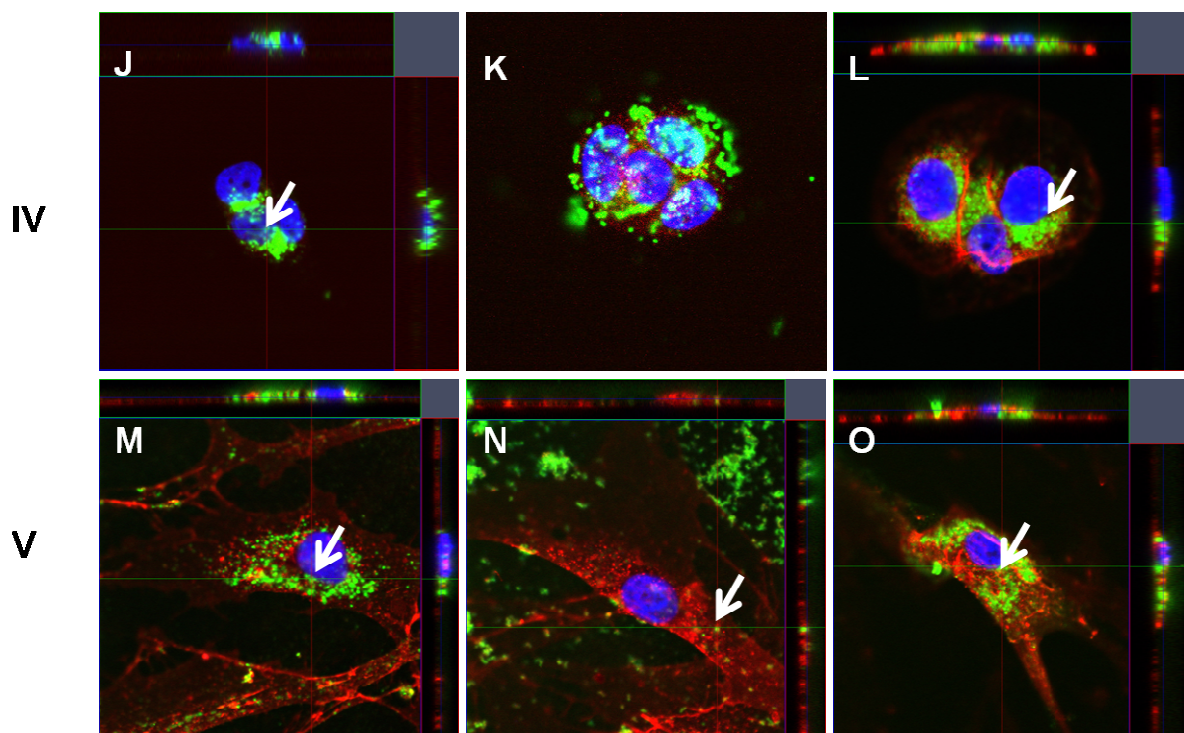


Figure 7.3 Cellular uptake after 24 h on HaCat (IV) and NHDF-p (V) cells: FA-PLGÁ-Protamine NPs (J/M), FA-PLGA-Chitosan NPs (K/N) and FA-PLGA-CatStarch NPs (L/O). White arrow marks the point of z-x and z-y stacks (for K N/A).

Depending on the cationic coating material the total amount of particles inside the cell was different. A large number of FA-PLGA-CatSt NPs could be found in the cytosol of both cells types – the same with FA-PLGA-Prot NPs. However, FA-PLGA-Cs NPs again demonstrated a binding of aggregates to the plasma membrane.

Considering cell-specific differences particles seemed to have entered keratinocytic cells rather than the fibroblastic ones. As small keratinocytes have a higher turnover rate than larger fibroblasts [221] an enhanced uptake mechanism of HaCat cells might be possible. Incubating HeLa cells with coated FA-PLGA NPs showed a similar behavior (see Figure 7.4; (P: FA-PLGA-Prot, Q: FA-PLGA-Cs, R: FA-PLGA-CatSt; z-stacks were not available)): moderate particle uptake of FA-PLGA-Prot NPs, a weak uptake of FA-PLGA-Cs NPs next to partially membrane bound aggregates and an improved uptake of FA-PLGA-CatSt NPs.

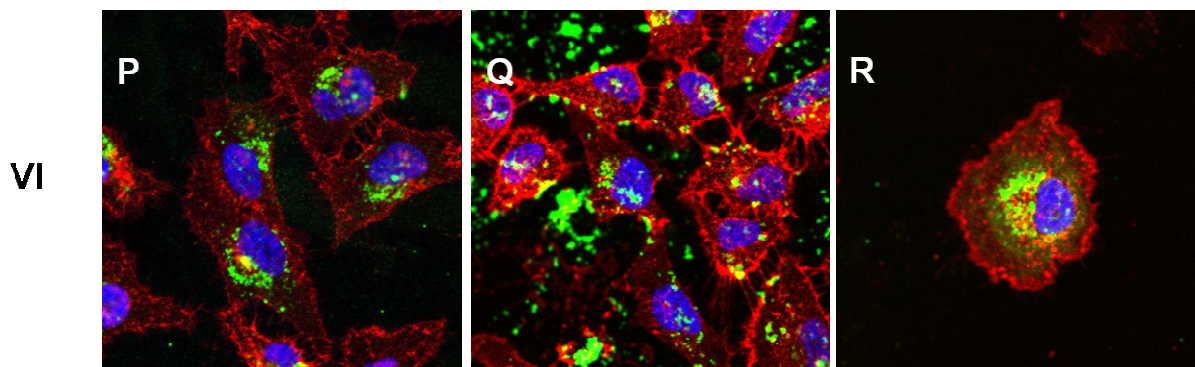


Figure 7.4 Cellular uptake after 24 h HeLa (VI) cells: FA-PLGA-Protamine NPs (P), FA-PLGA-Chitosan NPs (Q) and FA-PLGA-CatStarch NPs (R). Cell membrane (red), nuclei (blue), nanoparticles (green), z-stacks of P/Q/R were N/A.

7.3.1 Localization via LysoTracker[®] dye on A549 cells

Knowing from preliminary experiments (performed at 4 °C) that there is almost no passive transport (or diffusion) of NPs into the cell. Nanoparticles were presumably incorporated via endocytosis. As a test for this hypothesis, lysosomes as acidic cell compartments were specifically visualized by LysoTracker[®] red. This fluorescent dye accumulated in lysosomes or endosomes. An overlay of red stained lysosomes and green nanoparticles indicated an endosomal particle uptake (see yellow spots at Figure 7.5; (S: FA-PLGA, T: FA-PLGA-Prot, U: FA-PLGA-Cs, V: FA-PLGA-CatSt; z-

stack of S was not available). As expected no particles were taken up by A549 cells after incubation with uncoated FA-PLGA NPs which resulted in red stained vesicles. Incubation with FA-PLGA-Prot NPs showed some particles located inside the cell. Some endosomes contained particles and some not whereas all vesicles contained FA-PLGA-Cs or FA-PLGA-CatSt NPs.

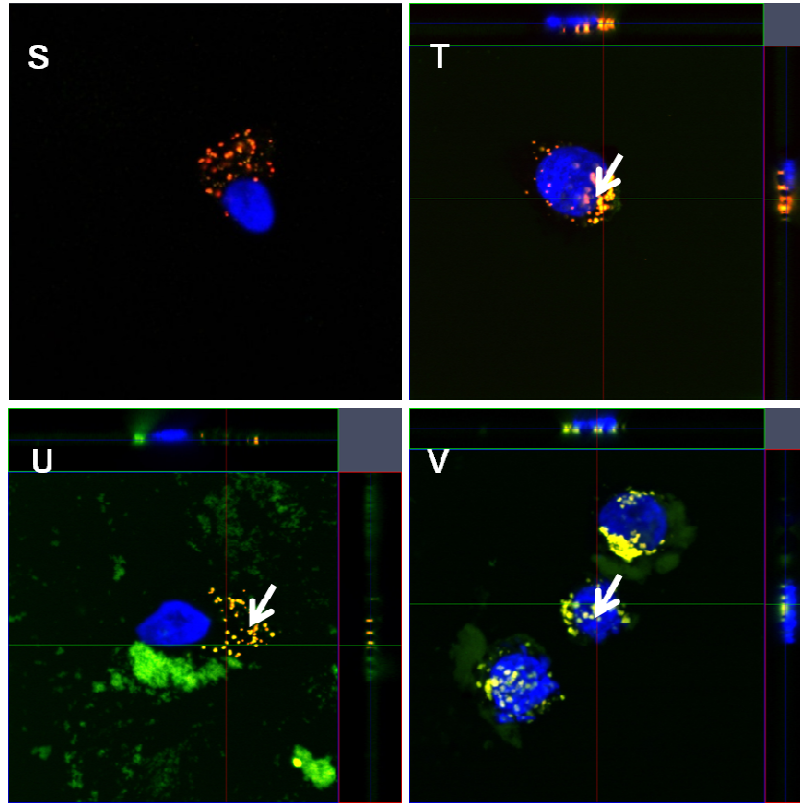


Figure 7.5 Cellular uptake after 24h on A549: FA-PLGA NPs (S), FA-PLGA-Protamine NPs (T), FA-PLGA-Chitosan NPs (U) and FA-PLGA-CatStarch NPs (V). Visualization of lysosomes with LysoTracker[®] Red (red), nuclei with DAPI (blue), nanoparticles (green), overlay of nanoparticles in lysosomes (yellow). White arrow marks the point of z-x and z-y stacks (for S N/A).

7.3.2 FCS analysis

Initial uptake studies with labeled siRNA (ALEXA568 and ALEXA647 siRNA were available) showed a suitable fluorescein labeling of the PLGA NPs and a superior ability of ALEXA647siRNA to evaluate fluorescent signals. With ALEXA568siRNA a dissociation of sample signals from the background was limited as cells showed a strong auto-fluorescence at that wavelength. Thus, only ALEXA647siRNA was applied for the following studies. FA-PLGA NPs as an uncoated control sample with

an anionic surface charge did not internalize well or seemed to bind labeled siRNA (see Figure 7.6 A). FA-PLGA-Prot NPs, however, were strongly bound to the ALEXA-labeled siRNA and to the plasma membrane; after 6 h a complete internalization was visible (see Figure 7.6 B).

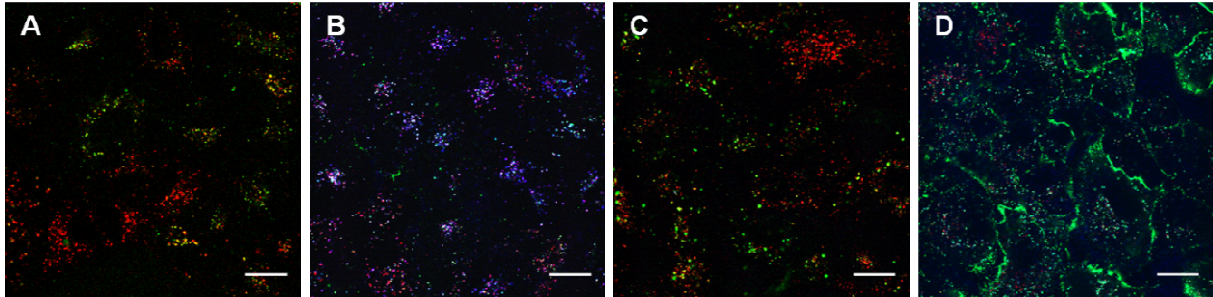


Figure 7.6 Overlay images from endosomal tracking (2 h pulse, 4 h chase) after incubation with 100 $\mu\text{g}/\text{mL}$ NPs and 50 $\mu\text{g}/\text{mL}$ Dextran-A546 in FBS-containing media; FA-PLGA (A), FA-PLGA-Prot (B), FA-PLGA-Cs (C), FA-PLGA-CatSt (D); lysosomes (red), NPs (green), siRNA (blue); Scale bar: 20 μm .

Having a look at FA-PLGA-Cs NPs, images merely showed a low siRNA associated fluorescence signal, but some internalized NPs (see Figure 7.6 C). FA-PLGA-CatSt NPs achieved (in comparison with the other DDSs) a very strong binding to the plasma membrane, but additionally showed initial siRNA binding and internalization (see Figure 7.6 D).

Because of the strong membrane binding internalization might occur by a combination of membrane turnover and fluid phase endocytosis. Observing the fluorescence intensity of fluorescein over time, decreasing signal intensities might be related to the lower pH (pH 5.5) inside late endosomes or lysosomes.

7.3.3 Correlative microscopy

Correlative microscopy was used to combine SEM and light microscopy or CLSM to produce one joint image (see Figure 7.7). Due to the fixation procedure with glutaraldehyde, the cells showed a rough appearing cell membrane. Paraformaldehyde (PMA) as an alternative fixation reagent would be suitable to obtain a smoother cell membrane, but cells would show a strong auto-fluorescence then. Hence, a fixation with PMA was adverse and worked well. FA-PLGA-Prot NPs

and FA-PLGA-CatSt NPs (see Figure 7.7 B and D) showed green spots located around the nucleus (= internalized NPs). Dependent on the applied cationic coating material Protamine-coated NPs showed little less green spots than PLGA-CatSt NPs.

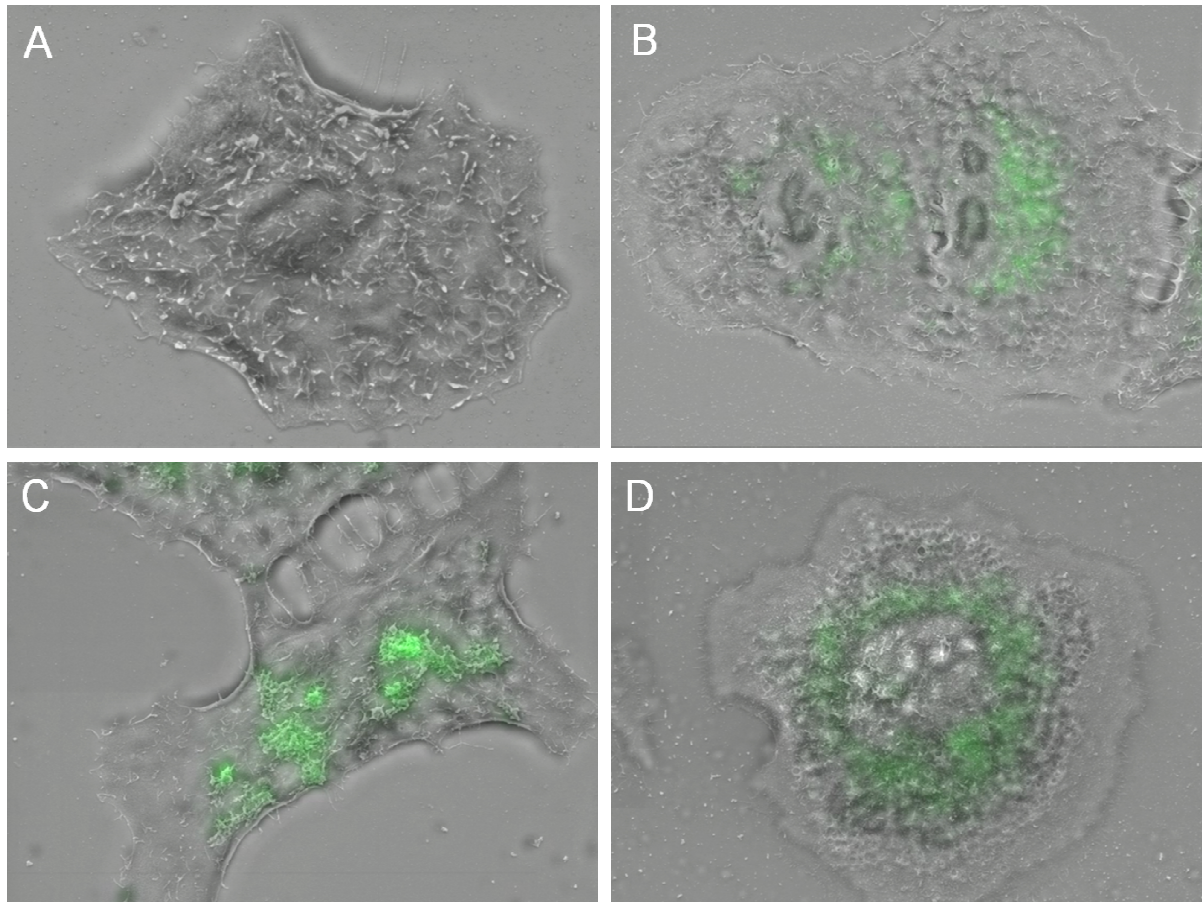


Figure 7.7 Image of a correlative microscopy (overlay of SEM, light and confocal microscopy): coated FA-labeled particles (0.01 mg/mL) were incubated for 24 h on A549 cells. A: no particles, B: FA-PLGA-Prot NPs, C: FA-PLGA-Cs NPs, D: FA-PLGA-CatSt NPs.

As no particles were visible on the cell membrane, the significance of confocal z-stack images (see Figure 7.2) can be supported. Hence, the presence of particles inside the cell is probable. However, FA-PLGA-Cs NPs (see Figure 7.7) stuck as an aggregated cluster on the cell. Here, some internalization might occur, but internalized particles were not visible because of the strong signal intensity from the particles which could be found outside the cell onto the plasma membrane.

7.4 Conclusion

Comparable with cell-specific differences in transfection efficacy (see Chapter 6) a significantly varying uptake behavior of human cancer cell lines (e.g. A549 and Calu-3) and human immortalized non-tumor cells (hAELVi) could be observed. Non-tumor cells, in general, showed the most limited uptake of all applied NPs whereas the amount of internalized particles between cell lines (A549, Calu-3, HaCat, NHDF-p and HeLa cells) underlie slighter variations. Here, the cationic material of the coated NPs seemed to have a greater impact on the transport of NPs into the cell. Incubation with CatStarch-coated NPs resulted in increased fluorescent signals at intracellular compartments, followed by FA-PLGA-Prot NPs with some fluorescent spots around the nuclear region and a few punctual signals after the addition of FA-PLGA-Cs NPs inside the cytosol. As the fluorescence intensity of fluorescein is known to be decreased at a lower pH and the fluorescence itself differs among the coated NPs (see section 3.3.2.5), a particle quantification based on the signal intensities would not be reliable. A specific staining of acidic cell compartments (LysoTracker[®]) successfully dyed endosomes or lysosomes and confirmed the internalization of nanoparticles into these cell compartments.

In principle, FCS experiments confirmed an improved uptake of CatSt-coated and Protamine-coated NPs. Additionally, the amount of internalized ALEXA647 was visualized and a stronger signal associated with FA-PLGA-Prot NPs (see section 3.3.2.4) in comparison to FA-PLGA-CatSt NPs, was shown. This means that the uptake mechanism is affected by several parameters. To collect more information about uptake and localization, however, detailed tracking experiments need to be performed. This includes studies focused on the endosomal escape of siRNA (regardless of NPs) as siRNA can only act effectively when located in the cytosol.

Chapter 8 - Summary and outlook

Within this work different polymer-based nanoparticulate drug delivery systems (DDSs) were developed to transport nucleic acids (in specific: siRNA) into the lung to overcome the cellular barrier. For this purpose, Chitosan (Cs), a synthesized cationic starch derivate (CatStarch) and Protamine (Prot) were chosen as biodegradable polymers to coat PLGA nanoparticles (NPs). The established preparation technique (emulsion-diffusion-evaporation technique) to create PLGA-Cs nanoparticles was applied and could be optimized plus partially automatized. DLS measurements of resulting particles obtained a diameter range between 130 and 170 nm, although the only changing parameter was the usage of a different cationic polymer. Depending on the molecular weight of the polymer different diameters became visible. The higher the molecular weight the larger the resulting NPs. Additionally, different surface charges could be determined. PLGA-Prot NPs showed a minor ζ -potential of 14 mV, whereas greater values of 32 mV and 37 mV were measured for PLGA-Cs and PLGA-CatSt NPs, respectively. The ζ -potential is presumably referable to the amount of protonable amine groups of the polymer. Investigations regarding particle stability showed a decreasing surface charge of PLGA-Chitosan NPs after repeating washing with water. In contrast to Protamine and Starch, Chitosan seems to have a different attachment behavior towards PLGA. Due to weak binding, significant amounts of Chitosan were sluiced down. But a specific reason for that could not be evaluated and need to be the subject of further studies.

An absolute quantification of surface-bound siRNA could only be performed for PLGA-Chitosan by an indirect UV-quantification and resulted at a loading efficiency of 84 %. Fluorometric analyses suffered from quenching effects and unspecific binding of fluorescent dyes on unloaded PLGA-Chitosan NPs. Employing gel electrophoresis (and replacement of siRNA through heparin) the amount of bound siRNA could be measured. As the supernatant of PLGA-Prot NPs contained less siRNA than the supernatant of PLGA-Cs NPs and PLGA-CatSt NPs. Most siRNA seemed to be bound on PLGA-Prot NPs. However, a quantification method to determine the absolute amount of bound API should be found.

The developed DDS should be suitable for the desired inhalative application and thus be available as a powder or suspension formulation. During stability studies, particles were analyzed under different storage conditions and after nebulization (using different devices). At a temperature between 4 °C and 20 °C nanoparticulate suspensions can be stored for up to 5 weeks. Using lyophilization to create a dry powder was unrestrictedly feasible for PLGA-CatSt NPs, whereas PLGA-Prot NPs and PLGA-Cs NPs required a cryoprotectant (e.g. Trehalose) to obtain recovered NPs after re-dispersion with water. All examined nebulization devices could create a fine mist out of the nanoparticulate-suspensions. Especially PLGA-Chitosan NPs showed an increased ability to form aggregates by devices using an oscillating membrane.

Moreover, the effect of particles on cells or cell culture models was evaluated. Within the applied concentrations no toxic effects based on the addition of NPs could be observed. Merely a slight activation of dendritic cells for all formulations at higher concentrations became visible. However, this activation could not be attributed to an activation of TLR2 and 4. As the developed DDSs were made to bind nucleic acids, positive controls for TLR3, 7 and 9 (dsRNA, ssRNA, and CPG DNA) were attached to the particulate system possible non-activation could not be excluded. The presence of bound siRNA resulted in no differing observations.

Finally, the efficiency of a transport system to convey the siRNA into the cell was crucial. As no stable transfected cell line was available, a co-transfection method was developed to enable the detection of a decreased expression of Luciferase. However, the received results were not only influenced by the particle load or the buffering capacity (for release from endosomes) of the polymer. In addition, polymer-siRNA interactions were responsible for successful transfections. A drawback of this method is the necessary use of transfection agents. Consequently, obtained results need to be confirmed by transfection studies on stably transfected cell lines or a knock-down and quantification of GAPDH via qPCR. CLSM measurements showed an uptake of fluorescent labeled NPs into different cells and localization at endosomes/lysosomes, although particles tend to attach to the cell membrane.

Recapitulating three promising carrier systems for the transport of nucleic acids with differing characteristics could be developed and analyzed. Prospective, transfection

studies of nebulized NPs on cellular co-culture (e.g hAELVi + THP-1) or inflamed *in-vitro* models will be possible followed by *in-vivo* inflammation models (e.g. TNF α) and biodistribution studies to identify regions where NPs may accumulate. Additionally, as soon as a suitable transgenic mouse model with luciferase expression in the lung is build up and the corresponding siRNA is available, *in-vivo* transfection studies will represent an important milestone for the development of a novel DDS.

Chapter 9 - Zusammenfassung und Ausblick

Im Rahmen dieser Arbeit wurden verschiedene polymerbasierte nanopartikuläre Transportsysteme entwickelt, mit dem Ziel Nukleinsäuren (im Speziellen: siRNA) in die Lunge zu transportieren, um dort die zelluläre Barriere zu überwinden. Zu den ausgewählten bioabbaubaren Polymeren gehörten neben Chitosan (Cs), eine eigens synthetisierte kationische Stärke (CatSt) und Protamin (Prot). Eine bereits etablierte Methode (Emulsions-Diffusions-Verdunstungs-Methode) zur Herstellung von Chitosan-überzogenen PLGA Nanopartikeln konnte optimiert und teilweise automatisiert werden. Zusätzlich war eine Übertragung dieser Methode auf weitere eingesetzte Polymere (hier: Prot und CatSt) möglich. Die resultierenden Partikeln wurden analysiert und miteinander verglichen. Dynamische Streulichtmessungen ergaben trotz identischer Mengen an eingesetztem Polymer, Partikeldurchmesser zwischen 130 und 170 nm. Diese erheblichen Größenunterschiede konnten durch die jeweiligen Molekulargewichte erklärt werden. Je höher das Molekulargewicht des kationischen Polymers, desto größer die PLGA-basierten Nanopartikel (NP). Des Weiteren wurden Abweichungen bei der Oberflächenladung festgestellt. PLGA-Prot NPs zeigten mit 14 mV das geringste ζ -Potential, wohingegen bei PLGA-Cs und PLGA-CatSt NPs mit jeweils 32 mV und 37 mV höhere Werte gemessen wurden. Dies ist voraussichtlich auf die unterschiedliche Anzahl protonierbarer Amine im Polymer zurückzuführen. Untersuchungen auf Partikelstabilität zeigten eine sinkende Oberflächenladung von ausschließlich PLGA-Cs NPs nach mehrmaligem Waschen mit Wasser. Chitosan scheint somit im Vergleich zu Prot und CatSt ein anderes Bindungsverhalten zum PLGA zu besitzen. Durch die schwache Bindung zu PLGA konnte eine große Menge an Polymer abgewaschen werden. Die konkrete Ursache konnte noch nicht in Gänze analysiert werden und bedarf daher weiterer Nachforschungen.

Eine absolute Quantifizierung der oberflächengebundenen siRNA war nur bedingt durchführbar. Eine indirekte UV-Quantifizierung freier siRNA im umgebenen Medium konnte nur bei PLGA-Cs NPs erreicht werden und ergab eine Beladungseffizienz (LE) von circa 84 %. Eine fluorimetrische Analyse war aufgrund von Quenchingeffekten und einer unspezifischen Bindung von Fluoreszenzfarbstoffen an

unbeladenen PLGA-Cs NPs ausgeschlossen. Mittels Gelelektrophorese konnte jedoch (nach Verdrängung der siRNA durch Heparin) die gebundene Menge an siRNA bestimmt werden. Da der Überstand von PLGA-Prot NPs die geringste Menge siRNA und der von PLGA-CatSt NPs die größte Menge enthielt, scheint der Hauptteil an siRNA auf der Oberfläche von PLGA-Prot NPs gebunden zu sein. Hier konnten lediglich vergleichende Aussagen getroffen werden, wobei eine geeignete Quantifizierungsmethode zur absoluten Bestimmung gebundener siRNA nicht zur Verfügung stand und entwickelt werden müsste.

Die entwickelten Partikel sind für eine spätere Anwendung in der inhalativen Therapie vorgesehen und sollten daher als Pulver oder Flüssigformulierung vorliegen können. Innerhalb der Stabilitätsstudien wurde sowohl Lagerungsverhalten über die Zeit, als auch die Partikelstabilität nach Vernebelung mit verschiedenen Gerätschaften untersucht. Bei Temperaturen zwischen 4 und 20 °C ist die Lagerung einer Nanopartikelsuspension bis zu 5 Wochen möglich. Die Herstellung eines Lyophilisats (als lagerfähige oder finale Formulierung) ist hingegen nur uneingeschränkt für PLGA-CatSt sinnvoll. Die beiden anderen Systeme benötigen die Zugabe eines Cryoprotectants (z.B. Trehalose) wobei die Eigenschaften von PLGA-Cs NPs nicht mehr vollständig wiederhergestellt werden konnten. Bei der Verwendung von oszillierenden Membranen zur Vernebelung traten durch die applizierten physikalischen Kräfte im Allgemeinen vermehrt Aggregationen auf.

Des Weiteren wurde sich mit dem Einfluss von Partikeln auf Zellen bzw. Zellkulturmodellen befasst. In den eingesetzten Mengen konnte eine Zellschädigung durch die Zugabe von NPs ausgeschlossen werden. Eine leichte Aktivierung dendritischer Zellen durch alle drei Systeme konnte zwar in höheren Konzentrationen beobachtet werden, war allerdings nicht auf eine Aktivierung von TLR2 und 4 zurückzuführen. Eine fehlende Aktivierung von TLR3, 7 und 9 konnte aufgrund von Bindungstendenzen zu den Positivkontrollen (dsRNA, ssRNA and CPG DNA) nicht ausgeschlossen werden. Dies war allerdings zu erwarten, da die entwickelten Transporter Nucleinsäuren an der Partikeloberfläche binden sollen. Eine Beladung mit siRNA führte zu keinerlei abweichenden Ergebnissen.

Letztendlich ist die Effektivität eines Transportsystems, um enthaltene siRNA in die Zelle zu befördern, entscheidend. Da bis zum Ende der Ausarbeitung keine

geeignete, stabil transfizierte Zelllinie zur Verfügung stand, konnte mittels einer simultanen Co-Transfektion eine verminderte Expression des eingeschleusten Luciferase-Plasmids sichtbar gemacht werden. Die Resultate sind jedoch nicht alleinig auf eine möglichst hohe Beladung oder eine verbesserte Pufferkapazität (Freisetzung aus Endosomen) zurückzuführen. Das Zusammenspiel aus Beladung, Pufferkapazität und Polymer-siRNA-Interaktion scheint gemeinsam für die Transfektionseffizienz verantwortlich zu sein. Da eine Co-Transfektion jedoch dem Einsatz von Transfektionsreagentien bedarf, ist eine Bestätigung dieser Ergebnisse durch den Einsatz einer stabil transfizierten Zelllinie oder eine Bestimmung von GAPDH mittels qPCR unabdingbar.

Eine Aufnahme von Fluoreszenz-markierten NPs in die Zelle und eine Lokalisierung in Endosomen/Lysosomen konnte mittels CLSM gezeigt werden, wenn gleich ein Großteil der Partikel sich an der Außenmembran der Zelle anlagerten.

Zusammenfassend konnten demnach drei vielversprechende Trägersysteme entwickelt und beschrieben werden. Neben Versuche zur Bestätigung der Co-Transfektionsergebnisse, können Studien auf Co-Kultur-Zellmodelle (bsp. hAELVi + THP-1) oder auf krankhafte bzw. entzündete Zellmodelle ausgeweitet werden. Ein Aufbringen von vernebelten Transportsystemen ist ebenfalls vorstellbar. Folgen sollten dann auch *in-vivo* Studien zur Verteilung der Partikel im Körper von Mäusen, um mögliche Ansammlungen von Partikeln und eine einhergehende Belastung von Organen zu identifizieren. Sobald ein geeignetes TNF α -Tiermodell mit transgenen Mäusen und die dazugehörige siRNA verfügbar sind, bilden solche *in-vivo* Transfektionsstudien einen wichtigen Meilenstein bei der Entwicklung neuartiger Trägersysteme.

Abbreviations

AFM	atomic force microscopy = scanning force microscopy (SFM)
ALI	air-liquid interface
API	active pharmaceutical ingredient
ASO	antisense oligonucleotide
ATR	attenuated total reflectance (sampling technique in IR spectroscopy)
A549	adenocarcinomic human alveolar basal epithelial cells
BCA	bicinchoninic assay
BCA-RAC	bicinchoninic assay reactive agent compatible
BP	biopharmaceuticals
BPE	bovine pituitary extract
BSA	bovine serum albumin
BSA-FAF	bovine serum albumin, fatty acid free
CA	cellulose acetate
CatStarch	cationic starch derivative (own synthesis)
CCLR	cell culture lysis reagent
CD _x	cluster of differentiation x (x = 4, 40, 86, 11c)
COMPACT	Collaboration on the Optimization of Macromolecular Pharmaceutical Access to Cellular Targets
COPD	chronic obstructive pulmonary disease
Cs	Chitosan
CTA	cellulose triacetate
DAPI	4',6-diamidino-2-phenylindole
DC	dendritic cell
DEPC	Diethy pyrocarbonate = diethyl dicarbonate
Dil	1,1'-Dioctadecyl-3,3,3',3'-tetramethylindocarbocyanine perchlorate
DLS	Dynamic light scattering = photon correlation spectroscopy (PCS)

DMEM	Dulbecco's Modified Eagle Medium
DNA	deoxyribonucleic acid
dog	drop on grid
dsRNA	double-stranded RNA
DTT	dithiothreitol
EDTA	ethylenediaminetetraacetic acid
EFPIA	European Federation of Pharmaceutical Industries and Associations
EMA	European Medicines Agency
FA	fluoresceinamine
FBS	fetal bovine serum = fetal calf serum (abbreviated 'FCS')
FCS	fluorescent correlation spectroscopy
FDA	Food and Drug Administration
FSC	forward scatter
GA	gentamicin amphotericin
god	grid on drop
hAELVi	human alveolar epithelial lentivirus immortalized
HBSS	Hank's Balanced Salt Solution
HDMS	hexamethyldisilazane = Bis(trimethylsilyl)amine
HEK293	human embryonic kidney 293 cells
HIPS	Helmholtz-Institute for Pharmaceutical research Saarland
Hsp70	heat shock proteins, 70 kDa
IMI	Innovative Medicine Initiative
IR	infra-red (spectral range: $\sim 14,000\text{ cm}^{-1}$ to 10 cm^{-1} or 1 mm to 800 nm)
KRB	Krebs-Ringer Buffer
LC	loading capacity
LDH	lactate dehydrogenase
LE	loading efficiency
LF iMAX	Lipofectamine [®] RNAiMax

LCC	liquid covered conditions
LPS	lipopolysaccharide (endotoxin)
mBMDC	murine bone marrow-derived dendritic cells
MHCII	major histocompatibility complex class II
mRNA	messenger RNA
miRNA	micro RNA
MMD	mass mean diameter
MTT	methyl-thiazoyl-tetrazolium
M_w	'relative' molecular weight or mass
MWCO	molecular weight cut-off
NF- κ B	nuclear factor 'kappa-light-chain-enhancer' of activated B-cells
nt	nucleotides
NTA	nanoparticle tracking analysis
PAGE	polyacrylamide gel electrophoresis
PBS	Phosphate Buffered Saline
PCS	Photon correlation spectroscopy = dynamic light scattering (DLS)
PDI	polydispersity index
PES	polyethersulfone
pDNA	plasmid DNA
PEG	polyethylene glycol
PEI	polyethyleneimine
PES	polyethersulfone
PFA	paraformaldehyde
piRNA	piwi-interacting RNA
PIWI or piwi	P-element induced wimpy testis
PLGA	Poly(lactic-co-glycolic acid)
PLGA-CatSt	CatStarch-coated PLGA NPs
PLGA-Cs	chitosan-coated PLGA NPs
PLGA-Prot	protamine-coated PLGA NPs

PMA	phorbol 12-myristate 13-acetate
Prot	Protamine
P/S	penicillin streptomycin
PVOH	polyvinyl alcohol
rasiRNA	repeat associated small interfering RNA
RC	regenerated cellulose
rhEGF	recombinant human Epidermal Growth Factor
RISC	RNA-induced Silencing Complex
RLU	relative light units
RNA	ribonucleic acid
RNAi	RNA interference
rpm	revolutions per minute
RPMI	Roswell Park Memorial Institute
RT	room temperature [20 °C]
SAGM	Small Airway Growth Medium
SDS	sodium dodecylsulfate
SEC	size exclusion chromatography
SEM	scanning electron microscopy
SFM	scanning force microscopy = atomic force microscopy (AFM)
shRNA	short hairpin RNA
siRNA	small interfering RNA
SPM	scanning probe microscopy (e.g. AFM or SFM)
SSC	side scatter
ssRNA	single-stranded RNA
TAE	TRIS/Acetic acid/EDTA
TBE	Tris/Borate/EDTA
TE	Tris/EDTA
TEER	transepithelial electric resistance
TLR	toll-like receptor

TNF	tumor necrosis factor
UV	ultraviolet
VMD	volumetric mean diameter
WP	work package
ZP	zeta potential

References

- [1] H. Staudinger and J. Fritschi, "Über Isopren und Kautschuk. 5. Mitteilung. Über die Hydrierung des Kautschuks und über seine Konstitution," *Helvetica Chimica Acta*, vol. 5, pp. 785-806, 02 Sep 1922.
- [2] W. Wang, "Protein aggregation and its inhibition in biopharmaceutics," *Int J Pharm*, vol. 289, pp. 1-30, Jan 31 2005.
- [3] S. Frokjaer and D. E. Otzen, "Protein drug stability: a formulation challenge," *Nat Rev Drug Discov*, vol. 4, pp. 298-306, Apr 2005.
- [4] Y. Kamiya, J. Takai, H. Ito, K. Murayama, H. Kashida, and H. Asanuma, "Enhancement of stability and activity of siRNA by terminal substitution with serinol nucleic acid (SNA)," *Chembiochem*, vol. 15, pp. 2549-55, Nov 24 2014.
- [5] A. A. Kaspar and J. M. Reichert, "Future directions for peptide therapeutics development," *Drug Discov Today*, vol. 18, pp. 807-17, Sep 2013.
- [6] K. Fosgerau and T. Hoffmann, "Peptide therapeutics: current status and future directions," *Drug Discov Today*, vol. 20, pp. 122-8, Jan 2015.
- [7] B. J. Bruno, G. D. Miller, and C. S. Lim, "Basics and recent advances in peptide and protein drug delivery," *Ther Deliv*, vol. 4, pp. 1443-67, Nov 2013.
- [8] P. J. Carter, "Introduction to current and future protein therapeutics: a protein engineering perspective," *Exp Cell Res*, vol. 317, pp. 1261-9, May 15 2011.
- [9] T. Cullen. (2015, 18 Dec). *Isis Pharmaceuticals to change its name Ionis Pharmaceuticals*. Available: <http://www.cnbc.com/2015/12/18/isis-pharmaceuticals-to-change-its-name-ionis-pharmaceuticals.html>
- [10] E. M. A. T. C. f. M. P. f. H. Use. (2013, 21 Mar). *Refusal of the marketing authorisation for Kynamro (mipomersen)* [online]. Available: http://www.ema.europa.eu/docs/en_GB/document_library/Summary_of_opinion_-_Initial_authorisation/human/002429/WC500140678.pdf
- [11] G. McClorey and M. J. Wood, "An overview of the clinical application of antisense oligonucleotides for RNA-targeting therapies," *Curr Opin Pharmacol*, vol. 24, pp. 52-8, Oct 2015.
- [12] A. Pharmaceuticals. (2014, 11 Dec). *Alynlam Initiates ENDEAVOUR Phase 3 Clinical Trial with Revusiran (ALN-TTRsc), an Investigational RNAi Therapeutic Targeting Transthyretin (TTR) for the Treatment of TTR Cardiac Amyloidosis* [online]. Available: <http://investors.alnylam.com/releasedetail.cfm?ReleaseID=887340>
- [13] A. Pharmaceuticals. (2016, 02 Jan). *Alynlam Completes Enrollment in APOLLO Phase 3 Study with Patisiran, an Investigational RNAi Therapeutic for Patients with Transthyretin (TTR)-Mediated Amyloidosis (ATTR Amyloidosis)* [online]. Available: <http://investors.alnylam.com/releasedetail.cfm?ReleaseID=952545>
- [14] U. S. N. I. o. Health. (2016, Apr 03). *ENDEAVOUR: Phase 3 Multicenter Study of Revusiran (ALN-TTRSC) in Patients With Transthyretin (TTR) Mediated Familial Amyloidotic Cardiomyopathy (FAC)* [online]. Available: <https://clinicaltrials.gov/ct2/show/NCT02319005>
- [15] S. T. Crooke, "Molecular mechanisms of action of antisense drugs," *Biochim Biophys Acta*, vol. 1489, pp. 31-44, Dec 10 1999.
- [16] N. M. Dean and C. F. Bennett, "Antisense oligonucleotide-based therapeutics for cancer," *Oncogene*, vol. 22, pp. 9087-96, Dec 8 2003.

- [17] S. M. Hammond, E. Bernstein, D. Beach, and G. J. Hannon, "An RNA-directed nuclease mediates post-transcriptional gene silencing in *Drosophila* cells," *Nature*, vol. 404, pp. 293-6, Mar 16 2000.
- [18] M. K. Montgomery, S. Xu, and A. Fire, "RNA as a target of double-stranded RNA-mediated genetic interference in *Caenorhabditis elegans*," *Proc Natl Acad Sci U S A*, vol. 95, pp. 15502-7, Dec 22 1998.
- [19] E. Bernstein, A. A. Caudy, S. M. Hammond, and G. J. Hannon, "Role for a bidentate ribonuclease in the initiation step of RNA interference," *Nature*, vol. 409, pp. 363-6, Jan 18 2001.
- [20] A. Fire, S. Xu, M. K. Montgomery, S. A. Kostas, S. E. Driver, and C. C. Mello, "Potent and specific genetic interference by double-stranded RNA in *Caenorhabditis elegans*," *Nature*, vol. 391, pp. 806-11, Feb 19 1998.
- [21] N. M. AB. (2014). *The Nobel Prize in Physiology or Medicine 2006* [online]. Available: http://www.nobelprize.org/nobel_prizes/medicine/laureates/2006/
- [22] J. G. Izant and H. Weintraub, "Inhibition of thymidine kinase gene expression by anti-sense RNA: a molecular approach to genetic analysis," *Cell*, vol. 36, pp. 1007-15, Apr 1984.
- [23] S. Guo and K. J. Kemphues, "par-1, a gene required for establishing polarity in *C. elegans* embryos, encodes a putative Ser/Thr kinase that is asymmetrically distributed," *Cell*, vol. 81, pp. 611-20, May 19 1995.
- [24] C. E. Rocheleau, W. D. Downs, R. Lin, C. Wittmann, Y. Bei, Y. H. Cha, *et al.*, "Wnt signaling and an APC-related gene specify endoderm in early *C. elegans* embryos," *Cell*, vol. 90, pp. 707-16, Aug 22 1997.
- [25] P. D. Zamore, T. Tuschl, P. A. Sharp, and D. P. Bartel, "RNAi: double-stranded RNA directs the ATP-dependent cleavage of mRNA at 21 to 23 nucleotide intervals," *Cell*, vol. 101, pp. 25-33, Mar 31 2000.
- [26] R. C. Lee and V. Ambros, "An extensive class of small RNAs in *Caenorhabditis elegans*," *Science*, vol. 294, pp. 862-4, Oct 26 2001.
- [27] N. C. Lau, L. P. Lim, E. G. Weinstein, and D. P. Bartel, "An abundant class of tiny RNAs with probable regulatory roles in *Caenorhabditis elegans*," *Science*, vol. 294, pp. 858-62, Oct 26 2001.
- [28] M. Lagos-Quintana, R. Rauhut, W. Lendeckel, and T. Tuschl, "Identification of novel genes coding for small expressed RNAs," *Science*, vol. 294, pp. 853-8, Oct 26 2001.
- [29] C. D. Novina and P. A. Sharp, "The RNAi revolution," *Nature*, vol. 430, pp. 161-4, Jul 8 2004.
- [30] J. K. Lam, M. Y. Chow, Y. Zhang, and S. W. Leung, "siRNA Versus miRNA as Therapeutics for Gene Silencing," *Mol Ther Nucleic Acids*, vol. 4, p. e252, 2015.
- [31] G. Ozcan, B. Ozpolat, R. L. Coleman, A. K. Sood, and G. Lopez-Berestein, "Preclinical and clinical development of siRNA-based therapeutics," *Adv Drug Deliv Rev*, vol. 87, pp. 108-19, Jun 29 2015.
- [32] B. L. Davidson and P. B. McCray, "Current prospects for RNA interference-based therapies," *Nat Rev Genet*, vol. 12, pp. 329-340, 05//print 2011.
- [33] Q. Liu, T. A. Rand, S. Kalidas, F. Du, H. E. Kim, D. P. Smith, *et al.*, "R2D2, a bridge between the initiation and effector steps of the *Drosophila* RNAi pathway," *Science*, vol. 301, pp. 1921-5, Sep 26 2003.
- [34] S. M. Elbashir, J. Harborth, W. Lendeckel, A. Yalcin, K. Weber, and T. Tuschl, "Duplexes of 21-nucleotide RNAs mediate RNA interference in cultured mammalian cells," *Nature*, vol. 411, pp. 494-8, May 24 2001.

- [35] P. D. Zamore and B. Haley, "Ribo-gnome: the big world of small RNAs," *Science*, vol. 309, pp. 1519-24, Sep 2 2005.
- [36] Y. Lee, C. Ahn, J. Han, H. Choi, J. Kim, J. Yim, *et al.*, "The nuclear RNase III Drosha initiates microRNA processing," *Nature*, vol. 425, pp. 415-9, Sep 25 2003.
- [37] E. P. Murchison and G. J. Hannon, "miRNAs on the move: miRNA biogenesis and the RNAi machinery," *Curr Opin Cell Biol*, vol. 16, pp. 223-9, Jun 2004.
- [38] S. M. Hammond, "Dicing and slicing: the core machinery of the RNA interference pathway," *FEBS Lett*, vol. 579, pp. 5822-9, Oct 31 2005.
- [39] G. Hutvagner, "Small RNA asymmetry in RNAi: function in RISC assembly and gene regulation," *FEBS Lett*, vol. 579, pp. 5850-7, Oct 31 2005.
- [40] Y. Tomari and P. D. Zamore, "MicroRNA biogenesis: drosha can't cut it without a partner," *Curr Biol*, vol. 15, pp. R61-4, Jan 26 2005.
- [41] B. P. Lewis, C. B. Burge, and D. P. Bartel, "Conserved seed pairing, often flanked by adenosines, indicates that thousands of human genes are microRNA targets," *Cell*, vol. 120, pp. 15-20, Jan 14 2005.
- [42] T. Du and P. D. Zamore, "microPrimer: the biogenesis and function of microRNA," *Development*, vol. 132, pp. 4645-52, Nov 2005.
- [43] P. Svoboda, P. Stein, and R. M. Schultz, "RNAi in mouse oocytes and preimplantation embryos: effectiveness of hairpin dsRNA," *Biochem Biophys Res Commun*, vol. 287, pp. 1099-104, Oct 12 2001.
- [44] Y. W. Iwasaki, M. C. Siomi, and H. Siomi, "PIWI-Interacting RNA: Its Biogenesis and Functions," *Annu Rev Biochem*, vol. 84, pp. 405-33, 2015.
- [45] V. Ambros, "The functions of animal microRNAs," *Nature*, vol. 431, pp. 350-5, Sep 16 2004.
- [46] D. D. Rao, J. S. Vorhies, N. Senzer, and J. Nemunaitis, "siRNA vs. shRNA: similarities and differences," *Adv Drug Deliv Rev*, vol. 61, pp. 746-59, Jul 25 2009.
- [47] S. T. Grivna, E. Beyret, Z. Wang, and H. Lin, "A novel class of small RNAs in mouse spermatogenic cells," *Genes Dev*, vol. 20, pp. 1709-14, Jul 1 2006.
- [48] R. W. Williams and G. M. Rubin, "ARGONAUTE1 is required for efficient RNA interference in Drosophila embryos," *Proc Natl Acad Sci U S A*, vol. 99, pp. 6889-94, May 14 2002.
- [49] C. Klattenhoff and W. Theurkauf, "Biogenesis and germline functions of piRNAs," *Development*, vol. 135, pp. 3-9, Jan 2008.
- [50] A. A. Aravin, M. Lagos-Quintana, A. Yalcin, M. Zavolan, D. Marks, B. Snyder, *et al.*, "The small RNA profile during Drosophila melanogaster development," *Dev Cell*, vol. 5, pp. 337-50, Aug 2003.
- [51] R. M. Effros. (2006, May 16). *Anatomy, development, and physiology of the lungs* [online]. Available: <http://www.nature.com/gimo/contents/pt1/full/gimo73.html>
- [52] M. Bur and C. M. Lehr, "Pulmonary cell culture models to study the safety and efficacy of innovative aerosol medicines," *Expert Opin Drug Deliv*, vol. 5, pp. 641-52, Jun 2008.
- [53] M. E. K. Morgenroth, "Anatomy: Morphology of the small airways," in *Mechanical Ventilation: Clinical Applications and Pathophysiology*
- P. J. P. B. Lachmann, Ed., 1 ed: Saunders Elsevier 2008, pp. 74-80.

-
- [54] A. Steimer, E. Haltner, and C. M. Lehr, "Cell culture models of the respiratory tract relevant to pulmonary drug delivery," *J Aerosol Med*, vol. 18, pp. 137-82, Summer 2005.
- [55] J. S. Patton and P. R. Byron, "Inhaling medicines: delivering drugs to the body through the lungs," *Nat Rev Drug Discov*, vol. 6, pp. 67-74, Jan 2007.
- [56] L. A. Creuwels, L. M. van Golde, and H. P. Haagsman, "The pulmonary surfactant system: biochemical and clinical aspects," *Lung*, vol. 175, pp. 1-39, 1997.
- [57] L. G. Dobbs, "Isolation and culture of alveolar type II cells," *Am J Physiol*, vol. 258, pp. L134-47, Apr 1990.
- [58] G. J. Gibson, R. Loddenkemper, B. Lundback, and Y. Sibille, "Respiratory health and disease in Europe: the new European Lung White Book," *Eur Respir J*, vol. 42, pp. 559-63, Sep 2013.
- [59] L. Fromer and C. B. Cooper, "A review of the GOLD guidelines for the diagnosis and treatment of patients with COPD," *Int J Clin Pract*, vol. 62, pp. 1219-36, Aug 2008.
- [60] M. E. Wechsler, "Managing asthma in primary care: putting new guideline recommendations into context," *Mayo Clin Proc*, vol. 84, pp. 707-17, Aug 2009.
- [61] R. A. Wise, A. Anzueto, D. Cotton, R. Dahl, T. Devins, B. Disse, *et al.*, "Tiotropium Respimat inhaler and the risk of death in COPD," *N Engl J Med*, vol. 369, pp. 1491-501, Oct 17 2013.
- [62] N. Taniguchi, "On the Basic Concept of 'Nano-Technology'," *Proc. Intl. Conf. Prod. Eng. Tokyo, Part II, Japan Society of Precision Engineering*, pp. 18-23, 1974.
- [63] P. Vettiger, G. Cross, M. Despont, U. Drechsler, U. Durig, B. Gotsmann, *et al.*, "The "millipede" - Nanotechnology entering data storage," *Ieee Transactions on Nanotechnology*, vol. 1, pp. 39-55, Mar 2002.
- [64] S. De Franceschi and L. Kouwenhoven, "Nanotechnology - Electronics and the single atom," *Nature*, vol. 417, pp. 701-702, Jun 13 2002.
- [65] P. Singh and A. Nanda, "Enhanced sun protection of nano-sized metal oxide particles over conventional metal oxide particles: an in vitro comparative study," *Int J Cosmet Sci*, vol. 36, pp. 273-83, Jun 2014.
- [66] S. K. Sahoo and V. Labhasetwar, "Nanotech approaches to drug delivery and imaging," *Drug Discov Today*, vol. 8, pp. 1112-20, Dec 15 2003.
- [67] H. Liu and T. J. Webster, "Nanomedicine for implants: A review of studies and necessary experimental tools," *Biomaterials*, vol. 28, pp. 354-369, Jan 2007.
- [68] N. Sozer and J. L. Kokini, "Nanotechnology and its applications in the food sector," *Trends in Biotechnology*, vol. 27, pp. 82-89, Feb 2009.
- [69] C. Buzea, Pacheco, II, and K. Robbie, "Nanomaterials and nanoparticles: sources and toxicity," *Biointerphases*, vol. 2, pp. MR17-71, Dec 2007.
- [70] V. Weissig, T. K. Pettinger, and N. Murdock, "Nanopharmaceuticals (part 1): products on the market," *Int J Nanomedicine*, vol. 9, pp. 4357-73, 2014.
- [71] R. Iyer, C. C. Hsia, and K. T. Nguyen, "Nano-Therapeutics for the Lung: State-of-the-Art and Future Perspectives," *Curr Pharm Des*, vol. 21, pp. 5233-44, 2015.
- [72] T. Stylianopoulos and R. K. Jain, "Design considerations for nanotherapeutics in oncology," *Nanomedicine*, vol. 11, pp. 1893-907, Nov 2015.

- [73] V. Mishra, P. Kesharwani, and N. K. Jain, "siRNA nanotherapeutics: a Trojan horse approach against HIV," *Drug Discov Today*, vol. 19, pp. 1913-20, Dec 2014.
- [74] M. V. Yezhelyev, X. Gao, Y. Xing, A. Al-Hajj, S. Nie, and R. M. O'Regan, "Emerging use of nanoparticles in diagnosis and treatment of breast cancer," *Lancet Oncol*, vol. 7, pp. 657-67, Aug 2006.
- [75] K. K. Jain, "Nanotechnology in clinical laboratory diagnostics," *Clin Chim Acta*, vol. 358, pp. 37-54, Aug 2005.
- [76] K. K. Alharbi and Y. A. Al-Sheikh, "Role and implications of nanodiagnostics in the changing trends of clinical diagnosis," *Saudi J Biol Sci*, vol. 21, pp. 109-17, Apr 2014.
- [77] Y. Barenholz, "Doxil(R)--the first FDA-approved nano-drug: lessons learned," *J Control Release*, vol. 160, pp. 117-34, Jun 10 2012.
- [78] V. Weissig and D. Guzman-Villanueva, "Nanopharmaceuticals (part 2): products in the pipeline," *Int J Nanomedicine*, vol. 10, pp. 1245-57, 2015.
- [79] C. A. Ruge, J. Kirch, and C. M. Lehr, "Pulmonary drug delivery: from generating aerosols to overcoming biological barriers-therapeutic possibilities and technological challenges," *Lancet Respir Med*, vol. 1, pp. 402-13, Jul 2013.
- [80] B. K. Rubin, "Physiology of airway mucus clearance," *Respir Care*, vol. 47, pp. 761-8, Jul 2002.
- [81] M. B. Antunes and N. A. Cohen, "Mucociliary clearance--a critical upper airway host defense mechanism and methods of assessment," *Curr Opin Allergy Clin Immunol*, vol. 7, pp. 5-10, Feb 2007.
- [82] W. Hofmann and B. Asgharian, "The effect of lung structure on mucociliary clearance and particle retention in human and rat lungs," *Toxicol Sci*, vol. 73, pp. 448-56, Jun 2003.
- [83] M. R. Knowles and R. C. Boucher, "Mucus clearance as a primary innate defense mechanism for mammalian airways," *J Clin Invest*, vol. 109, pp. 571-7, Mar 2002.
- [84] J. Kirch, A. Schneider, B. Abou, A. Hopf, U. F. Schaefer, M. Schneider, *et al.*, "Optical tweezers reveal relationship between microstructure and nanoparticle penetration of pulmonary mucus," *Proc Natl Acad Sci U S A*, vol. 109, pp. 18355-60, Nov 6 2012.
- [85] M. Geiser, "Update on macrophage clearance of inhaled micro- and nanoparticles," *J Aerosol Med Pulm Drug Deliv*, vol. 23, pp. 207-17, Aug 2010.
- [86] J. A. Frank, "Claudins and alveolar epithelial barrier function in the lung," *Ann N Y Acad Sci*, vol. 1257, pp. 175-83, Jun 2012.
- [87] J. S. Patton and P. R. Byron, "Inhaling medicines: delivering drugs to the body through the lungs," *Nature Reviews Drug Discovery*, vol. 6, pp. 67-74, Jan 2007.
- [88] C. A. Ruge, J. Kirch, O. Canadas, M. Schneider, J. Perez-Gil, U. F. Schaefer, *et al.*, "Uptake of nanoparticles by alveolar macrophages is triggered by surfactant protein A," *Nanomedicine-Nanotechnology Biology and Medicine*, vol. 7, pp. 690-693, Dec 2011.
- [89] C. A. Ruge, U. F. Schaefer, J. Herrmann, J. Kirch, O. Canadas, M. Echaide, *et al.*, "The interplay of lung surfactant proteins and lipids assimilates the macrophage clearance of nanoparticles," *PLoS One*, vol. 7, p. e40775, 2012.
- [90] J. Kirch, C. A. Ruge, S. C., J. Hanes, and C. M. Lehr, "Nanostructures for Overcoming the Pulmonary Barriers: Physiological Considerations and

- Mechanistic Issues," in *Nanostructured Biomaterials for Overcoming Biological Barriers*, M. J. Alonso, N. S. Csaba, and A. Matinez, Eds., ed: Cambridge: Royal Society of Chemistry, 2012, pp. 239-71.
- [91] C. de Souza Carvalho, N. Daum, and C. M. Lehr, "Carrier interactions with the biological barriers of the lung: advanced in vitro models and challenges for pulmonary drug delivery," *Adv Drug Deliv Rev*, vol. 75, pp. 129-40, Aug 2014.
- [92] J. Wang, Z. Lu, M. G. Wientjes, and J. L. Au, "Delivery of siRNA therapeutics: barriers and carriers," *AAPS J*, vol. 12, pp. 492-503, Dec 2010.
- [93] R. W. Niven, "Delivery of biotherapeutics by inhalation aerosol," *Crit Rev Ther Drug Carrier Syst*, vol. 12, pp. 151-231, 1995.
- [94] D. Goula, N. Becker, G. F. Lemkine, P. Normandie, J. Rodrigues, S. Mantero, *et al.*, "Rapid crossing of the pulmonary endothelial barrier by polyethylenimine/DNA complexes," *Gene Ther*, vol. 7, pp. 499-504, Mar 2000.
- [95] M. Geiser, B. Rothen-Rutishauser, N. Kapp, S. Schurch, W. Kreyling, H. Schulz, *et al.*, "Ultrafine particles cross cellular membranes by nonphagocytic mechanisms in lungs and in cultured cells," *Environ Health Perspect*, vol. 113, pp. 1555-60, Nov 2005.
- [96] H. Herd, N. Daum, A. T. Jones, H. Huwer, H. Ghandehari, and C. M. Lehr, "Nanoparticle geometry and surface orientation influence mode of cellular uptake," *ACS Nano*, vol. 7, pp. 1961-73, Mar 26 2013.
- [97] J. K. Lam, W. Liang, and H. K. Chan, "Pulmonary delivery of therapeutic siRNA," *Adv Drug Deliv Rev*, vol. 64, pp. 1-15, Jan 2012.
- [98] J. D. Byrne, T. Betancourt, and L. Brannon-Peppas, "Active targeting schemes for nanoparticle systems in cancer therapeutics," *Adv Drug Deliv Rev*, vol. 60, pp. 1615-26, Dec 14 2008.
- [99] I. M. Initiative. (2010). *Introducing IMI* [online]. Available: <http://www.imi.europa.eu/content/mission>
- [100] N. Nafee, S. Taetz, M. Schneider, U. F. Schaefer, and C. M. Lehr, "Chitosan-coated PLGA nanoparticles for DNA/RNA delivery: effect of the formulation parameters on complexation and transfection of antisense oligonucleotides," *Nanomedicine*, vol. 3, pp. 173-83, Sep 2007.
- [101] D. K. Jensen, L. B. Jensen, S. Koocheki, L. Bengtson, D. Cun, H. M. Nielsen, *et al.*, "Design of an inhalable dry powder formulation of DOTAP-modified PLGA nanoparticles loaded with siRNA," *J Control Release*, vol. 157, pp. 141-8, Jan 10 2012.
- [102] S. Ni, Y. Xie, Y. Tang, Y. Liu, J. Chen, and S. Zhu, "Nebulized anionic guanidinylated O-carboxymethyl chitosan/N-2-hydroxypropyltrimethyl ammonium chloride chitosan nanoparticles for siRNA pulmonary delivery: preparation, characterization and in vitro evaluation," *J Drug Target*, vol. 25, pp. 451-462, Jun 2017.
- [103] E. J. Jeong, M. Choi, J. Lee, T. Rhim, and K. Y. Lee, "The spacer arm length in cell-penetrating peptides influences chitosan/siRNA nanoparticle delivery for pulmonary inflammation treatment," *Nanoscale*, vol. 7, pp. 20095-104, Dec 21 2015.
- [104] E. J. Nielsen, J. M. Nielsen, D. Becker, A. Karlas, H. Prakash, S. Z. Glud, *et al.*, "Pulmonary gene silencing in transgenic EGFP mice using aerosolised chitosan/siRNA nanoparticles," *Pharm Res*, vol. 27, pp. 2520-7, Dec 2010.
- [105] O. Taratula, A. Kuzmov, M. Shah, O. B. Garbuzenko, and T. Minko, "Nanostructured lipid carriers as multifunctional nanomedicine platform for

- pulmonary co-delivery of anticancer drugs and siRNA," *J Control Release*, vol. 171, pp. 349-57, Nov 10 2013.
- [106] P. O. Yoon, J. W. Park, C. M. Lee, S. H. Kim, H. N. Kim, Y. Ko, *et al.*, "Self-assembled Micelle Interfering RNA for Effective and Safe Targeting of Dysregulated Genes in Pulmonary Fibrosis," *J Biol Chem*, vol. 291, pp. 6433-46, Mar 18 2016.
- [107] A. Hibbitts, A. M. O'Mahony, E. Forde, L. Nolan, J. Ogier, S. Desgranges, *et al.*, "Early-stage development of novel cyclodextrin-siRNA nanocomplexes allows for successful postnebulization transfection of bronchial epithelial cells," *J Aerosol Med Pulm Drug Deliv*, vol. 27, pp. 466-77, Dec 2014.
- [108] S. Jin, J. C. Leach, and K. Ye, "Nanoparticle-mediated gene delivery," *Methods Mol Biol*, vol. 544, pp. 547-57, 2009.
- [109] P. Pantazis, K. Dimas, J. H. Wyche, S. Anant, C. W. Houchen, J. Panyam, *et al.*, "Preparation of siRNA-encapsulated PLGA nanoparticles for sustained release of siRNA and evaluation of encapsulation efficiency," *Methods Mol Biol*, vol. 906, pp. 311-9, 2012.
- [110] M. D. Buschmann, A. Merzouki, M. Lavertu, M. Thibault, M. Jean, and V. Darras, "Chitosans for delivery of nucleic acids," *Adv Drug Deliv Rev*, vol. 65, pp. 1234-70, Aug 2013.
- [111] X. Q. Zhang, J. Intra, and A. K. Salem, "Comparative study of poly (lactic-co-glycolic acid)-poly ethyleneimine-plasmid DNA microparticles prepared using double emulsion methods," *J Microencapsul*, vol. 25, pp. 1-12, Feb 2008.
- [112] M. N. Kumar, S. S. Mohapatra, X. Kong, P. K. Jena, U. Bakowsky, and C. M. Lehr, "Cationic poly(lactide-co-glycolide) nanoparticles as efficient in vivo gene transfection agents," *J Nanosci Nanotechnol*, vol. 4, pp. 990-4, Nov 2004.
- [113] M. N. Ravi Kumar, U. Bakowsky, and C. M. Lehr, "Preparation and characterization of cationic PLGA nanospheres as DNA carriers," *Biomaterials*, vol. 25, pp. 1771-7, May 2004.
- [114] S. Prabha, W. Z. Zhou, J. Panyam, and V. Labhasetwar, "Size-dependency of nanoparticle-mediated gene transfection: studies with fractionated nanoparticles," *Int J Pharm*, vol. 244, pp. 105-15, Sep 5 2002.
- [115] D. Luo and W. M. Saltzman, "Synthetic DNA delivery systems," *Nat Biotechnol*, vol. 18, pp. 33-7, Jan 2000.
- [116] S. C. Richardson, H. V. Kolbe, and R. Duncan, "Potential of low molecular mass chitosan as a DNA delivery system: biocompatibility, body distribution and ability to complex and protect DNA," *Int J Pharm*, vol. 178, pp. 231-43, Feb 15 1999.
- [117] B. Sarmiento, das Neves, *Chitosan-Based Systems for Biopharmaceuticals: Delivery, Targeting and Polymer Therapeutics*, 2012.
- [118] C. Song, V. Labhasetwar, X. Cui, T. Underwood, and R. J. Levy, "Arterial uptake of biodegradable nanoparticles for intravascular local drug delivery: results with an acute dog model," *J Control Release*, vol. 54, pp. 201-11, Jul 31 1998.
- [119] I. Serr, R. W. Furst, V. B. Ott, M. G. Scherm, A. Nikolaev, F. Gokmen, *et al.*, "miRNA92a targets KLF2 and the phosphatase PTEN signaling to promote human T follicular helper precursors in T1D islet autoimmunity," *Proc Natl Acad Sci U S A*, vol. 113, pp. E6659-E6668, Oct 25 2016.
- [120] E. Hood, E. Simone, P. Wattamwar, T. Dziubla, and V. Muzykantov, "Nanocarriers for vascular delivery of antioxidants," *Nanomedicine (Lond)*, vol. 6, pp. 1257-72, Sep 2011.

- [121] Y. L. Yuan, B. M. Chesnutt, W. O. Haggard, and J. D. Bumgardner, "Deacetylation of Chitosan: Material Characterization and in vitro Evaluation via Albumin Adsorption and Pre-Osteoblastic Cell Cultures," *Materials*, vol. 4, pp. 1399-1416, Aug 2011.
- [122] E. Horisawa, K. Kubota, I. Tuboi, K. Sato, H. Yamamoto, H. Takeuchi, *et al.*, "Size-dependency of DL-lactide/glycolide copolymer particulates for intra-articular delivery system on phagocytosis in rat synovium," *Pharm Res*, vol. 19, pp. 132-9, Feb 2002.
- [123] B. Weiss, U. F. Schaefer, J. Zapp, A. Lamprecht, A. Stallmach, and C. M. Lehr, "Nanoparticles made of fluorescence-labelled Poly(L-lactide-co-glycolide): preparation, stability, and biocompatibility," *J Nanosci Nanotechnol*, vol. 6, pp. 3048-56, Sep-Oct 2006.
- [124] L. Song, E. J. Hennink, I. T. Young, and H. J. Tanke, "Photobleaching kinetics of fluorescein in quantitative fluorescence microscopy," *Biophys J*, vol. 68, pp. 2588-600, Jun 1995.
- [125] J. R. Saylor, "Photobleaching of disodium fluorescein in water," *Experiments in Fluids*, vol. 18, pp. 445-447, 1995.
- [126] S. Taetz, N. Nafee, J. Beisner, K. Piotrowska, C. Baldes, T. E. Murdter, *et al.*, "The influence of chitosan content in cationic chitosan/PLGA nanoparticles on the delivery efficiency of antisense 2'-O-methyl-RNA directed against telomerase in lung cancer cells," *Eur J Pharm Biopharm*, vol. 72, pp. 358-69, Jun 2009.
- [127] N. Nafee, "Cationically-modified nanoparticles for the pulmonary delivery of the telomerase inhibitor 2'-O-Methyl RNA for the treatment of lung cancer," S. University, Ed., ed, 2008.
- [128] A. Bootz, V. Vogel, D. Schubert, and J. Kreuter, "Comparison of scanning electron microscopy, dynamic light scattering and analytical ultracentrifugation for the sizing of poly(butyl cyanoacrylate) nanoparticles," *Eur J Pharm Biopharm*, vol. 57, pp. 369-75, Mar 2004.
- [129] D. Fillion, M. Lavertu, and M. D. Buschmann, "Ionization and solubility of chitosan solutions related to thermosensitive chitosan/glycerol-phosphate systems," *Biomacromolecules*, vol. 8, pp. 3224-34, Oct 2007.
- [130] L. Illum, "Chitosan and its use as a pharmaceutical excipient," *Pharm Res*, vol. 15, pp. 1326-31, Sep 1998.
- [131] F. L. Graham and A. J. van der Eb, "A new technique for the assay of infectivity of human adenovirus 5 DNA," *Virology*, vol. 52, pp. 456-67, Apr 1973.
- [132] P. L. Felgner, T. R. Gadek, M. Holm, R. Roman, H. W. Chan, M. Wenz, *et al.*, "Lipofection: a highly efficient, lipid-mediated DNA-transfection procedure," *Proc Natl Acad Sci U S A*, vol. 84, pp. 7413-7, Nov 1987.
- [133] M. Ogris, P. Steinlein, S. Carotta, S. Brunner, and E. Wagner, "DNA/polyethylenimine transfection particles: influence of ligands, polymer size, and PEGylation on internalization and gene expression," *AAPS PharmSci*, vol. 3, p. E21, 2001.
- [134] J. R. Baker, Jr., A. U. Bielinska, and J. F. Kukowska-Latallo, "Dendrimer-mediated cell transfection in vitro," *Methods Mol Biol*, vol. 245, pp. 67-82, 2004.
- [135] J. S. Pagano and A. Vaheri, "Enhancement of infectivity of poliovirus RNA with diethylaminoethyl-dextran (DEAE-D)," *Arch Gesamte Virusforsch*, vol. 17, pp. 456-64, 1965.

- [136] S. C. McBain, U. Griesenbach, S. Xenariou, A. Keramane, C. D. Batich, E. W. Alton, *et al.*, "Magnetic nanoparticles as gene delivery agents: enhanced transfection in the presence of oscillating magnet arrays," *Nanotechnology*, vol. 19, p. 405102, Oct 08 2008.
- [137] F. Scherer, M. Anton, U. Schillinger, J. Henke, C. Bergemann, A. Kruger, *et al.*, "Magnetofection: enhancing and targeting gene delivery by magnetic force in vitro and in vivo," *Gene Ther*, vol. 9, pp. 102-9, Jan 2002.
- [138] C. Plank, U. Schillinger, F. Scherer, C. Bergemann, J. S. Remy, F. Krotz, *et al.*, "The magnetofection method: using magnetic force to enhance gene delivery," *Biol Chem*, vol. 384, pp. 737-47, May 2003.
- [139] E. Neumann, M. Schaefer-Ridder, Y. Wang, and P. H. Hofschneider, "Gene transfer into mouse lymphoma cells by electroporation in high electric fields," *EMBO J*, vol. 1, pp. 841-5, 1982.
- [140] I. P. Sugar and E. Neumann, "Stochastic model for electric field-induced membrane pores. Electroporation," *Biophys Chem*, vol. 19, pp. 211-25, May 1984.
- [141] H. Wolf, M. P. Rols, E. Boldt, E. Neumann, and J. Teissie, "Control by pulse parameters of electric field-mediated gene transfer in mammalian cells," *Biophys J*, vol. 66, pp. 524-31, Feb 1994.
- [142] R. M. Klein, E. D. Wolf, R. Wu, and J. C. Sanford, "High-velocity microprojectiles for delivering nucleic acids into living cells. 1987," *Biotechnology*, vol. 24, pp. 384-6, 1992.
- [143] J. C. Sanford, T. M. Klein, E. D. Wolf, and N. Allen, "Delivery of substances into cells and tissues using a particle bombardment process," *Particulate Science and Technology*, vol. 5, pp. 27-37, 1987/01/01 1987.
- [144] M. Tsukakoshi, S. Kurata, Y. Nomiya, Y. Ikawa, and T. Kasuya, "A novel method of DNA transfection by laser microbeam cell surgery," *Applied Physics B*, vol. 35, pp. 135-140, 1984.
- [145] E. G. Diacumakos, "Methods for micromanipulation of human somatic cells in culture," *Methods Cell Biol*, vol. 7, pp. 287-311, 1973.
- [146] D. H. Hamer, K. D. Smith, S. H. Boyer, and P. Leder, "SV40 recombinants carrying rabbit beta-globin gene coding sequences," *Cell*, vol. 17, pp. 725-35, Jul 1979.
- [147] R. C. Mulligan, B. H. Howard, and P. Berg, "Synthesis of rabbit beta-globin in cultured monkey kidney cells following infection with a SV40 beta-globin recombinant genome," *Nature*, vol. 277, pp. 108-14, Jan 11 1979.
- [148] M. A. Kay, "State-of-the-art gene-based therapies: the road ahead," *Nat Rev Genet*, vol. 12, pp. 316-28, May 2011.
- [149] M. A. Mintzer and E. E. Simanek, "Nonviral vectors for gene delivery," *Chem Rev*, vol. 109, pp. 259-302, Feb 2009.
- [150] H. Yin, R. L. Kanasty, A. A. Eltoukhy, A. J. Vegas, J. R. Dorkin, and D. G. Anderson, "Non-viral vectors for gene-based therapy," *Nature Reviews Genetics*, vol. 15, pp. 541-555, Aug 2014.
- [151] M. Ramamoorth and A. Narvekar, "Non viral vectors in gene therapy- an overview," *J Clin Diagn Res*, vol. 9, pp. GE01-6, Jan 2015.
- [152] H. Yin, R. L. Kanasty, A. A. Eltoukhy, A. J. Vegas, J. R. Dorkin, and D. G. Anderson, "Non-viral vectors for gene-based therapy," *Nat Rev Genet*, vol. 15, pp. 541-555, 08/print 2014.
- [153] S. Mao, W. Sun, and T. Kissel, "Chitosan-based formulations for delivery of DNA and siRNA," *Adv Drug Deliv Rev*, vol. 62, pp. 12-27, Jan 31 2010.

- [154] H. Ragelle, K. Vanvarenberg, G. Vandermeulen, and V. Preat, "Chitosan Nanoparticles for SiRNA Delivery In Vitro," *Methods Mol Biol*, vol. 1364, pp. 143-50, 2016.
- [155] H. Ragelle, G. Vandermeulen, and V. Preat, "Chitosan-based siRNA delivery systems," *J Control Release*, vol. 172, pp. 207-18, Nov 28 2013.
- [156] P. V. Dileep, H. Su-Ji, and H. Leaf, "Lipid-Protamine-DNA-Mediated Antigen Delivery," *Current Drug Delivery*, vol. 2, pp. 401-406, 2005.
- [157] Y. Tsuchiya, T. Ishii, Y. Okahata, and T. Sato, "Characterization of protamine as a transfection accelerator for gene delivery," *Journal of Bioactive and Compatible Polymers*, vol. 21, pp. 519-537, Nov 2006.
- [158] H. Yamada, B. Loretz, and C. M. Lehr, "Design of starch-graft-PEI polymers: an effective and biodegradable gene delivery platform," *Biomacromolecules*, vol. 15, pp. 1753-61, May 12 2014.
- [159] M. Kunishima, C. Kawachi, J. Monta, K. Terao, F. Iwasaki, and S. Tani, "4-(4,6-dimethoxy-1,3,5-triazin-2-yl)-4-methyl-morpholinium chloride: an efficient condensing agent leading to the formation of amides and esters," *Tetrahedron*, vol. 55, pp. 13159-13170, 11/12/ 1999.
- [160] N. Blumenkrantz and G. Asboe-Hansen, "New method for quantitative determination of uronic acids," *Anal Biochem*, vol. 54, pp. 484-9, Aug 1973.
- [161] H. Yamada, "Starch based cationic polymers for gene delivery," Saarländische Universitäts- und Landesbibliothek, Saarbrücken, 2014.
- [162] E. Wagner, "Effects of membrane-active agents in gene delivery," *J Control Release*, vol. 53, pp. 155-8, Apr 30 1998.
- [163] T. I. Kim, T. Rothmund, T. Kissel, and S. W. Kim, "Bioreducible polymers with cell penetrating and endosome buffering functionality for gene delivery systems," *J Control Release*, vol. 152, pp. 110-9, May 30 2011.
- [164] W. Liang and J. K. W. Lam, *Endosomal Escape Pathways for Non-Viral Nucleic Acid Delivery Systems*, 2012.
- [165] K. Braeckmans, K. Buyens, B. Naeye, D. Vercauteren, H. Deschout, K. Raemdonck, *et al.*, "Advanced fluorescence microscopy methods illuminate the transfection pathway of nucleic acid nanoparticles," *J Control Release*, vol. 148, pp. 69-74, Nov 20 2010.
- [166] K. Buyens, B. Lucas, K. Raemdonck, K. Braeckmans, J. Vercammen, J. Hendrix, *et al.*, "A fast and sensitive method for measuring the integrity of siRNA-carrier complexes in full human serum," *J Control Release*, vol. 126, pp. 67-76, Feb 18 2008.
- [167] S. Barthold, "Nanotechnology enabled drug delivery of proteins and peptides to the lung," Saarländische Universitäts- und Landesbibliothek, Saarbrücken, 2016.
- [168] N. P. Gabrielson and D. W. Pack, "Acetylation of polyethylenimine enhances gene delivery via weakened polymer/DNA interactions," *Biomacromolecules*, vol. 7, pp. 2427-35, Aug 2006.
- [169] S. W. Stein, P. Sheth, P. D. Hodson, and P. B. Myrdal, "Advances in metered dose inhaler technology: hardware development," *AAPS PharmSciTech*, vol. 15, pp. 326-38, Apr 2014.
- [170] P. J. Atkins, "Dry Powder Inhalers: An Overview," *Respiratory Care*, vol. 50, pp. 1304-1312, 2005.
- [171] M. B. Snipes, "Biokinetics of inhaled radionuclides," *Internal Radiation Dosimetry*, pp. 181-196, 1994.

- [172] C. o. A. M. f. T. I. A. A. B. Agents, *Overcoming Challenges to Develop Countermeasures Against Aerosolized Bioterrorism Agents: Appropriate Use of Animal Models* National Academy of Sciences, 2006.
- [173] N. K. Jain and I. Roy, "Effect of trehalose on protein structure," *Protein Sci*, vol. 18, pp. 24-36, Jan 2009.
- [174] M. Rinaudo, "Chitin and chitosan: Properties and applications," *Progress in Polymer Science*, vol. 31, pp. 603-632, 7// 2006.
- [175] K. Donaldson, V. Stone, C. L. Tran, W. Kreyling, and P. J. A. Borm, "Nanotoxicology," *Occupational and Environmental Medicine*, vol. 61, pp. 727-728, Sep 2004.
- [176] C. M. Keck and R. H. Muller, "Nanotoxicological classification system (NCS) - a guide for the risk-benefit assessment of nanoparticulate drug delivery systems," *Eur J Pharm Biopharm*, vol. 84, pp. 445-8, Aug 2013.
- [177] C. M. Lehr and H. Groß, "Wirksamere und sicherere Medikamente mit Hilfe der Nanotechnologie," *Nanotechnologie aktuell*, vol. 7, pp. 112-116, 2014.
- [178] S. Barthold, N. Kunschke, X. Murgia, B. Loretz, C. de Souza Carvalho-Wodarz, and C.-M. Lehr, "Overview of Inhaled Nanopharmaceuticals," in *ISAM Textbook of Aerosol Medicine*, B. a. D. Rothen-Rutishauser, R., Ed., ed, 2015, pp. 330-351.
- [179] T. B. Casale and E. J. Carolan, "Cytokine-induced sequential migration of neutrophils through endothelium and epithelium," *Inflamm Res*, vol. 48, pp. 22-7, Jan 1999.
- [180] M. I. Hermanns, R. E. Unger, K. Kehe, K. Peters, and C. J. Kirkpatrick, "Lung epithelial cell lines in coculture with human pulmonary microvascular endothelial cells: development of an alveolo-capillary barrier in vitro," *Lab Invest*, vol. 84, pp. 736-52, Jun 2004.
- [181] B. M. Rothen-Rutishauser, S. G. Kiama, and P. Gehr, "A three-dimensional cellular model of the human respiratory tract to study the interaction with particles," *Am J Respir Cell Mol Biol*, vol. 32, pp. 281-9, Apr 2005.
- [182] F. Blank, M. Wehrli, A. Lehmann, O. Baum, P. Gehr, C. von Garnier, *et al.*, "Macrophages and dendritic cells express tight junction proteins and exchange particles in an in vitro model of the human airway wall," *Immunobiology*, vol. 216, pp. 86-95, Jan-Feb 2011.
- [183] S. Tsuchiya, M. Yamabe, Y. Yamaguchi, Y. Kobayashi, T. Konno, and K. Tada, "Establishment and characterization of a human acute monocytic leukemia cell line (THP-1)," *Int J Cancer*, vol. 26, pp. 171-6, Aug 1980.
- [184] H. G. Drexler, H. Quentmeier, and R. A. MacLeod, "Malignant hematopoietic cell lines: in vitro models for the study of MLL gene alterations," *Leukemia*, vol. 18, pp. 227-32, Feb 2004.
- [185] S. Tsuchiya, Y. Kobayashi, Y. Goto, H. Okumura, S. Nakae, T. Konno, *et al.*, "Induction of maturation in cultured human monocytic leukemia cells by a phorbol diester," *Cancer Res*, vol. 42, pp. 1530-6, Apr 1982.
- [186] H. Schwende, E. Fitzke, P. Ambs, and P. Dieter, "Differences in the state of differentiation of THP-1 cells induced by phorbol ester and 1,25-dihydroxyvitamin D3," *J Leukoc Biol*, vol. 59, pp. 555-61, Apr 1996.
- [187] D. J. Giard, S. A. Aaronson, G. J. Todaro, P. Arnstein, J. H. Kersey, H. Dosik, *et al.*, "In vitro cultivation of human tumors: establishment of cell lines derived from a series of solid tumors," *J Natl Cancer Inst*, vol. 51, pp. 1417-23, Nov 1973.

- [188] D. L. Shapiro, L. L. Nardone, S. A. Rooney, E. K. Motoyama, and J. L. Munoz, "Phospholipid biosynthesis and secretion by a cell line (A549) which resembles type II alveolar epithelial cells," *Biochim Biophys Acta*, vol. 530, pp. 197-207, Aug 25 1978.
- [189] M. Lieber, B. Smith, A. Szakal, W. Nelson-Rees, and G. Todaro, "A continuous tumor-cell line from a human lung carcinoma with properties of type II alveolar epithelial cells," *Int J Cancer*, vol. 17, pp. 62-70, Jan 15 1976.
- [190] J. Fogh, J. M. Fogh, and T. Orfeo, "One hundred and twenty-seven cultured human tumor cell lines producing tumors in nude mice," *J Natl Cancer Inst*, vol. 59, pp. 221-6, Jul 1977.
- [191] T. Mosmann, "Rapid colorimetric assay for cellular growth and survival: application to proliferation and cytotoxicity assays," *J Immunol Methods*, vol. 65, pp. 55-63, Dec 16 1983.
- [192] T. M. Buttke, J. A. McCubrey, and T. C. Owen, "Use of an aqueous soluble tetrazolium/formazan assay to measure viability and proliferation of lymphokine-dependent cell lines," *J Immunol Methods*, vol. 157, pp. 233-40, Jan 04 1993.
- [193] R. C. Squatrito, J. P. Connor, and R. E. Buller, "Comparison of a novel redox dye cell growth assay to the ATP bioluminescence assay," *Gynecol Oncol*, vol. 58, pp. 101-5, Jul 1995.
- [194] S. Nayak and R. W. Herzog, "Progress and prospects: immune responses to viral vectors," *Gene Ther*, vol. 17, pp. 295-304, Mar 2010.
- [195] R. Gardlik, R. Palffy, J. Hodossy, J. Lukacs, J. Turna, and P. Celec, "Vectors and delivery systems in gene therapy," *Med Sci Monit*, vol. 11, pp. RA110-21, Apr 2005.
- [196] N. Nayerossadat, T. Maedeh, and P. A. Ali, "Viral and nonviral delivery systems for gene delivery," *Adv Biomed Res*, vol. 1, p. 27, 2012.
- [197] X. Zeng, A. M. de Groot, A. J. Sijts, F. Broere, E. Oude Blenke, S. Colombo, et al., "Surface coating of siRNA-peptidomimetic nano-self-assemblies with anionic lipid bilayers: enhanced gene silencing and reduced adverse effects in vitro," *Nanoscale*, vol. 7, pp. 19687-98, Dec 14 2015.
- [198] A. K. L. Abbas, A. H.; Pillai, S., *Cellular and Molecular Immunology*, 8th ed.: Elsevir, 2014.
- [199] J. Banchereau and R. M. Steinman, "Dendritic cells and the control of immunity," *Nature*, vol. 392, pp. 245-52, Mar 19 1998.
- [200] A. Lanzavecchia and F. Sallusto, "Regulation of T cell immunity by dendritic cells," *Cell*, vol. 106, pp. 263-6, Aug 10 2001.
- [201] K. Shortman and Y. J. Liu, "Mouse and human dendritic cell subtypes," *Nat Rev Immunol*, vol. 2, pp. 151-61, Mar 2002.
- [202] R. S. Mahla, M. C. Reddy, D. V. Prasad, and H. Kumar, "Sweeten PAMPs: Role of Sugar Complexed PAMPs in Innate Immunity and Vaccine Biology," *Front Immunol*, vol. 4, p. 248, 2013.
- [203] Y. Delneste, C. Beauvillain, and P. Jeannin, "[Innate immunity: structure and function of TLRs]," *Med Sci (Paris)*, vol. 23, pp. 67-73, Jan 2007.
- [204] T. Letoha, C. Somlai, T. Takacs, A. Szabolcs, K. Jarmay, Z. Rakonczay, Jr., et al., "A nuclear import inhibitory peptide ameliorates the severity of cholecystokinin-induced acute pancreatitis," *World J Gastroenterol*, vol. 11, pp. 990-9, Feb 21 2005.
- [205] M. V. Berridge and A. S. Tan, "Characterization of the cellular reduction of 3-(4,5-dimethylthiazol-2-yl)-2,5-diphenyltetrazolium bromide (MTT): subcellular

- localization, substrate dependence, and involvement of mitochondrial electron transport in MTT reduction," *Arch Biochem Biophys*, vol. 303, pp. 474-82, Jun 1993.
- [206] H. Tada, O. Shiho, K. Kuroshima, M. Koyama, and K. Tsukamoto, "An improved colorimetric assay for interleukin 2," *J Immunol Methods*, vol. 93, pp. 157-65, Nov 06 1986.
- [207] M. J. Stoddart, "Cell viability assays: introduction," *Methods Mol Biol*, vol. 740, pp. 1-6, 2011.
- [208] T. L. Riss, R. A. Moravec, A. L. Niles, S. Duellman, H. A. Benink, T. J. Worzella, *et al.*, "Cell Viability Assays," in *Assay Guidance Manual*, G. S. Sittampalam, N. P. Coussens, K. Brimacombe, A. Grossman, M. Arkin, D. Auld, *et al.*, Eds., ed Bethesda (MD), 2004.
- [209] S. Hacein-Bey-Abina, C. Von Kalle, M. Schmidt, M. P. McCormack, N. Wulffraat, P. Leboulch, *et al.*, "LMO2-associated clonal T cell proliferation in two patients after gene therapy for SCID-X1," *Science*, vol. 302, pp. 415-9, Oct 17 2003.
- [210] A. Kuehn, S. Kletting, C. de Souza Carvalho-Wodarz, U. Repnik, G. Griffiths, U. Fischer, *et al.*, "Human alveolar epithelial cells expressing tight junctions to model the air-blood barrier," *ALTEX*, Mar 17 2016.
- [211] F. Manford, A. Tronde, A. B. Jeppsson, N. Patel, F. Johansson, and B. Forbes, "Drug permeability in 16HBE14o- airway cell layers correlates with absorption from the isolated perfused rat lung," *Eur J Pharm Sci*, vol. 26, pp. 414-20, Dec 2005.
- [212] K. A. Foster, C. G. Oster, M. M. Mayer, M. L. Avery, and K. L. Audus, "Characterization of the A549 cell line as a type II pulmonary epithelial cell model for drug metabolism," *Exp Cell Res*, vol. 243, pp. 359-66, Sep 15 1998.
- [213] J. R. Pappenheimer, E. M. Renkin, and L. M. Borrero, "Filtration, diffusion and molecular sieving through peripheral capillary membranes; a contribution to the pore theory of capillary permeability," *Am J Physiol*, vol. 167, pp. 13-46, Oct 1951.
- [214] L. Gonzalez-Mariscal, S. Hernandez, and J. Vega, "Inventions designed to enhance drug delivery across epithelial and endothelial cells through the paracellular pathway," *Recent Pat Drug Deliv Formul*, vol. 2, pp. 145-76, 2008.
- [215] K. Murugan, Y. E. Choonara, P. Kumar, D. Bijukumar, L. C. du Toit, and V. Pillay, "Parameters and characteristics governing cellular internalization and trans-barrier trafficking of nanostructures," *Int J Nanomedicine*, vol. 10, pp. 2191-206, 2015.
- [216] B. D. Grant and J. G. Donaldson, "Pathways and mechanisms of endocytic recycling," *Nat Rev Mol Cell Biol*, vol. 10, pp. 597-608, Sep 2009.
- [217] F. R. Maxfield and T. E. McGraw, "Endocytic recycling," *Nat Rev Mol Cell Biol*, vol. 5, pp. 121-32, Feb 2004.
- [218] I. Mellman, "Endocytosis and molecular sorting," *Annu Rev Cell Dev Biol*, vol. 12, pp. 575-625, 1996.
- [219] J. A. Mindell, "Lysosomal acidification mechanisms," *Annu Rev Physiol*, vol. 74, pp. 69-86, 2012.
- [220] G. Griffiths, B. Hoflack, K. Simons, I. Mellman, and S. Kornfeld, "The mannose 6-phosphate receptor and the biogenesis of lysosomes," *Cell*, vol. 52, pp. 329-341, 1988.
- [221] D. J. Tobin, "Biochemistry of human skin--our brain on the outside," *Chem Soc Rev*, vol. 35, pp. 52-67, Jan 2006.

Danksagung

Zuerst möchte ich meinem Doktorvater Herrn Prof. Claus-Michael Lehr für die Möglichkeit danken, an diesem überaus interessanten Thema arbeiten zu dürfen. Er bot mir den nötigen Freiraum, mich im Rahmen dieser Arbeit selbstständig zu finden und zu entwickeln. Darüber hinaus durfte ich die Möglichkeit ergreifen, die Ausbildung zum Fachapotheker für pharmazeutische Technologie durchzuführen. Danke für das offene und freundliche Miteinander und den kreativen Input.

Darüber hinaus möchte ich mich bei denen bedanken, die mich während dieser Zeit begleitet und unterstützt haben.

Thorsten Lehr, der einem stets mit Rat und Tat beiseite stand und so viel Interesse an einem für ihn eher fachfremden Thema zeigte. Vielen Dank ebenfalls für das Zweitgutachten.

Ich danke dem Prüfungsgremium für die Zeit und die Mühe sich mit meinem Thema zu beschäftigen.

Danke an das COMPACT Konsortium, hier durfte ich eine projektbezogene Arbeitsweise zwischen universitärer und industrieller Forschung kennenlernen.

Brigitta vielen Dank für die fachliche Unterstützung und den hilfreichen Anregungen, Maike für den Rückhalt in der Lehrtätigkeit und dem stets offenen Ohr, Nicole & Cristiane für die Hilfe bei allen Belangen rund um die Zellkultur.

Nicht zu vergessen die Techniker am HIPS und der Uni, besonders Chiara (SEM, TEM und irgendwie alles andere), Petra & Jana (Zellkultur); Büro (Sarah und Stephanie) Hilfe im Bürokratie-Wust und gemeinsame Suche nach dem „Passierschein A38“ (auch Reisekostenerstattung genannt) und nicht zu vergessen Karin für den Überblick über das große Ganze.

AK Schneider, (Marc Schneider, Carolin, Agnes, Michael, Marcel, Nashrawan und Nazende) für den kleinen Schnack zwischendurch und dem Willkommen sein trotz Umzug in das Helmholtz-Forschungsgebäude.

COMPACT-Girls (Sarah, Stephanie, Remi) und die COMPACT-Partner. Es war schön, gemeinsam in einem Projekt zu arbeiten und Probleme zusammen besprechen zu können.

Dankeschön an die Arbeitskollegen am Institut, besonders an Hiroe für die Einweisung in die hohe Kunst der Stärkesynthese), Marius (der sich gegen eine Bezahlung in Gerstensaft ☺ dazu hinreißen ließ, mir die korrelative Mikroskopie zu zeigen, René als Büroverbündeter gegen den Rest der Welt). Viele Leute, die ich in der Zeit kennengelernt habe werde ich in guter Erinnerung behalten und hoffe, dass sich die Wege mal wieder kreuzen werden.

An all die Lieben, die mir während der Zeit in der Apotheke geholfen haben, mal auf andere Gedanken zu kommen und mich haben Apotheker sein lassen.

Vielen Dank an meine „BioIng“-Familie, die die Anstrengungen einer Promotion stets nachvollziehen konnte und mir Mut machten weiterhin durchzuhalten, meinen Pharma-Mädels, besonders Sarah & Janine, die mir immer gezeigt haben (egal wo ich gerade bin) was im Leben wirklich wichtig ist – wahre Freunde sind wie eine zweite Familie!

Meinen Eltern die (auch wenn sie nicht genau verstanden haben, was ich während der Promotion überhaupt mache) sowie mein Bruder Markus, unfassbaren Stolz zeigten.

Till, es gibt keine Worte die beschreiben, welchen Anteil du trägst. Auch wenn es nicht einfach war, konnte ich immer auf deine Unterstützung vertrauen. Der letzte Dank geht an meinem kleinen Milan, der die Verzögerung meiner Arbeit und die Erschöpfung durch schlaflose Nächte mit nur einem Lächeln vergessen lässt.

Ihr beide lasst uns eine Familie sein und gebt meinem Leben somit einen Sinn!

Scientific output

Publications

- 10/2017 Contribution to the manuscript in Science Translational Medicine
I. Serr, M.G. Scherm, A.M. Zahm, J. Schug, V.K. Flynn, M. Hippich
et al.
*"A miRNA181a/NFAT5 axis links impaired T cell tolerance induction
with autoimmune Type 1 diabetes"*
- 10/2016: Contribution to the manuscript in Proceedings of the National Academy
of Sciences (PNAS)
I. Serr, R. W. Furst, V. B. Ott, M. G. Scherm, A. Nikolaev, F. Gokmen,
et al.
*"2a targets KLF2 and the phosphatase PTEN signaling to
promote human T follicular helper precursors in T1D islet
autoimmunity,"*
- 05/2015: Contribution to the book chapter in ISAM Textbook of Aerosol Medicine
S. Barthold, N. Kunschke, X. Murgia, B. Loretz, C. de Souza Carvalho-
Wodarz, and C.-M. Lehr
"Overview of Inhaled Nanopharmaceuticals"

Presentations

- 09/2015: Poster at DPhG annual conference 2015; Düsseldorf, Germany
N. Kunschke, B. Loretz, and C.-M. Lehr
*"Impact of cationic polymer coatings on PLGA nanoparticle
characteristics, immunogenicity and uptake"*

- 07/2015: Poster at the 42nd CRS Annual Meeting; Edinburgh, United Kingdom
N. Kunschke, A. M. de Groot, B. Loretz, E.J.A.M. Sijts and C. M. Lehr;
“Impact of cationic polymer coatings on PLGA nanoparticle characteristics, immunogenicity and uptake”
- 02/2015: Poster at CRS – Germany local chapter meeting; Basel, Switzerland
N. Kunschke, B. Loretz, and C.-M. Lehr
„PLGA-Chitosan Nanoparticles for pulmonary siRNA delivery (WP2)”
- 11/2014: Poster at 2. Doktorandentag der Naturwissenschaftlich-Technischen Fakultät III; Saarbrücken, Germany
N. Kunschke, B. Loretz, and C.-M. Lehr
„PLGA-Chitosan Nanoparticles for pulmonary siRNA delivery (WP2)”
- 06/2014: Poster at 4th HIPS Symposium; Saarbrücken, Germany
S. Kletting, S. Barthold, N. Kunschke, C. Carvalho, B. Loretz, N. Daum and C.M. Lehr;
“COMPACT – a European Collaboration on the Optimization of Macromolecular Pharmaceutical Access to Cellular Targets”

Curriculum Vitae

Personal Data

Name Nicole Liebsch, geb Kunschke
Date of Birth 27.02.1984 in Lippstadt, Germany
E-Mail Address nicole.liebsch@outlook.com

Dissertation

11/2012 – 11/2015 PhD candidate,
Helmholtz-Institute for pharmaceutical Research Saarland,
Saarbrücken, Germany; Department of Drug Delivery
Topic: Development of a Nanotechnology enabled
Drug Delivery System for Pulmonary siRNA Delivery

Education

09/2011 Approbation as pharmacist
2005 – 2011 Pharmacy at Technical University
'Carolo Wilhelmina', Braunschweig, Germany
2003-2005 Biological Engineering at Technical University
'Carolo Wilhelmina', Braunschweig, Germany
1994 – 2003 priv. Mauritius-Gymnasium, Büren, Germany

Internships

05/2012 – 10/2012 Apotheke in der alten Seilerei, Mannheim, Germany
11/2011 – 04/2012 Boehringer Ingelheim Pharma GmbH & Co. KG,
Launch & Production Site / Pharma Biberach,
Biberach an der Riß, Germany